# Quality assessment & monitoring of recycled coarse aggregates

Chang, C.

**DOI**
10.4233/uuid:ca80614c-747f-4ef8-95aa-78c0b193d261

**Publication date**
2025

**Document Version**
Final published version

**Citation (APA)**
Chang, C. (2025). *Quality assessment & monitoring of recycled coarse aggregates*. [Dissertation (TU Delft), Delft University of Technology]. https://doi.org/10.4233/uuid:ca80614c-747f-4ef8-95aa-78c0b193d261

# QUALITY ASSESSMENT & MONITORING OF RECYELED COARSE AGGREGATES

常成 Chang Cheng

# Quality Assessment & Monitoring of Recycled Coarse Aggregates

# Quality Assessment & Monitoring of Recycled Coarse Aggregates

## Dissertation

for the purpose of obtaining the degree of doctor
at Delft University of Technology
by the authority of the Rector Magnificus Prof.dr.ir. T.H.J.J. van der Hagen
chair of the Board for Doctorates
to be defended publicly on
Tuesday 7 January 2025 at 10:00 o'clock

by

**Cheng CHANG**

Master of Architecture, Southeast University, China,
born in Taixing, China.

Dit proefschrift is goedgekeurd door de promotoren.

Samenstelling promotiecommissie bestaat uit:

| | |
|---|---|
| Rector Magnificus | voorzitter |
| Prof. dr. ir. P. C. Rem | Technische Universiteit Delft, promotor |
| Dr. F. Di Maio | Technische Universiteit Delft, copromotor |
| | |
| *Onafhankelijke leden:* | |
| Prof. dr. ir. M. A. N. Hendriks | Technische Universiteit Delft |
| Prof. dr. ir. J. Brouwers | Technische Universiteit Eindhoven |
| Prof. dr. ir. J. Dai | City University of Hong Kong, China |
| Dr. M. W. N. Buxton | Technische Universiteit Delft |
| Dr. Y. Wu | Technische Universiteit Delft |
| Prof. dr. ir. M. Veljkovic | Technische Universiteit Delft, reservelid |

*Keywords:* Recycled coarse aggregates (RCA), Quality inspection, Concrete recycling, Laser-induced breakdown spectroscopy (LIBS), 3D Scanner Gocator, Inline

*Front & Back:* Cheng Chang



ISBN/EAN 978-94-6384-709-4(E-book)
ISBN/EAN 978-94-6384-708-7 (Paperback)

An electronic version of this dissertation is available at
http://repository.tudelft.nl/.

为者常成

# CONTENTS

# SUMMARY

This doctoral dissertation explores the development and application of innovative technologies designed to improve the sustainability of the construction industry by effectively using recycled coarse aggregates (RCA). The primary aim of this research is to develop, implement, and validate novel methods that incorporate advanced technologies for accurate grading and quality assurance of RCA. By enhancing the efficiency of RCA repurposing, this work seeks to broaden its use in construction projects, significantly contributing to environmental sustainability.

The research begins by introducing a novel mobile system specifically designed to conduct on-site quality inspections of unscreened RCA streams. This technology provides an easily transportable and efficient solution to assess and categorize RCA on-site, facilitating its immediate and effective reuse in various construction applications. This system leverages advanced technologies from the field of raw materials sorting and real-time data processing to ensure the quality and usability of recycled materials, aiming to reduce construction waste and enhance material lifecycle management.

The study further investigates the integration of RCA in the production of high-performance concrete through the industrial-scale implementation of intelligent optimal grading techniques. These techniques detail the integration of optimized grading algorithms that adjust the composition of RCA to enhance the mechanical properties of concrete. This methodology not only improves the quality of final concrete but also demonstrates the practical and scalable use of RCA in demanding construction environments.

A significant portion of the research is dedicated to the characterization of RCA using Laser-Induced Breakdown Spectroscopy (LIBS). This technique offers a quick and non-destructive way to accurately identify and classify materials and contaminants for in-line quality inspection of RCA. The precision and accuracy of LIBS allow for a detailed assessment of the RCA quality, crucial for ensuring the structural integrity and longevity of RCA-based concrete structures.

Further advancements are achieved by integrating LIBS with 3D scanning technologies. This combination establishes a more precise quality control system for RCA streams. By enhancing the detection and quantification of undesirable contaminants within RCA streams, this approach ensures that the materials in the final recycled products meet the required standards, thereby improving the overall reliability of RCA. This not only maintains but also improves the structural quality of the final concrete.

The dissertation concludes by synthesizing the technological innovations and research findings, emphasizing their implications for both the scientific community and the construction industry at large. It highlights the environmental benefits of adopting RCA, including reduced reliance on virgin materials and enhancing the sustainability of construction practices. Additionally, it outlines a series of future research directions that focus on refining these technologies, exploring their economic impacts and com-

mercial viability, and evaluating the long-term performance of structures built with RCA concrete.

Overall, this thesis provides a substantial contribution to the field of sustainable construction, offering practical, technology-driven solutions that pave the way for a more sustainable and environmentally conscious construction industry. The methodologies developed herein not only push the boundaries of academic research but also present viable, industry-ready applications that can significantly impact the way construction materials are recycled and utilized.

# SAMENVATTING

Dit proefschrift onderzoekt de ontwikkeling en toepassing van innovatieve technologieën ontworpen om de duurzaamheid van de bouwindustrie te verbeteren door effectief gebruik te maken van gerecyclede grove aggregaten (RCA). Het primaire doel van dit onderzoek is het ontwikkelen, implementeren en valideren van nieuwe methoden die geavanceerde technologieën incorporeren voor nauwkeurige sortering en kwaliteitsborging van RCA. Door het verbeteren van de efficiëntie van het hergebruik van RCA, streeft dit werk naar een bredere toepassing in bouwprojecten, wat aanzienlijk bijdraagt aan de milieuduurzaamheid.

Het onderzoek begint met de introductie van een nieuw mobiel systeem dat specifiek is ontworpen om ter plaatse kwaliteitsinspecties uit te voeren van ongezeefde RCA-stromen. Deze technologie biedt een gemakkelijk transporteerbare en efficiënte oplossing om RCA ter plaatse te beoordelen en te categoriseren, waardoor het direct en effectief hergebruikt kan worden in verschillende bouwtoepassingen. Dit systeem maakt gebruik van geavanceerde technologieën op het gebied van grondstoffen sorteren en realtime gegevensverwerking om de kwaliteit en bruikbaarheid van gerecycleerde materialen te waarborgen, met als doel bouwafval te verminderen en het beheer van de materiaalcyclus te verbeteren.

De studie onderzoekt verder de integratie van RCA in de productie van hoogwaardig beton door de industriële implementatie van intelligente optimale sorteertechnieken. Deze technieken beschrijven de integratie van geoptimaliseerde sorteeralgoritmen die de samenstelling van RCA aanpassen om de mechanische eigenschappen van beton te verbeteren. Deze methodologie verbetert niet alleen de kwaliteit van het uiteindelijke beton, maar toont ook het praktische en schaalbare gebruik van RCA in veeleisende bouwomgevingen.

Een aanzienlijk deel van het onderzoek is gewijd aan de karakterisering van RCA met behulp van Laser-Induced Breakdown Spectroscopy (LIBS). Deze techniek biedt een snelle en niet-destructieve manier om materialen en verontreinigingen nauwkeurig te identificeren en te classificeren voor in-line kwaliteitsinspectie van RCA. De precisie en nauwkeurigheid van LIBS maken een gedetailleerde beoordeling van de RCA-kwaliteit mogelijk, cruciaal voor het waarborgen van de structurele integriteit en levensduur van op RCA gebaseerde betonconstructies.

Verdere vooruitgang wordt bereikt door LIBS te integreren met 3D-scantechnologieën. Deze combinatie realiseert een nauwkeuriger kwaliteitscontrolesysteem voor RCA-stromen. Door het detecteren en kwantificeren van ongewenste verontreinigingen binnen RCA-stromen te verbeteren, zorgt deze aanpak ervoor dat de materialen in de uiteindelijke gerecyclede producten aan de vereiste normen voldoen, waardoor de algehele betrouwbaarheid van RCA verbetert. Dit behoudt niet alleen, maar verbetert ook de structurele kwaliteit van het uiteindelijke beton.

Het proefschrift wordt afgesloten door de technologische innovaties en onderzoeksresultaten te integreren, waarbij de implicaties voor zowel de wetenschappelijke gemeenschap als de bouwindustrie in het algemeen worden benadrukt. Het benadrukt de milieuvoordelen van het adopteren van RCA, inclusief verminderde afhankelijkheid van uitputbare grondstoffen materialen en het versterken van de duurzaamheid van bouwpraktijken. Daarnaast schetst het een reeks toekomstige onderzoeksrichtingen die zich richten op het verfijnen van deze technologieën, het verkennen van hun economische impact en commerciële levensvatbaarheid, en het evalueren van de langetermijnprestaties van bouwwerken uit RCA-beton.

Over het algemeen levert deze thesis een substantiële bijdrage aan het gebied van duurzame bouw, en biedt zij praktische, technologiegedreven oplossingen die de weg banen voor een duurzamere en milieubewustere bouwindustrie. De ontwikkelde methodologieën verleggen niet alleen de grenzen van academisch onderzoek, maar presenteren ook haalbare, industrie–rijpe toepassingen die significant kunnen impact hebben op de manier waarop bouwmaterialen worden gerecycled en gebruikt.

# 1

# Introduction

1

THE construction industry is at a pivotal crossroads, as it grapples with the dual challenges of meeting the increasing demand for infrastructure while minimizing its environmental footprint. Traditional construction practices, particularly the extensive use of concrete, have led to significant environmental concerns, including resource depletion, energy consumption, and land degradation. In response to these challenges, the adoption of sustainable construction practices has become a global imperative. This dissertation explores the role of recycled coarse aggregates (RCA) as a sustainable alternative to natural aggregates, examining the challenges of quality control and monitoring associated with their utilization.

The introduction is structured as follows: Section 1.1 provides the background and motivation for this research, delving into the global need for sustainable construction, the role of RCA, and the challenges in their broader adoption. Section 1.2 outlines the specific research objectives that guide this study. Finally, Section 1.3 presents the overall structure of the dissertation, offering a roadmap for the topics and methodologies explored in subsequent chapters.

## 1.1. BACKGROUND AND MOTIVATION

### 1.1.1. GLOBAL NEED FOR SUSTAINABLE CONSTRUCTION

As the global population continues to grow and urbanize, the construction industry faces an unprecedented demand for infrastructure development. This rapid expansion places immense pressure on natural resources and the environment, highlighting the urgent need for sustainable construction practices. Traditional methods of construction, particularly the widespread use of concrete, have significant environmental impacts, including resource depletion, high energy consumption, and extensive land degradation. Addressing these challenges is critical to ensuring that future construction activities meet the needs of society without compromising the availability of our planet. This section explores the escalating demand for construction materials and the environmental consequences of conventional concrete practices, emphasizing the necessity of sustainable solutions in the construction industry.

#### ESCALATING DEMAND FOR CONSTRUCTION MATERIALS

The global population is projected to reach nearly 10 billion by 2050, predominantly concentrated in urban areas (Lee, 2011). This surge necessitates substantial construction activity to accommodate growing urban populations, including housing, commercial buildings, transportation networks, and other critical infrastructure. This growth is not only concentrated in developed regions but is particularly intense in developing countries where urbanization is accelerating at a rapid pace (X. Q. Zhang, 2016). According to the United Nations Environment Programme (UNEP), the construction sector accounts for more than 30% of global resource consumption (UNEP, 2002). This intensive use of resources highlights the urgent need for sustainable materials and practices that reduce environmental impact without compromising the demand for infrastructure.

**Urbanization and Infrastructure Expansion**

The rapid pace of urbanization and infrastructure expansion has become a defining characteristic of the 21st century, significantly influencing the demand for construction materials globally (Wei and Ewing, 2018). As more people migrate to urban areas in search of better economic opportunities and improved living standards, cities have experienced unprecedented growth. This urban expansion necessitates the development of a wide array of infrastructure, including residential buildings, commercial complexes, transportation networks, and public utilities.

The United Nations estimates that by 2050, nearly 70% of the global population will reside in urban areas, an increase from the current 56% (Hawksworth and Cookson, 2006). This shift not only drives the need for new construction but also the expansion and upgrading of existing infrastructure. Consequently, there is a substantial surge in the demand for essential construction materials, particularly concrete, which is the most widely used construction material globally. Concrete's primary component, coarse aggregates, is central to meeting the structural demands of this urban growth. However, the scale of current urbanization trends places immense pressure on the natural resources used to produce these materials, prompting a critical evaluation of their sustainability.

**Material Consumption Patterns**

The consumption patterns of construction materials have evolved in tandem with the growth in urbanization and infrastructure projects. Over the past few decades, the construction industry has witnessed a substantial increase in the extraction and use of natural resources, particularly in the production of cement, sand, and aggregates (Kisku et al., 2017). These materials form the backbone of modern construction, especially in developing nations where the need for new infrastructure is most acute.

In many regions, the demand for construction materials far outstrips the local supply, leading to increased importation and, consequently, higher costs and environmental impact (Bridge, 2009). The traditional linear consumption model—where resources are extracted, used, and disposed of—has led to inefficiencies and a significant waste problem, further exacerbating the sustainability challenges faced by the construction sector. As material consumption continues to rise, there is an urgent need to move towards more sustainable practices, such as the use of recycled materials, to mitigate the environmental footprint of construction activities.

**Resource Depletion and Sustainability Challenges**

The escalating demand for construction materials has brought to light the critical issue of resource depletion. Natural aggregates, a key component in concrete, are derived from finite geological resources, primarily consisting of crushed stone, sand, and gravel. The continuous extraction of these materials has led to the depletion of high-quality sources, pushing the industry to source aggregates from increasingly distant and environmentally sensitive areas.

This depletion poses significant sustainability challenges. The environmental impact of aggregate extraction includes habitat destruction, increased greenhouse gas emissions from transportation, and the loss of biodiversity (Bendixen et al., 2021). Furthermore, the reduced availability of quality aggregates has resulted in higher costs and the need for alternative materials.

## ENVIRONMENTAL IMPACT OF TRADITIONAL CONCRETE CONSTRUCTION PRACTICES

Traditional concrete construction practices, while foundational to modern infrastructure development, have significant environmental repercussions. The production and use of concrete involve processes that heavily deplete natural resources, consume vast amounts of energy, and contribute to extensive land degradation. These environmental impacts are increasingly becoming unsustainable, raising concerns about the long-term viability of conventional construction methods. This section examines the specific environmental challenges associated with traditional concrete practices, focusing on water resource depletion, energy consumption and emissions, and the degradation of land, thereby highlighting the urgent need for more sustainable alternatives in the construction industry.

### Water Resource Depletion

Traditional concrete construction practices are highly water-intensive, contributing significantly to global water resource depletion (Hong et al., 2019). Water is essential in concrete production for the hydration of cement, which is the binding agent in concrete. The process demands vast amounts of freshwater, not only for mixing but also for curing and cleaning purposes on construction sites. This excessive water usage has serious environmental implications, especially in regions where water scarcity is already a critical issue.

Globally, the construction industry is one of the largest consumers of freshwater, with concrete production alone accounting for approximately 9% of total industrial water usage in 2012 (Miller et al., 2018). In water-stressed regions, this demand exacerbates the competition for limited water resources, affecting both ecosystems and communities. Over-extraction of water for concrete production can lead to the depletion of local aquifers, reduced water quality, and disruption of natural water cycles. It is important to note that the high water demand for cement hydration persists regardless of whether natural aggregates or recycled aggregates are used. The unsustainable use of water in concrete production highlights the need for more efficient practices and alternative materials that reduce water dependency in construction.

### Energy Consumption and Emissions

The production of traditional concrete is an energy-intensive process with significant environmental consequences. The primary energy consumption stems from the production of cement, the most crucial component of concrete. Cement production involves the calcination of limestone at high temperatures in kilns, which requires substantial amounts of energy, predominantly from fossil fuels. This process not only consumes a large amount of energy but also results in the emission of carbon dioxide ($CO_2$) and other greenhouse gases.

Cement production is responsible for approximately 8% of global $CO_2$ emissions, making it one of the largest single industrial contributors to climate change (Shen et al., 2015). Additionally, the overall lifecycle of concrete—from raw material extraction to transportation and construction—further adds to the carbon footprint of the construction industry. The energy consumed in the production and transportation of aggregates, as well as the operation of construction machinery, all contribute to the industry's high

energy demands and associated emissions.

These emissions have far-reaching impacts on global warming, air quality, and public health (Shah et al., 2022). The urgent need to mitigate the environmental impact of energy consumption in concrete production has spurred research into low-carbon alternatives and more sustainable construction practices, including the adoption of recycled materials and innovative technologies.

**Land Degradation**

Land degradation is another significant environmental impact associated with traditional concrete construction practices (Habert et al., 2010). The extraction of raw materials for concrete, such as sand, gravel, and limestone, requires large-scale mining operations that often lead to severe ecological disruption. These activities cause the destruction of natural landscapes, loss of biodiversity, and alteration of ecosystems.

Quarrying and mining for aggregates result in the removal of topsoil and vegetation, leading to soil erosion, loss of fertile land, and increased vulnerability to flooding. In many cases, abandoned quarries and mines are left as scarred landscapes, contributing to long-term environmental degradation. The expansion of mining activities to meet the growing demand for construction materials also encroaches on agricultural land and protected areas, further exacerbating land use conflicts.

Moreover, the disposal of construction and demolition waste, which often includes concrete debris, contributes to land degradation (Rao et al., 2007). Inadequate waste management practices lead to the accumulation of waste in landfills, occupying vast areas of land and potentially contaminating soil and groundwater.

These traditional practices underscore an unsustainable trajectory that, if continued, could lead to irreversible environmental damage, including exacerbating climate change, depleting natural resources, and reducing biodiversity. This in turn would hinder future construction capabilities and jeopardize sustainability goals. To address these significant impacts, several mitigation strategies have been developed and are being increasingly implemented:

**(1) Use of supplementary cementitious materials (SCMs)** Materials such as fly ash, slag, and silica fume can be used to replace a portion of cement in concrete mixtures (Samad and Shah, 2017). These materials can improve the mechanical properties of concrete while significantly reducing the carbon footprint associated with cement production.

**(2) Enhanced recycling of concrete** Developing more efficient methods for recycling concrete can reduce the need for virgin aggregate extraction and can decrease the overall energy consumption and emissions associated with new concrete production.

**(3) Innovations in concrete composition** Recent advancements include the development of low-carbon cements and carbon capture, utilization, and storage (CCUS) technologies (McLaughlin et al., 2023). These innovations aim to reduce the carbon emissions from cement manufacturing and enhance the sustainability of concrete structures.

1

### THE DRIVE FOR SUSTAINABLE CONSTRUCTION

With the increasing recognition of the unsustainable nature of traditional concrete construction, there has been a global push towards sustainable construction practices. The impetus for embracing sustainable construction practices stems from a confluence of ecological, economic, and social drivers that collectively address the pressing challenges posed by conventional construction methods. This shift is essential to achieving environmental sustainability while meeting the increasing demands of urban development. This shift is motivated by the need for:

**Reduction of Greenhouse Gas Emissions**

A fundamental aspect of sustainable construction is its potential to significantly curtail emissions associated with global warming (Chen et al., 2024). Innovative construction methodologies, such as the use of carbon-capturing technologies during the concrete curing process, actively convert $CO_2$ into minerals within the building materials themselves. This not only helps reduce the overall carbon footprint but also transforms buildings into carbon sinks rather than emitters.

**Enhancing Resource Efficiency**

Sustainable construction promotes the efficient use of materials throughout the lifecycle of a building, from construction to demolition (Kabirifar et al., 2020). Techniques such as prefabrication and modular construction reduce onsite waste and increase the precision in material usage. These methods not only streamline the construction process but also allow for the dismantling and reuse of components, thereby extending the material lifecycle and reducing the demand for new raw materials.

**Adoption of Circular Economy Principles**

Moving beyond the traditional linear economic model (make, use, dispose), sustainable construction embraces a circular economy where materials are continually repurposed (Ghisellini et al., 2018). This approach encourages the use of recycled aggregates and reclaimed building materials, which conserves resources and decreases dependence on virgin materials. For example, the use of demolished concrete as recycled aggregate in new construction projects not only alleviates the pressure on natural resources but also tackles the problem of construction and demolition waste.

**Integration of Smart Technologies**

The incorporation of smart technologies in construction processes and building management systems plays a crucial role in enhancing efficiency and sustainability (Nižetić et al., 2019). Technologies such as intelligent HVAC systems and automated lighting, driven by IoT (Internet of Things), optimize energy use and reduce operational costs. Moreover, the use of Building Information Modeling (BIM) allows for better planning and management of resources throughout a building's lifecycle, minimizing waste and maximizing efficiency.

**Policy and Regulatory Frameworks**

Strong governmental support is crucial for fostering sustainable construction (Darko et

al., 2018). This can be seen in the implementation of stricter building codes that mandate energy efficiency and resource conservation. Incentive programs, such as tax rebates for green building projects, further encourage developers and builders to adopt sustainable practices. Additionally, international collaborations and frameworks, like the United Nations' Sustainable Development Goals (SDGs), provide a global blueprint for reducing environmental impact through sustainable construction. Many countries have adopted national policies to promote green building standards (Y. Zhang et al., 2017), such as LEED (Leadership in Energy and Environmental Design) in the United States and BREEAM (Building Research Establishment Environmental Assessment Method) in the UK, which encourage the adoption of sustainable practices in the construction sector.

These expanded elements illustrate a comprehensive approach to sustainable construction that aligns with global sustainability objectives. By integrating innovative technologies, adopting efficient practices, and supporting these through robust policy frameworks, the construction industry can significantly mitigate its environmental impact while continuing to thrive economically and socially. As the world continues to urbanize, the construction industry must embrace sustainable practices to ensure that it can meet future infrastructure needs while preserving the planet for future generations. This holistic approach not only mitigates the adverse impacts associated with construction but also aligns with broader sustainability goals, fostering a resilient, inclusive, and sustainable urban future.

### 1.1.2. RECYCLED COARSE AGGREGATES

RCA are derived from the processed rubble of demolished concrete structures. As the construction industry seeks sustainable practices due to environmental concerns and resource depletion, RCA has emerged as a viable alternative to natural aggregates. Concrete is the most widely used construction material globally, and its production consumes considerable natural resources, particularly aggregates. The demolition of old concrete yields significant amounts of waste, which, if recycled properly, can provide a sustainable source of aggregates for new construction projects.

#### SOURCES AND PRODUCTION OF RCA

RCA is typically produced through the demolition of concrete buildings, roads, bridges, and other structures. Once a concrete structure is earmarked for demolition, it undergoes a series of processes to become usable aggregate. The primary steps include demolition, debris collection, and crushing. The demolition is carried out using mechanical breakers, wrecking balls, or controlled explosions. The resulting debris is then collected and often sorted to separate it into different materials. The concrete chunks are transported to recycling plants where they are crushed, screened, classified, and washed to produce aggregates of desired sizes. Advanced technologies such as hydraulic crushers and mechanical screens help in achieving precise sizes and removing contaminants such as rebar, metal, and glass.

#### QUALITY OF RCA

The quality of RCA can vary significantly depending on the source of the original concrete and the processing method used. Factors such as the age of the concrete, the presence of reinforcements, and the type of additives used in the original mix can affect the properties of RCA. Commonly, RCA is found to be more porous and has a higher absorption rate than natural aggregates due to the presence of old cement paste attached to the aggregate particles. This residual cement paste also gives RCA weaker mechanical properties compared to new aggregates. However, with proper processing and quality control, RCA can meet the specifications required for many construction applications, including road base, landscaping, and even new concrete production.

#### ENVIRONMENTAL AND ECONOMIC IMPLICATIONS OF RCA

The use of RCA is aligned with the principles of sustainable development and circular economy. By recycling concrete waste, the construction industry can significantly reduce its environmental footprint. The production of RCA reduces the need for quarrying natural aggregates, which can lead to habitat destruction and biodiversity loss. Moreover, it helps in reducing the amount of construction waste sent to landfills, thereby mitigating landfill usage and associated environmental issues. In addition to RCA, the recycling process also produces by-products rich in sand and cement, which opens up new opportunities for reusing these components of concrete in an economically efficient way. This further enhances the sustainability of the recycling process by maximizing the value extracted from concrete waste and reducing the demand for new raw materials.

Economically, the use of RCA can lead to cost savings in materials for construction projects. Although the initial investment in recycling equipment and technology may be high, the long-term savings in materials and landfill fees can offset these costs. Furthermore, as regulations on waste disposal tighten and natural aggregates become scarcer, the economic benefits of RCA are likely to increase.

RCA represent a key element in the pursuit of sustainable construction. Through technological advancements and improved regulatory frameworks, the potential of RCA to replace natural aggregates can be fully realized, leading to more sustainable construction practices worldwide. As such, RCA not only offers a pathway to reduce the construction industry's environmental impact but also presents a viable economic opportunity in the face of decreasing natural resources.

### 1.1.3. CHALLENGES IN RECYCLED COARSE AGGREGATES UTILIZATION

RCA present a promising avenue for sustainable construction, offering a way to repurpose waste from demolished structures and reduce the environmental impact associated with new construction. However, despite these benefits, the utilization of RCA faces several significant challenges that hinder its broader acceptance and application in the construction industry. These challenges can be broadly categorized into quality concerns, regulatory and standardization issues, economic considerations, and technical hurdles.

#### QUALITY CONCERNS

**Variability in Material Properties**

One of the primary concerns with RCA is the variability in its physical and chemical

properties. Unlike natural aggregates, whose properties are relatively consistent and predictable, RCA can vary widely depending on the source of the original concrete, the strategy of dismantling and demolition, and the methods used for its processing. This variability can affect the strength, durability, and performance of the concrete made with RCA.

**Presence of Contaminants**
RCA is often contaminated with other materials, such as bricks, glass, wood, gypsum, and plastics, which can significantly affect the quality and safety of the aggregate. These contaminants can interfere with the cement's hydration process, leading to weaker concrete. Moreover, harmful substances like lead or asbestos, if present in the demolished concrete, can pose serious health risks during handling and use.

**Residual Mortar Content**
RCA contains residual mortar from the original concrete, which can increase the water absorption and porosity of the aggregates. This residual mortar also contributes to a higher surface area compared to natural aggregates, requiring more cement paste to achieve adequate workability in concrete, thus increasing material costs and potentially affecting the final strength and durability.

### REGULATORY AND STANDARDIZATION ISSUES

**Lack of Consistent Standards**
The standards for RCA vary significantly across different regions and countries. Without consistent, universally accepted standards, it's challenging for the construction industry to adopt RCA broadly. This lack of standardization also complicates the quality assurance process, making it difficult for engineers and architects to confidently specify RCA for high-stakes projects.

**Certification and Compliance Difficulties**
Gaining certification for RCA-based products can be challenging due to the stringent requirements set by many building codes, which are often designed with natural aggregates in mind. These regulatory barriers can discourage the use of RCA in public and high-profile projects where compliance with building codes is strictly enforced.

### ECONOMIC CONSIDERATIONS

**Cost of Processing**
Although using RCA reduces waste and can potentially lower material costs, the initial costs for processing RCA (including sorting, crushing, and treating) can be higher than those for natural aggregates. These higher upfront costs can deter businesses from investing in RCA production, particularly when the price of dumping waste is low.

**Market Perception and Acceptance**
RCA often suffers from a market perception issue, where it is seen as a lower-quality alternative to natural aggregates. This perception can reduce market demand and limit its use to non-structural applications. Overcoming this perception requires education and

demonstrated success stories in RCA's effective implementation. Educating the market on the environmental and technical benefits of recycled aggregates is essential for its broader acceptance (de Larrard and Colina, 2019). Providing insights into best practices for the production and application of recycled concrete can help address common misconceptions and drive wider industry adoption.

#### TECHNICAL HURDLES

**Inferior Mechanical Properties**

Studies have shown that concrete made with RCA can exhibit reduced compressive strength and slower strength development compared to those made with natural aggregates. This is partly due to the weaker bond that forms between the old cement mortar and the new cement paste in RCA concrete.

**Durability Issues**

The higher porosity and water absorption of RCA can lead to durability issues in concrete, especially in environments exposed to freeze-thaw cycles and chemical attacks. These durability concerns are critical for infrastructures such as bridges and roads, where long-term performance is paramount.

**Predictability and Modelling Difficulties**

The variability in RCA makes it difficult to predict the exact performance of RCA-based concrete, complicating the engineering and design processes. Advanced models and simulations are required to accurately predict how RCA will behave in different conditions, which can be a barrier for smaller firms or projects with limited technical resources.

To mitigate these challenges and enhance the utilization of RCA, several strategies can be employed. These include developing advanced technologies for better sorting and treatment of RCA, establishing clearer regulatory standards, and conducting extensive research to better understand the material properties and behavior of RCA in concrete. Additionally, educational initiatives to improve the perception of RCA and demonstrate its viability and benefits in real-world applications are crucial. For all of these strategies, the availability of data on the quality of RCA is an essential prerequisite for success. By addressing these challenges head-on, the potential of RCA as a sustainable construction material can be fully realized, contributing to more environmentally friendly and cost-effective building practices worldwide.

## 1.2. RESEARCH OBJECTIVES

### 1.2.1. PRIMARY OBJECTIVE

The primary objective of this doctoral research is to enhance the efficiency and reliability of RCA for sustainable construction by addressing critical challenges in their quality assessment and grading. This study is dedicated to developing and implementing cutting-edge technologies to improve the quality inspection process of RCA. Specifically, the research aims to integrate advanced sensor technologies and data analytics into a

streamlined, real-time quality inspection system, thereby promoting sustainability and reducing the environmental impact of construction practices.

To achieve this, the research focuses on the development and validation of a novel mobile sensor-based quality inspection system for RCA. This system leverages advanced sensor technology to provide real-time, accurate data on RCA quality, enhancing their usability in sustainable construction practices. This overarching goal guides the entire research effort, aiming to establish a reliable, efficient, and scalable method for assessing the quality of RCA, thus offering scalable and innovative solutions for the construction industry.

### 1.2.2. SPECIFIC GOALS

#### ENHANCE REAL-TIME PARTICLE SIZE DISTRIBUTION (PSD) ANALYSIS

**To achieve accurate, real-time PSD analysis of RCA using a novel sensor-based system that integrates 3D scanning technology**

This technology enables the dynamic assessment of particle size and distribution on a conveyor belt system, processing over 100 tons of RCA per hour, thus ensuring high throughput with minimal human intervention.

#### IMPROVE CONTAMINANT DETECTION

**To enhance the detection and identification of contaminants in RCA by incorporating advanced spectral analysis using Laser-Induced Breakdown Spectroscopy (LIBS)**

This method allows for the immediate identification of various material compositions, including hazardous substances, directly influencing the purity and safety of RCA used in construction.

#### INCREASE PROCESSING EFFICIENCY

**To develop a system capable of monitoring large quantities of RCA efficiently through the integration of automated feeding and real-time data feedback**

This system includes a high-capacity conveyor setup and advanced rating algorithms designed to optimize the monitoring and processing of RCA at significantly higher speeds than traditional methods.

#### ENSURE SYSTEM MOBILITY AND ADAPTABILITY

**To create a mobile, containerized system that can be easily transported and deployed at various demolition sites**

This system is designed to withstand different environmental conditions and setup scenarios, offering flexibility in on-site recycling operations and enabling efficient RCA processing directly at demolition sites to reduce transportation costs and environmental impact.

#### VALIDATE SYSTEM ACCURACY AND RELIABILITY

**To rigorously test and validate the accuracy and reliability of the sensor-based inspection system through extensive field trials and comparative analysis with traditional methods**

This includes validating the system's performance across various operational conditions and RCA quality levels to ensure consistent and dependable results.

#### PROMOTE SCALABLE AND SUSTAINABLE CONSTRUCTION PRACTICES

**To promote scalable and sustainable construction practices by integrating advanced sensor technologies into the recycling and concrete production workflows**
This approach is aimed at improving the quality assurance of RCA and fostering a circular economy within the construction industry. The system's design facilitates scalability, allowing it to be adapted for larger or smaller operations without loss of effectiveness.

By addressing these specific goals, this research contributes significantly to advancing sustainable construction practices, improving the quality and usability of RCA, and providing a scalable solution for the construction industry.

## 1.3. OUTLINE

This outline provides a structured preview, organizing the dissertation into six cohesive chapters. Each chapter focuses on essential aspects of monitoring the quality of RCA, which are pivotal for advancing sustainable infrastructure. The framework of this dissertation is depicted in Figure 1.1.

**Chapter 1: Introduction**

This introductory chapter sets the stage for the dissertation by underscoring the urgent global need for sustainable construction practices, with a special focus on the use of RCA. It delves into the pressing environmental challenges posed by construction waste and articulates the substantial potential of RCA to alleviate these concerns. This chapter critically examines the primary barriers to RCA adoption, particularly the variability in quality that contributes to industry reluctance to embrace these materials more widely. By defining the research context and outlining the objectives, this section highlights the novel contributions of this study and its significance in propelling forward the practices of sustainable construction.

**Chapter 2: A Mobile System for Quality Control and Monitoring: Design and Implementation**

This chapter introduces a novel mobile system specifically designed for the in-situ quality inspection of unscreened RCA streams providing a comprehensive look at its design, setup, and technical specifications. The system is specifically engineered to meet the rigorous demands of modern sustainable construction, with a detailed rationale behind each component enhancing its efficiency and effectiveness. Through an in-depth examination, this chapter highlights how the system functions within real-world scenarios, playing a pivotal role in advancing quality assurance processes. By detailing the system's operational capabilities, it underscores its potential to significantly improve the handling and usability of RCA, thus driving efficiency in sustainable construction practices.

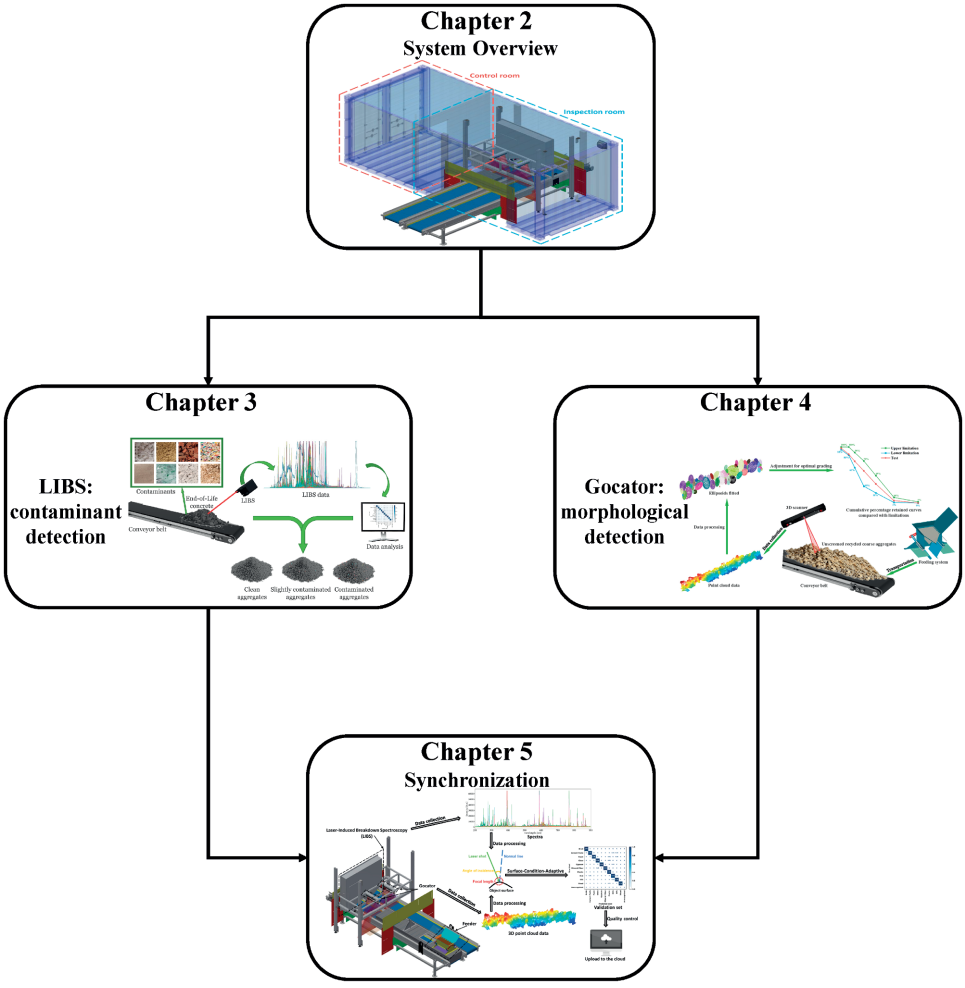


Figure 1.1: Structure of this dissertation

**Chapter 3: In-line Recycled Coarse Aggregates Characterization Using Laser-Induced Breakdown Spectroscopy**

This chapter explores the use of LIBS for the detailed characterization of RCA. The focus is on efficiently identifying and classifying materials within end-of-life (EoL) concrete, often contaminated by different waste components which degrade the quality of RCA. A cluster-based identification algorithm is developed to enhance the precision of in-line quality inspection of these aggregates as they are processed on a conveyor belt. This methodology not only supports the high-grade recycling of EoL concrete but also contributes to closing the material loop in a sustainable manner. The effectiveness of this approach is demonstrated through rigorous validation, showing high accuracy and

reliability in identifying contaminants and ensuring the production of clean RCA.

**Chapter 4: 3D Surface Analysis to Assess Particle Size Distribution in Unscreened Recycled Coarse Aggregates for Quality Assurance**

This chapter discusses the integration of unscreened RCA in high-performance concrete production through an advanced, intelligent grading system. The system employs automated, non-destructive technology for PSD analysis, markedly enhancing the efficiency of RCA grading. Utilizing sophisticated 3D scanning technology that processes RCA on a conveyor belt, it analyzes high-resolution point clouds in real time to achieve optimal aggregate grading. Capable of processing at least 50 tons per hour per conveyor belt, this innovative technology offers rapid, precise feedback that drives operational decisions and optimizes the recycling process. This approach not only reduces waste but also promotes the reuse of materials, advancing the quality of concrete production and reinforcing the sustainability of construction practices.

**Chapter 5: Optimizing Contaminant Detection Precision in Recycled Coarse Aggregates via Surface-Condition-Adaptive Method**

This chapter presents a quality control system that capitalizes on the integrated technologies of LIBS and 3D scanning, building upon the foundational insights discussed in previous chapters. This advanced system is designed to facilitate rapid and precise detection of contaminants in RCA, significantly enhancing the identification and classification processes crucial for maintaining RCA quality in construction applications. The system's capability to perform real-time, non-destructive analysis allows for the immediate assessment of large volumes of RCA, significantly enhancing the efficiency of recycling processes. This method not only boosts the reliability of RCA but also sets the groundwork for automated, high-throughput quality control systems in the recycling industry.

**Chapter 6: Conclusion**

The final chapter synthesizes the core findings of this dissertation, highlighting their implications for the recycling industry and sustainable construction. This research significantly advances RCA quality inspection through the development of a novel mobile sensor-based system, integrating 3D scanning and LIBS for real-time, on-site assessments. These innovations enhance the efficiency, accuracy, and scalability of RCA processing, supporting the industry's shift towards sustainability and circular economy principles. While the research presents significant advancements, challenges such as scalability, cost, and integration into existing processes remain. Future research should focus on refining sensor technologies, exploring economic feasibility, and ensuring long-term performance and regulatory compliance. These efforts will further enhance the adoption of RCA in construction, contributing to a more sustainable and resilient built environment.

# BIBLIOGRAPHY


Bendixen, M., Iversen, L. L., Best, J., Franks, D. M., Hackney, C. R., Latrubesse, E. M., & Tusting, L. S. (2021). Sand, gravel, and un sustainable development goals: Conflicts, synergies, and pathways forward. *One Earth*, *4*(8), 1095–1111.

Bridge, G. (2009). Material worlds: Natural resources, resource geography and the material economy. *Geography compass*, *3*(3), 1217–1244.

Chen, L., Hu, Y., Wang, R., Li, X., Chen, Z., Hua, J., Osman, A. I., Farghali, M., Huang, L., Li, J., et al. (2024). Green building practices to integrate renewable energy in the construction sector: A review. *Environmental Chemistry Letters*, *22*(2), 751–784.

Darko, A., Chan, A. P. C., Yang, Y., Shan, M., He, B.-J., & Gou, Z. (2018). Influences of barriers, drivers, and promotion strategies on green building technologies adoption in developing countries: The ghanaian case. *Journal of Cleaner Production*, *200*, 687–703.

de Larrard, F., & Colina, H. (2019). *Concrete recycling: Research and practice*. CRC Press.

Ghisellini, P., Ripa, M., & Ulgiati, S. (2018). Exploring environmental and economic costs and benefits of a circular economy approach to the construction and demolition sector. a literature review. *Journal of Cleaner Production*, *178*, 618–643.

Habert, G., Bouzidi, Y., Chen, C., & Jullien, A. (2010). Development of a depletion indicator for natural resources used in concrete. *Resources, conservation and recycling*, *54*(6), 364–376.

Hawksworth, J., & Cookson, G. (2006). The world in 2050. *How big will the major emerging market economies get and how can the OECD compete*.

Hong, J., Zhong, X., Guo, S., Liu, G., Shen, G. Q., & Yu, T. (2019). Water-energy nexus and its efficiency in china's construction industry: Evidence from province-level data. *Sustainable Cities and Society*, *48*, 101557.

Kabirifar, K., Mojtahedi, M., Wang, C., & Tam, V. W. (2020). Construction and demolition waste management contributing factors coupled with reduce, reuse, and recycle strategies for effective waste management: A review. *Journal of cleaner production*, *263*, 121265.

Kisku, N., Joshi, H., Ansari, M., Panda, S., Nayak, S., & Dutta, S. C. (2017). A critical review and assessment for usage of recycled aggregate as sustainable construction material. *Construction and building materials*, *131*, 721–740.

Lee, R. (2011). The outlook for population growth. *Science*, *333*(6042), 569–573.

McLaughlin, H., Littlefield, A. A., Menefee, M., Kinzer, A., Hull, T., Sovacool, B. K., Bazilian, M. D., Kim, J., & Griffiths, S. (2023). Carbon capture utilization and storage in review: Sociotechnical implications for a carbon reliant world. *Renewable and Sustainable Energy Reviews*, *177*, 113215.

Miller, S. A., Horvath, A., & Monteiro, P. J. (2018). Impacts of booming concrete production on water resources worldwide. *Nature Sustainability*, *1*(1), 69–76.

Nižetić, S., Djilali, N., Papadopoulos, A., & Rodrigues, J. J. (2019). Smart technologies for promotion of energy efficiency, utilization of sustainable resources and waste management. *Journal of cleaner production*, *231*, 565–591.

Rao, A., Jha, K. N., & Misra, S. (2007). Use of aggregates from recycled construction and demolition waste in concrete. *Resources, conservation and Recycling*, *50*(1), 71–81.

Samad, S., & Shah, A. (2017). Role of binary cement including supplementary cementitious material (scm), in production of environmentally sustainable concrete: A critical review. *International journal of Sustainable built environment*, *6*(2), 663–674.

Shah, I. H., Miller, S. A., Jiang, D., & Myers, R. J. (2022). Cement substitution with secondary materials can reduce annual global co2 emissions by up to 1.3 gigatons. *Nature communications*, *13*(1), 5758.

Shen, W., Cao, L., Li, Q., Zhang, W., Wang, G., & Li, C. (2015). Quantifying co2 emissions from china's cement industry. *Renewable and Sustainable Energy Reviews*, *50*, 1004–1012.

UNEP, G. M. A. (2002). United nations environment programme. *Chemicals, Geneva, Switzerland*.

Wei, Y. D., & Ewing, R. (2018). Urban expansion, sprawl and inequality.

Zhang, X. Q. (2016). The trends, promises and challenges of urbanisation in the world. *Habitat international*, *54*, 241–252.

Zhang, Y., Wang, J., Hu, F., & Wang, Y. (2017). Comparison of evaluation standards for green building in china, britain, united states. *Renewable and sustainable energy reviews*, *68*, 262–271.

# 2

# A Mobile System for Quality Control and Monitoring: Design and Implementation

*Incorporating recycled coarse aggregates (RCA) from End-of-Life (EoL) concrete into construction encounters industry resistance due to concerns over inconsistent quality. The quality of RCA varies from one batch to another, unlike the more consistent quality of natural aggregates. Thus, it is essential to automate RCA quality control for the recycling industry. Traditional methods often fall short of providing the detailed analysis necessary for quality assurance. This study emphasizes the critical need for reliable evaluations of RCA to align with industry standards. To address this issue, a new mobile, containerized sensor-based quality inspection system is proposed. This system features conveyor belts capable of processing over 100 tons of RCA per hour, substantially increasing efficiency over lab-based methods. It includes a 3D scanner, the Gocator, which can accurately measure the particle size distribution (PSD) of large quantities of RCA by rapidly approximating the shape of particles from just one side of the pile. The accuracy and validity of this approach are verified using X-ray tomography 3D modeling, comparable to traditional manual sieving. Additionally, the system uses a laser-induced breakdown spectroscopy (LIBS) sensor to monitor two conveyor belts simultaneously during high-speed operations. This enables the continuous production of stable spectral data that accurately reflects the material's composition. A modified cluster-based identification algorithm swiftly detects contaminants in RCA, thereby improving material purity assessments. Incremental learning techniques are implemented to update existing models as new spectral data becomes available, dynamically updating chi-square distribution parameters. This ensures continuous model refinement without the need for complete retraining, enhancing computational efficiency and sustaining high classification performance. Monitoring data are recorded on accompanying radio frequency identification (RFID) tags to enhance trace-*

Apart from minor updates, this chapter has been submitted for publication.

*ability. This integrated system provides a scalable and flexible solution that enhances the efficiency and reliability of EoL material management, supporting global sustainable infrastructure initiatives.*

## 2.1. INTRODUCTION

THE increasing demand for construction materials, alongside the urgency for sustainable waste management, has propelled the recycling of concrete from End-of-Life (EoL) infrastructures as a progressively feasible solution. This approach has garnered significant attention within the construction industry, aligning with its pivot towards sustainable practices. A key aspect of this shift is the increased use of recycled coarse aggregates (RCA), which are obtained from construction and demolition waste.



Recognizing the potential environmental detriments and the associated carbon footprint of unfettered natural aggregate extraction, many countries are promoting sustainable practices in the construction domain (Al Martini et al., 2023; Aslam et al., 2020; Kabirifar et al., 2020; Soto-Paz et al., 2023; Trivedi et al., 2023). The European Union (EU) has distinctly emerged as a frontrunner, adeptly incorporating sustainable recycling methodologies into mainstream construction practices (Akhtar and Sarmah, 2018; Gálvez-Martos et al., 2018; Lederer et al., 2020; Marique and Rossi, 2018; Zhang et al., 2022). This shift is not merely a reaction to environmental urgency, it marks a strategic transition towards resource conservation and a reduced carbon footprint for the entire construction sector.

However, the transition to RCA is fraught with challenges, chiefly concerning the assurance of the recycled aggregates' quality and purity (J. Kim, 2022; H. Wu et al., 2023). These challenges are accentuated when the RCA is sourced from a diverse range of dismantled infrastructures, bringing to the fore issues related to the presence and detection of contaminants (Alaejos et al., 2013). These contaminants, if not properly identified and managed, can significantly compromise the integrity and applicability of RCA in new construction projects (Poon and Chan, 2007; L. Wu et al., 2024). Consequently, addressing these quality-related concerns is critical to maintaining the performance, durability, and reliability of RCA-infused construction (Marín-Cortés et al., 2024; Vegas et al., 2015). It requires a focused approach towards standardizing the quality assessment methods and developing stringent guidelines to ensure that the recycled aggregates meet or surpass the performance metrics of their natural counterparts.

Historically, the assessment of RCA primarily relied on traditional methodologies, characterized by their labor-intensive nature, prolonged time frames, and manual procedures (Marie and Mujalli, 2019; Tuan et al., 2022). While these methods have served the industry for a significant period, their inherent limitations, such as potential imprecisions and inefficiencies, have become increasingly evident as the construction sector has progressed. As the industry's aspirations continue to shift towards achieving enhanced operational efficiencies without compromising quality, the imperative for a more innovative, efficient, and precise quality inspection mechanism has grown more pronounced.

Amidst the prevailing challenges, the emergence of sensor technology provides a promising solution (Barri et al., 2020; Cabral et al., 2023; Chang et al., 2022; Lotfi et al., 2015; Trotta et al., 2021; Xia and Bakker, 2014). The rising demand underscores the potential of recent advancements in sensor technology (Bonifazi et al., 2018; Nalon et al., 2022; Vegas et al., 2015), which offer real-time, on-site characterization of RCA. Such state-of-the-art methodologies not only enable prompt feedback, expediting the decision-making process and any necessary recalibrations in production but also aug-

ment the overall efficiency of the RCA production and usage cycle. Furthermore, the integration of real-time sensors into the RCA assessment process signifies more than just technological evolution, it represents a broader shift towards sustainable construction practices. By allowing for instant feedback and adjustments, these systems can reduce wastage, optimize resource use, and ensure that the resulting product meets the necessary quality benchmarks.

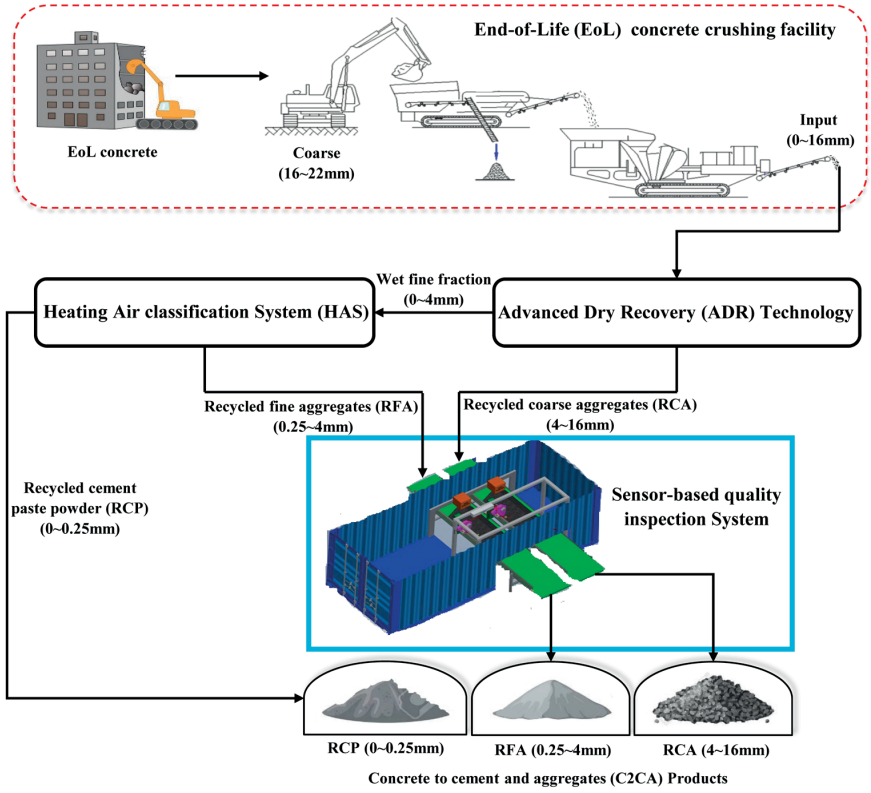


Figure 2.1: Concrete to Cement and Aggregate (C2CA) technology

This research delves into the sensor-based quality inspection system integrated into the Concrete to Cement and Aggregate (C2CA) technology (Figure 2.1). Figure 2.2 presents a flowchart summarizing the methodological steps of the quality inspection. This quality inspection system employs a 3D scanner Gocator and a laser-induced breakdown spectroscopy (LIBS) sensor to provide a comprehensive granulometric analysis of RCA and detect any contaminants. The accuracy and validity of the PSD measurement method are verified using 3D modeling with X-ray tomography, comparable to traditional manual sieving. Additionally, incremental learning techniques update existing models as new spectral data becomes available, dynamically adjusting chi-square distribution parameters. This approach ensures continuous model refinement without the need for complete retraining, enhancing computational efficiency and sustaining high

classification performance. The innovative use of advanced sensors enables real-time assessments on-site, which is particularly valuable in the dynamic context of demolition sites. By examining operational aspects and evaluating effectiveness in real-world scenarios, this research aims to highlight how this technology could improve the quality assessment of RCA. Through experimentation and analysis, the study emphasizes the advancements in RCA processing, presenting a pathway for industries to achieve sustainable growth while maintaining high-quality standards.

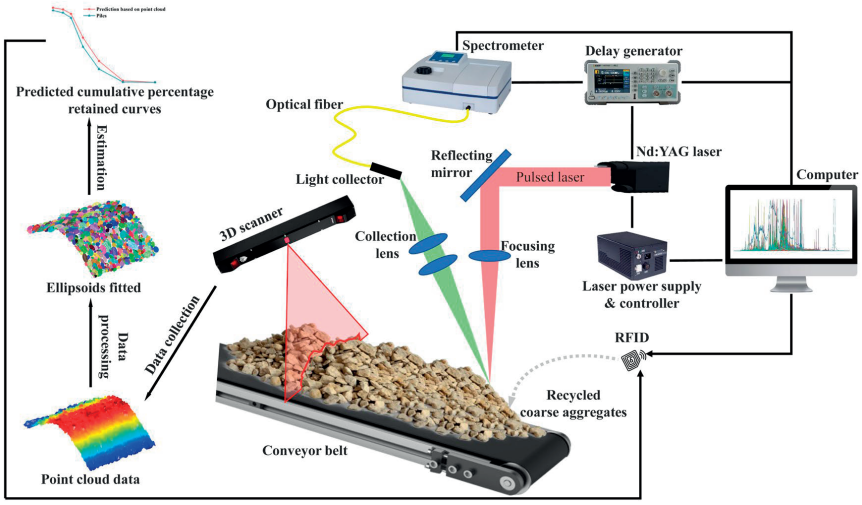


Figure 2.2: Schematic of quality inspection process

## 2.2. MATERIALS AND METHODS

### 2.2.1. MATERIAL SAMPLES

This study used recycled concrete aggregates obtained from discarded concrete, collected during the dismantling of various infrastructures throughout the Netherlands. To maintain the purity of the EoL concrete, selective demolition methodologies were employed. To avoid contamination of the samples, we manually separated other demolition residuals such as brick, foam, glass, gypsum, mineral fibers, plastics, and wood at the collection sites. This segregation process was part of the sample collection and preprocessing, aiming to preserve the integrity of the samples.

### 2.2.2. SENSOR-BASED QUALITY INSPECTION SYSTEM

#### CONTAINERIZATION

The sensor-based quality inspection system, depicted in Figure 2.3, plays a critical role in the C2CA technology framework. Housed within a specialized container, this system performs several vital functions.

The container is partitioned into two areas: an inspection room and a control room. These sections are separated to prevent any potential harm to operators from the lasers

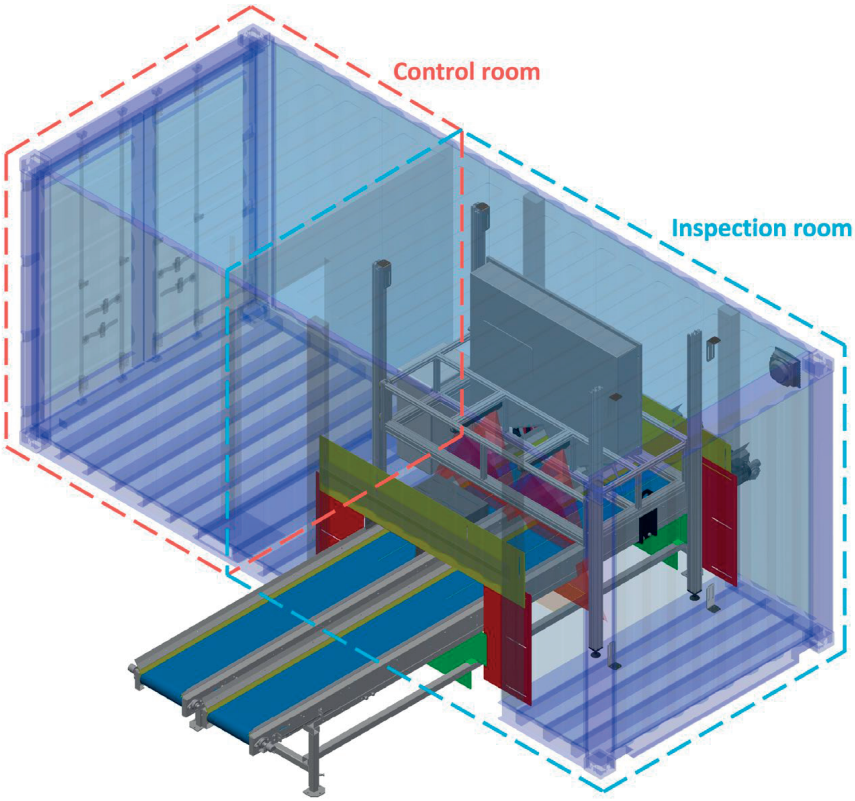


Figure 2.3: Sensor-based quality inspection system

used during the inspection process. The inspection room is equipped with sensors for material analysis, and it includes a vacuum system designed to reduce dust levels inside the inspection room. Reducing dust is essential, as it enhances the sensors' accuracy by lessening their interference with dust particles. The control room is set up to receive and process various data collected in real-time. It also uses a monitoring system to oversee activities within the inspection room to ensure operational safety and efficiency.

One of the primary advantages of the container is its mobility, which allows easy transport to various demolition sites. This mobility increases operational flexibility and optimizes resource allocation. The container is designed to facilitate the on-site recycling and testing of concrete directly at demolition sites. By processing the demolished concrete on-site, the need to transport it to a remote facility is eliminated. This not only reduces the costs associated with transportation but also minimizes the overall expenses related to the recycling process, as the material is reused or repurposed immediately without additional handling or processing steps.

Additionally, the container acts as a protective shield against adverse weather conditions, ensuring the system's functionality despite external environmental challenges. This safeguard is crucial for maintaining the accuracy of the sensors' measurements by

protecting the sensitive equipment from damage. Furthermore, beyond its role in adverse weather conditions, the container's presence demonstrates the system's adaptability in different field conditions. Such adaptability not only ensures the reliability of data but also strengthens the overall robustness, resilience, and effectiveness. Consequently, it expands the applicability of the system across various demolition and recycling contexts.

In summary, the containerized setup is fundamental in preserving data integrity, enhancing operational flexibility, and ensuring the system's adaptability. These attributes are key to the technology's effectiveness in a variety of demolition scenarios.

### COMPOSITION

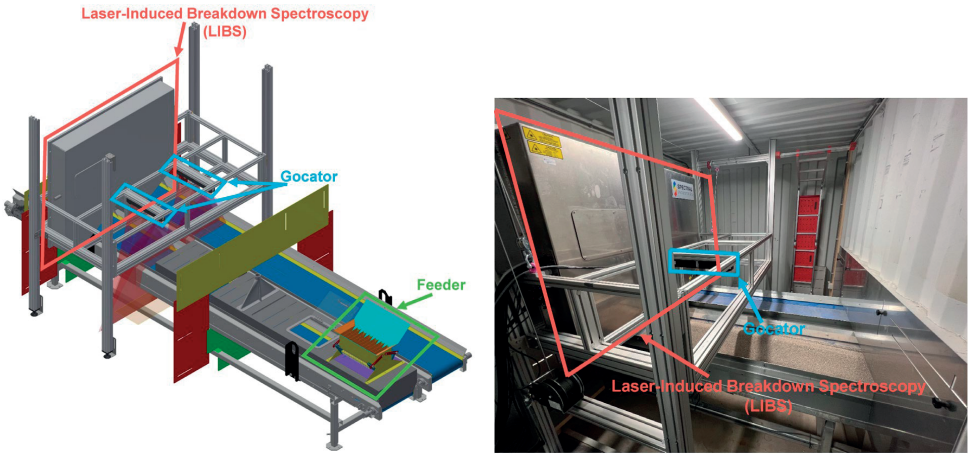


(a) 3D view (b) Close view

Figure 2.4: Sensor-based quality inspection system

The sensor-based quality inspection system (Figure 2.4) comprises two primary sensors: a 3D scanner Gocator and a LIBS sensor. Both sensors are positioned directly above the conveyor belt. The Gocator specializes in the granulometric analysis of RCA, pinpointing/measuring their PSD. This device is adept at generating high-resolution, three-dimensional point cloud data, capturing nuances in the surface topology and granular distribution. Meanwhile, the LIBS sensor (Figure 2.5) plays a crucial role in identifying contaminant compositions embedded within the RCA. It achieves this by focusing ultra-short pulse lasers on the sample's surface to create plasma, subsequently analyzing the emitted light spectrum from the plasma to determine the material composition and content of the sample.

A noteworthy aspect of the system's design is the ingenious incorporation of multiple reflective mirrors, which facilitates the simultaneous monitoring of RCA on two separate conveyor belts with the use of only one Nd:TAG laser. This innovative approach not only reduces the associated costs but also amplifies the system's overall operational efficacy.

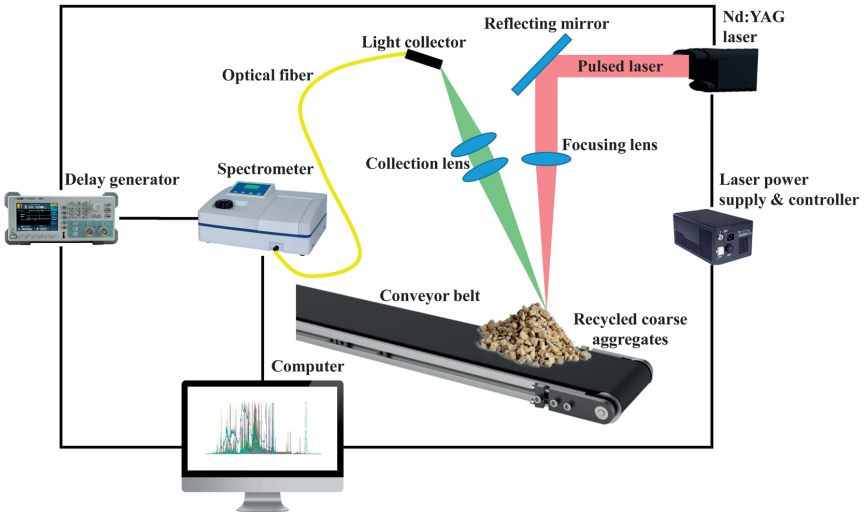


Figure 2.5: Schematic diagram of LIBS

#### Inspection

The inspection process begins with the introduction of RCA into the system via a feeder, followed by their deposition onto the conveyor belt, resulting in the formation of a triangular-shaped pile of RCA. This triangular configuration is designed to ensure a uniform distribution of the RCA, extending from the innermost region to the outer edges of the pile (Figure 2.6). This deliberate arrangement is particularly advantageous as it optimally facilitates the surface inspection conducted by the Gocator, allowing for precise assessment and estimation of RCA properties.

As RCA piles move along the conveyor belt, they are sequentially inspected by both the Gocator and LIBS sensors. The data generated during these inspections are instantaneously recorded in a computer system and subsequently uploaded to a secure cloud storage platform for long-term archiving and retrieval. Additionally, monitoring data are also linked to radio frequency identification (RFID) tags attached to the piles to enhance traceability. The conveyor belt operates at a constant velocity of 0.529 m/s, enabling a single conveyor belt to transport more than 50 tons of RCA per hour.

### 2.2.3. Analysis Methods

#### Particle Morphology

The primary objective of the particle morphology analysis is to achieve a statistical representativeness of RCA particles, ensuring that the morphological features such as size, shape, and orientation are comprehensively and reliably captured. This characterization is crucial for understanding the behavior and performance of RCA in various applications, particularly where particle size distribution significantly impacts material properties.

The feeding method for the RCA piles is meticulously designed to ensure symmetry,

Figure 2.6: Layered formation of RCA piles

which justifies focusing the analysis on only one side of the piles. This symmetric feeding method guarantees an even distribution of RCA particles across each layer, as well as each half-layer, within the piles formed on the conveyor belt (Figure 2.6). However, it should be noted that the actual PSD and composition throughout the pile are not perfectly uniform. Variations in PSD are commonly observed along the slope. For more detailed information on the equipment used and how uniformity is achieved, please refer to 4.2.2 Equipment. Despite these variations, this particle distribution allows the segmentation and analysis process to be both efficient and representative of the entire pile.

Employing the Fastscape algorithm (Braun and Willett, 2013), originally developed for terrain analytics, the system performs a watershed segmentation process (Steer et al., 2022) of 3D point clouds to accurately delineate RCA particles. The segmented regions are then encapsulated within ellipsoidal envelopes, enabling a quantifiable analysis of particle morphology, structure, and orientation. This method addresses challenges such as over-segmentation and ensures accurate geometrical representation through ellipsoidal fitting, providing a comprehensive statistical and geometrical description of RCA particles. The process involves several steps:

**Initial Segmentation**
The procedure begins by applying the watershed algorithm, traditionally used for 2D digital elevation models, to segment global 3D point cloud data. This adaptation allows the algorithm to effectively delineate individual particles by treating peaks in the data as watershed ridges, thereby dividing the data into distinct segments.

**Segmentation Correction**
Commonly, the initial segmentation results in over-segmentation, where particles are

divided into smaller, unnecessary parts. To correct this, the method merges particles that are closely located. This merging is based on two criteria: the proximity of the particles' summits and the alignment of their surface normals. Additionally, excessively flat or elongated particles are removed because they typically do not represent individual particles. Instead, they often correspond to clusters of fine particles with a size much smaller than the typical spacing between points in standard point clouds or are the result of improper particle segmentation. These steps refine the segmentation and enhance the overall quality.

**3D Ellipsoidal Fitting**
After the particles have been segmented and appropriately labeled, the next step is to characterize their geometrical properties. This is done by fitting 3D ellipsoids to each particle. Ellipsoidal fitting involves a complex optimization process where the best-fitting ellipsoid is calculated to approximate the shape and size of each particle. This step is crucial as it quantifies the particle structures, which can be vital for further analysis and applications.

**Morphological Analysis**
This method provides detailed geometrical information like the size, shape, and orientation of each particle. These properties are derived from the dimensions and orientation of the fitted ellipsoids. The key aspect of this ellipsoidal model is the choice of the second shortest axis as the main parameter for measuring graduation information. This particular axis is selected because it effectively represents the particle size, and consequently, helps in determining the PSD. The use of this axis is beneficial because it strikes a balance, being more informative than the shortest axis, which might be too small to provide useful data, and less variable than the longest axis, which could be too sensitive to minor changes in particle shape. This makes the second shortest axis a reliable and representative measure for assessing the characteristics of different particles in a sample.

A challenge in this process is the unequal probability of converting different particle sizes into ellipsoids when translating data obtained from scanning the top layer. This inequality arises due to several factors:

**Resolution Limitations** Smaller particles may not be captured with sufficient detail because of limitations in the resolution of the scanning equipment. This can result in a failure to properly detect and represent smaller particles in the ellipsoidal fitting process, leading to unequal representation across different particle sizes.

**Obscuration by Larger Particles** In a typical top-layer scanning process, smaller particles can be obscured or overshadowed by larger particles on the surface. Since scanning often captures the exposed or dominant features, smaller particles may be missed or inaccurately represented due to this overlap.

**Surface Visibility** Scanning data typically reflects the surface features of the particles. Particles that are partially embedded or not fully exposed may not be accurately captured, resulting in less reliable conversion into ellipsoids for PSD predictions.

**Particle Shape Sensitivity** The ellipsoidal fitting process tends to favor particles with regular, well-defined geometric features, which are easier to model. Particles with more irregular or subtle shapes may not be as easily translated into representative ellipsoids, leading to errors or oversimplifications in their representation.

These inconsistencies introduce potential errors in the morphological analysis. To mitigate this issue, it is essential to apply further calibration and adjust algorithms to ensure the ellipsoidal fitting process accurately represents particles of all sizes.

### 3D MODELING WITH X-RAY TOMOGRAPHY

To further verify the accuracy of algorithms simulating particle morphology, medical imaging techniques are employed to scan samples of RCA piles. It is important to note that this imaging process is not part of the container technology but is instead used for offline verification and calibration purposes. This enabled the creation of 3D models of their interior to capture the actual particle morphology for comparison. Computed Tomography (CT) imaging, a commonly used modality (Basu et al., 2011), employs X-rays to acquire multiple angular projections of an object, which are then used to reconstruct the object's linear attenuation coefficient distribution. The resulting images are typically assembled into a series of consecutive axial slices arranged in parallel (Pelc, 2014). CT scan information is digitally archived, frequently in a format referred to as Digital Imaging and Communications in Medicine (DICOM). This format arranges the information into an organized collection that includes both the imaging data and related metadata (Fajar et al., 2022). Metadata parameters like slice thickness, instance number, pixel spacing, rescale slope, and rescale intercept found in DICOM files are employed during the data preprocessing phase.

The Hounsfield unit (HU) scale, employed in CT imaging, quantifies the radiodensity of tissues and materials. It sets the baseline with water at 0 HU and air at roughly -1000 HU, where substances of greater density show higher HU values. The process of converting the linear attenuation coefficient of each material at a specified effective energy into HU uses the standard equation:

$$\mathrm{HU} = \left( \frac{\mu_{\mathrm{material}} - \mu_{\mathrm{water}}}{\mu_{\mathrm{water}}} \right) \times 1000 \tag{2.1}$$

where $\mu$ represents the linear attenuation coefficient. In the process known as Hounsfield scaling or CT number scaling (Huda and Slone, 1996), raw attenuation values derived from CT scans are converted into Hounsfield units using the equation:

$$\mathrm{HU} = (\mathrm{PV} \times \mathrm{RS}) + \mathrm{RI} \tag{2.2}$$

where $PV$ signifies the pixel value, representing the original value attributed to a pixel within a CT scan. $RS$, recognized as the rescale slope, is a scaling factor employed to modify the pixel values accordingly. Meanwhile, $RI$, identified as the rescale intercept, denotes a particular offset value applied to alter the pixel values.

Retrieving pixel arrays from DICOM files, organized by the instance number found in the metadata, involves adjusting each pixel's value in the CT image based on the rescale

slope and intercept values. This process standardizes the pixel values to accurately represent the actual attenuation coefficients. Following this standardization, the pixel values are then transformed into HU.

To facilitate a comprehensive comparison with algorithms that simulate particle morphology, adopting a distinct methodology involving the CT scanning of samples becomes imperative. Conventional CT scanning techniques typically involve making equidistant vertical incisions through the sample to capture cross-sectional imagery. However, to enhance the comparability, it is crucial that slices are made at uniform intervals along an oblique plane parallel to the surface of the sample. This procedure demands the compilation of CT scan images into a cohesive ensemble, which is then used to construct a 3D model of the sample, employing the transformed HU values. Subsequently, this model undergoes re-sectioning to align with the comparative analysis requirements.

### Dice Similarity Coefficient

To assess the extent of overlap between results obtained from algorithmic simulations and X-ray tomography, the Dice similarity coefficient (DSC) (Dice, 1945; Sorensen, 1948) is employed. The DSC, also known as the Sørensen–Dice coefficient, is a statistical metric used to measure similarity, often applied in image processing to gauge spatial overlap. This measurement method provides a quantitative way to compare the accuracy and alignment of the two sets of data, facilitating an objective evaluation of how closely the simulation results mimic the X-ray tomography findings. The DSC is defined as:

$$DSC = \frac{2 \times |A \cap B|}{|A| + |B|} \tag{2.3}$$

where: $|A \cap B|$ is the size of the intersection of two sets (in the context of images, these would be pixel sets) – basically, the number of pixels that are classified as the foreground (or as a particular object) in both images.$|A|$ is the number of pixels classified as the foreground in the first image. $|B|$ is the number of pixels classified as the foreground in the second image.

The value of the DSC ranges from 0 to 1, where 0 indicates no overlap and 1 indicates perfect overlap. This coefficient is particularly useful as it quantifies the similarity between two binary images. In an ideal case, if the predicted segmentation matches the ground truth segmentation exactly, the DSC would equal 1. Conversely, in an ideal case where two images have no overlap (anticorrelation), the DSC reaches 0. However, a DSC value of 0 is rare in practical applications, as it requires a complete absence of object overlap, meaning where an object exists in one image, it never exists in the corresponding location in the other image.

In more realistic cases, especially when comparing images that may be uncorrelated, it is essential to consider a more informative lower bound for the DSC. If a fraction $p$ of the first image contains objects and a fraction $q$ of the second image contains objects, the DSC for uncorrelated images can be derived as follows:

$$\text{DSC} = \frac{2pq}{p+q} \tag{2.4}$$

This formula gives the expected DSC when the two images have no correlation, and the placement of objects in the two images is independent. Here, $p$ and $q$ represent the proportions of the images that contain objects (foreground). This lower bound helps provide context for interpreting the actual DSC. This lower bound serves as a benchmark for understanding how much the actual DSC deviates from the expected value in an uncorrelated scenario. A comparison with this lower bound provides a clearer interpretation of image similarity, allowing us to discern meaningful correlations even when the DSC is not close to 1.

### CONTAMINANT DETECTION

Contaminant detection in RCA is achieved by employing spectral analysis. This study builds upon the cluster-based identification algorithm (Chang et al., 2022), which improved data representation. The current research focuses on refining this algorithm to further increase its operational efficiency and adaptability. These refinements lead to more reliable contaminant identification by improving the accuracy and speed of the detection process. In the dynamic field of spectroscopic analysis, environmental factors influence LIBS spectra, making adaptability to new data crucial for maintaining model accuracy and relevance (Chen et al., 2020; Wang et al., 2021). Therefore, periodic calibration is necessary. The incremental learning technique provides a practical approach for real-time spectral data analysis. This method significantly enhances performance and flexibility by eliminating the need for complete model retraining, making it well-suited for applications in environments where data is continuously generated.

#### Data Preprocessing

To efficiently process spectral data, it is necessary to preprocess the raw data. A first analysis of the spectra from typical constituents of different materials shows that focusing on the wavelength range of 200-900 nm is sufficient to achieve the desired outcomes, thereby improving computational efficiency. This preprocessing includes standardizing the spectral values to ensure uniform magnitude scales across different datasets, thereby highlighting unique data characteristics. Z-score standardization is used to maintain the data's distribution while aligning its mean and standard deviation to zero and one, respectively. This standardization captures essential data characteristics, such as the distribution patterns of peaks and troughs.

#### Parallel Processing for Enhanced Principal Component Analysis Computations

Each laser pulse generates a spectrum denoted as $S = (s_1, s_2, \ldots, s_N)$, where $s_i$ $(i = 1, 2, \ldots, N)$ represents the intensity of plasma emission at wavelengths $\lambda_i$. $N$ is the total number of measured wavelengths. This method positions each laser pulse into an $N$-dimensional space, creating distinct clusters for different materials based on their spectral signatures. New laser pulses are either assimilated into existing clusters or identified as outliers based on how much their spectra deviate from the norm.

The axes of the coordinate system of $S$ can be scaled and rotated to simplify the multi-dimensional normal distribution of points within a cluster. This simplification is achieved by defining a new orthonormal coordinate system, represented by $N$ unit

vectors $\alpha = (\alpha_1, \alpha_2, \ldots, \alpha_N)$. In this new coordinate system, the multi-dimensional normal distribution decomposes to $N$ independent one-dimensional normal distributions, each aligned with a new axis. Thus, the spectrum in the database transforms into the new coordinate system as:

$$\xi = (\xi_1, \xi_2, \ldots, \xi_N) = (S \cdot \alpha_1, S \cdot \alpha_2, \ldots, S \cdot \alpha_N) \tag{2.5}$$

Effective categorization does not require all $N$ dimensions; a smaller number $n$ is sufficient. This reduction minimizes the influence of irrelevant or noisy parts of the emission spectra. The significant information is projected into the leading dimensions of the new coordinate system. After the principal component analysis (PCA) process, the spectral database for a cluster consists consists of the number $n$, the principal component vectors $(\xi_1, \xi_2, \ldots, \xi_n)$, and a center point $\overline{\xi}$ with variances $\boldsymbol{\sigma^2}$, describing the multi-dimensional normal distribution of the spectra. For a comprehensive explanation of this process, please refer to 3.2.1 Principal Component Analysis.

By leveraging optimized Basic Linear Algebra Subprograms (BLAS) and Linear Algebra PACKage (LAPACK) libraries and implementing parallel processing (Abdelfattah et al., 2021; Psarras et al., 2022), we can significantly enhance the efficiency of PCA computations. These improvements are crucial for handling large datasets, particularly in applications involving spectral data analysis, where computational demands are high.

The BLAS and LAPACK libraries are fundamental tools for performing efficient linear algebra computations (Frison et al., 2018; Psarras et al., 2022). BLAS provides low-level routines for common operations such as vector addition, scalar multiplication, dot products, and matrix multiplication. Optimized implementations, such as OpenBLAS and Intel Math Kernel Library (MKL) (Frison et al., 2020; Yamazaki et al., 2018), exploit modern CPU architectures to deliver significant performance improvements through multi-threading and vectorization. LAPACK extends BLAS functionalities by offering routines for more complex linear algebra problems, including solving linear systems, eigenvalue problems, and singular value decomposition (SVD). By leveraging optimized BLAS libraries, LAPACK routines can achieve high performance across various hardware architectures. Parallel computing libraries can parallelize independent tasks like computations on different data chunks. Optimized BLAS libraries internally use multi-threading for operations like matrix multiplication, which can be configured to utilize multiple threads.

**Cluster-based Identification**

Post-PCA, the database catalogs a material by assigning a finite number of principal components, $n$. This step defines a new coordinate system through $n$ orthonormal vectors, facilitating the depiction of spectral data as multi-dimensional normal distributions around a centroid. Following normalization, principal component values are assumed to follow a chi-square distribution, which is crucial for classifying materials based on their spectral data. The conformity to the expected chi-square distribution is verified through $P$-value analysis, determining the significance level for recognizing specific materials.

Each component $\xi_m$ $(m = 1, 2, \ldots, n)$ in the set $(\xi_1, \xi_2, \ldots, \xi_n)$ follows a normal distribution with a mean of $\overline{\xi_m}$ and a variance of $\sigma_m^2$. After applying z-score standardization,

each standardized value $Z_m$ is calculated as:

$$Z_m = \frac{\xi_m - \overline{\xi_m}}{\sqrt{\sigma_m^2}} \tag{2.6}$$

These standardized values follow a normal distribution with a mean of 0 and a variance of 1. To test if the data comes from a $\chi_n^2$-distribution, the chi-square value is calculated as:

$$\chi^2 = \sum_{m=1}^{n} Z_m^2 = \sum_{m=1}^{n} \frac{(\xi_m - \overline{\xi}_m)^2}{\sigma_m^2} \tag{2.7}$$

This chi-square value helps determine the likelihood that the data follows the expected $\chi_n^2$-distribution. Each $\chi^2$ can be converted into a probability $P$-value for the $\chi_n^2$-distribution. A higher $\chi^2$ value corresponds to a lower $P$-value, indicating greater confidence that the data does not fit the expected distribution. $P$-values below a predetermined significance level indicate statistical significance. When this significance level is set as the acceptance criterion for a particular material, any spectra with $P$-value exceeding this threshold will be regarded as originating from that material.

**New Spectrum Assignment**

The $\chi_n^2$-distribution of the data within the database for specific materials is used to characterize each material's spectral signature. When a new spectrum is introduced, it is compared against the established $\chi_n^2$-distributions to determine if it could belong to a known material. The process involves evaluating the goodness-of-fit of the new spectrum within the bounds of each material's spectral $\chi_n^2$-distribution. This comparison provides a quantifiable level of confidence in assigning the new spectrum to a material, ensuring that false matches are minimized and the accuracy of material identification is improved.

**Incremental Learning**

Implement incremental learning techniques to update the model as new spectral data becomes available. This can be achieved through online PCA methods and updating chi-square distribution parameters dynamically.

Given a new spectral observation $S_t$ of a material at time $t$ (represents the index of the data point being introduced, i.e., it is the time step or the sequential position of the data point), the mean vector $\mu_t$ and covariance matrix $C_t$ of the spectral data in the original $N$-dimensional space are updated using the following equations (Oyama et al., 2008; Ozawa et al., 2006):

$$\mu_t = \mu_{t-1} + \frac{1}{t}(S_t - \mu_{t-1}) \tag{2.8}$$

$$C_t = \frac{t-1}{t} C_{t-1} + \frac{1}{t}(S_t - \mu_{t-1})(S_t - \mu_t)^T \tag{2.9}$$

Here, the covariance matrix $C_t$ is updated prior to performing PCA, capturing the variability of the spectral data in the original $N$-dimensional space. This updated covariance

matrix reflects the latest statistical characteristics of the data, which is essential for accurately calculating the principal components. Subsequently, the principal components are extracted from the updated covariance matrix $C_t$ using eigenvalue decomposition. In this approach, earlier spectral data are given the same weight as later spectral data, ensuring equal consideration throughout the time series. However, it is important to note that alternative methods exist, which prioritize more recent spectral data by assigning them higher weights, thereby adapting more swiftly to recent changes in the data.

Following PCA, the spectral data is transformed into a lower-dimensional space where each principal component follows a normal distribution. The chi-square distribution is then employed to evaluate the goodness-of-fit for new data points. To maintain the accuracy of this statistical test, it is essential to dynamically update the chi-square distribution parameters as new data is integrated.

Let $\xi_t$ represent the vector of principal components at time $t$. The mean $\overline{\xi}_t$ and variance $\sigma_t^2$ of the principal components are updated incrementally:

$$\overline{\xi}_t = \overline{\xi}_{t-1} + \frac{1}{t}\left(\xi_t - \overline{\xi}_{t-1}\right) \tag{2.10}$$

$$\sigma_t^2 = \sigma_{t-1}^2 + \frac{1}{t}\left[\left(\xi_t - \overline{\xi}_{t-1}\right)^2 - \sigma_{t-1}^2\right] \tag{2.11}$$

The chi-square statistic for the new observation $\xi_t$ is computed as:

$$\chi_t^2 = \sum_{i=1}^{n} \frac{(\xi_{t,i} - \overline{\xi}_{t,i})^2}{\sigma_{t,i}^2} \tag{2.12}$$

By continuously updating $\overline{\xi}_t$ and $\sigma_t^2$, the model dynamically adjusts to reflect the latest data distribution, thereby improving classification accuracy and robustness.

This method demonstrated a substantial reduction in computational load compared to traditional batch PCA, while maintaining similar levels of dimensionality reduction efficacy (Diaz-Chito et al., 2018). Additionally, the dynamic updating of chi-square parameters facilitated more accurate and responsive classification, particularly as new data was introduced.

## 2.3. RESULTS AND DISCUSSION

### 2.3.1. PSD CALCULATION

#### 3D POINT CLOUD DATA

Given the observed uniformity and consistency in the distribution pattern of constituents within the RCA piles, it becomes feasible to extrapolate the PSD characteristics of the entire pile through a focused analysis of the PSD associated exclusively with the outer surface layer of the pile. This method presents an effective means of obtaining a representative understanding of the overall PSD of the RCA piles. Using the Gocator scanner, a comprehensive scan of the RCA pile's external surface was conducted, yielding detailed 3D point cloud data (Figure 2.7 (a)).

The spatial resolution of this 3D point cloud data is crucial as it affects the accuracy and detail of the RCA particle measurements. In this context, it's paramount to note

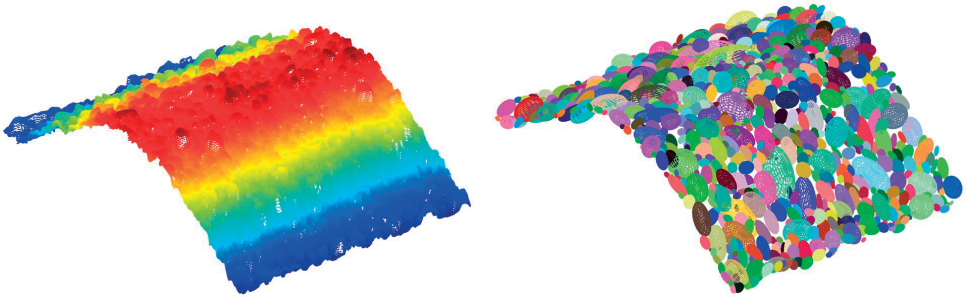

(a) 3D view of the point cloud data (b) Ellipsoids fitted to each particle

Figure 2.7: Point cloud processing

that the resolution of the point clouds under study demonstrated discernible variances across different spatial orientations—a phenomenon that has broader implications for the precision of granulometric assessments.

In the direction parallel to the motion of the conveyor belt, the resolution of 3D point cloud data is influenced by two factors. The first factor is the velocity of the conveyor belt, controlled by adjusting the rotational speed of the motor drive. This rotational speed adjustment is achieved through the manipulation of the motor's output frequency and the number of poles. Specifically, the motor drive in this study operates at 50 Hz with a 4-pole design, resulting in a rotational speed of 1500 rpm. Mechanical adjustments include a gearbox ratio of 19 and a wheel perimeter of 402.116 mm, resulting in a conveyor belt speed of 0.529 m/s. The second factor affecting the resolution is the encoder resolution of the Gocator, which was calibrated to record 1024 ticks per revolution, translating to a point cloud resolution of 0.393 mm along the conveyor belt's path.

Perpendicular to the conveyor belt, across its width, the resolution depends on the distance of the Gocator to the surface of the RCA pile. This resolution ranges from 0.375 mm to 1.100 mm, which is inherently tied to the Gocator's field of view at any given point in time. For accuracy, the transverse resolution was standardized at 0.375 mm in this study.

Vertically, concerning the height or depth of the RCA piles, the Gocator's advanced internal mechanisms come into play. The system provides a resolution gradient from a fine 0.092 mm to a coarser 0.488 mm. This variability highlights the scanner's versatility and adaptability in handling different granulometric scenarios, establishing it as a crucial tool in the comprehensive evaluation of RCA piles. In this study, the resolution was set at 0.092 mm in the vertical dimension.

### PSD CALCULATION

The PSD of RCA piles was determined using the method described previously. This involved fitting the 3D point cloud data of the RCA piles into ellipsoidal models (Figure 2.7 (b)) to capture morphological data for each particle. The resulting PSD was effectively demonstrated through a cumulative percentage retained graph, as depicted in Figure 8. This graph, supported by calculations of ellipsoidal volume and the RCA's apparent den-

sity, provided a clear visualization of the PSD characteristics inherent to the RCA piles. The insights gained from this analysis are crucial for understanding the aggregate structure and its potential influence on the performance of concrete.

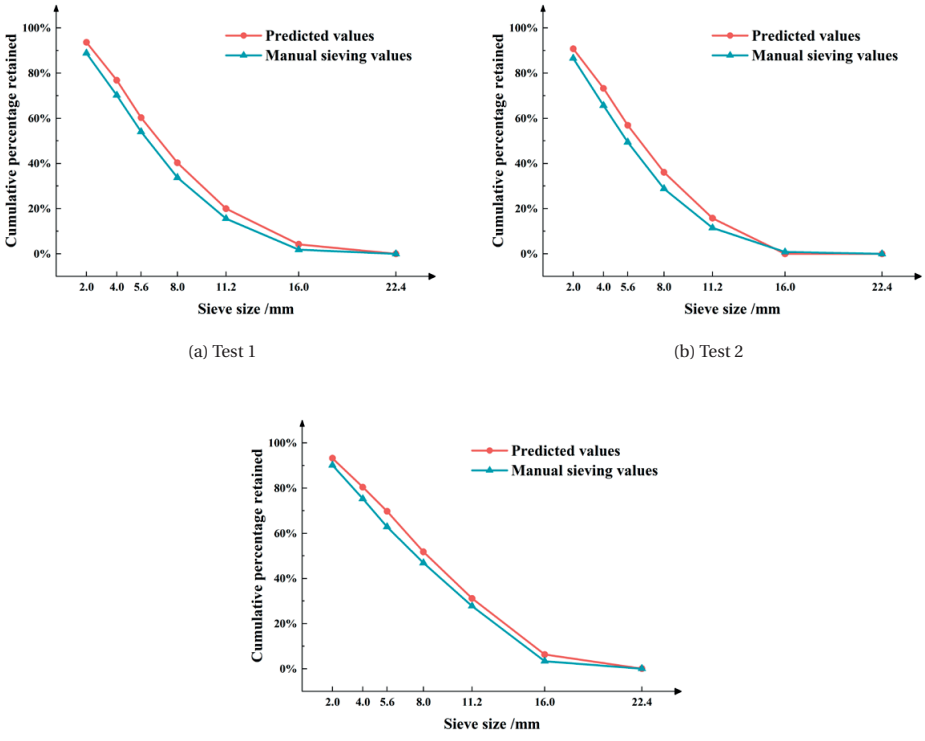


(a) Test 1

(b) Test 2

(c) Test 3

Figure 2.8: Cumulative percentage retained graphs

Subsequently, a cross-referential analysis was conducted to validate the accuracy and reliability of this non-intrusive, surface-based technique for PSD determination. This entailed comparing the PSD results from the 3D point cloud data with those obtained through the traditional, more invasive method - manual sieving. The comparison aimed to ascertain the degree of correlation and consistency between the surface PSD measurements and the actual overall PSD of the entire RCA piles. Figure 2.8 depicts this comparative study, showing the cumulative percentage retained curves as predicted from 3D point cloud analytics against those obtained from manual sieving, based on pilot scanning trials. The results indicate a minimal difference between the two methods, affirming a high degree of accuracy in the surface-based technique.

To further assess the precision and efficacy of this surface-based PSD measurement technique, the Root Mean Square Error (RMSE) was calculated between the predicted and manually derived values, resulting in deviations of 4.93%, 5.38%, and 4.27% across three experiments. These low RMSE values confirm the robustness and precision of this

surface-based technique in estimating the PSD of RCA piles on a conveyor belt. Initial results demonstrate a high degree of concordance between the two methods, suggesting that the 3D scanning approach could effectively approximate the comprehensive PSD with a significant reduction in manual effort and time.



### X-RAY TOMOGRAPHY VALIDATION

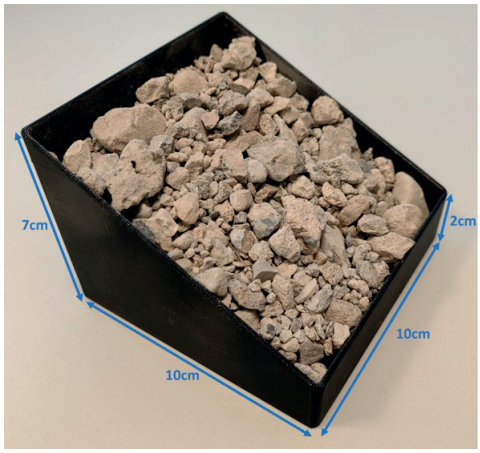


(a) Sample box

(b) Processed 3D scanning model

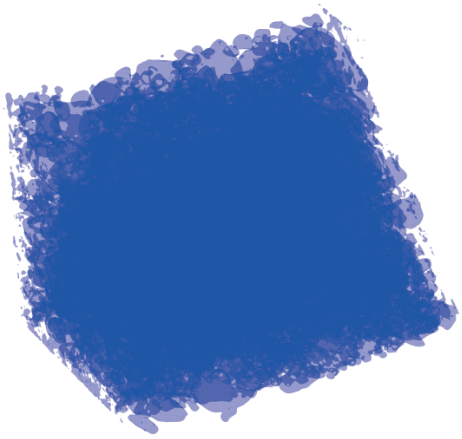

(c) Processed X-ray tomography model

Figure 2.9: RCA sample

To further validate this surface-based PSD measurement technique, X-ray tomography was employed to capture the morphology of particles beneath the surface of RCA plies. The internal structure captured by X-ray tomography was compared to the ellipsoids simulated from 3D point cloud data. A black box (as shown in Figure 2.9 (a)) was

used to simulate the inclined surface on one side of the formed piles, with RCA spread inside. The sample was scanned using both 3D scanning and X-ray tomography techniques. The data processed from these methods are shown in Figure 2.9 (b) and (c) respectively.

The ellipsoidal fitting model illustrated in Figure 2.9 (b) originated from 3D point cloud data obtained through 3D scanning with the Gocator. This process involved segmenting the 3D point cloud data and fitting it to the ellipsoidal shape. The 3D model in Figure 2.9 (c) was generated through layered scanning with X-ray tomography. This process involved compiling each scanned layer and isolating the particle components using thresholding. Both models were incrementally sliced from top to bottom, parallel to the inclined surface, allowing observation of each layer's cross-section. Then the two obtained cross-sectional images of each layer were overlapped for comparative analysis.

(a) Layer 1

(b) Layer 2

(c) Layer 3

(d) Layer 4

(e) Layer 5

(f) Layer 6

Figure 2.10: Cross-sectional details

Six representative layers were selected in Figure 2.10, following the top-down slicing depth (specific depths are provided in Table 2.1). On the left are the cross-sectional details of the simulated ellipsoidal model. In the middle are the cross-sectional details derived from the 3D model constructed using X-ray tomography, reflecting the real particle distribution. On the right are the overlapping cross-sections of the two methods for comparison.

To assess the similarity between cross-sections obtained by the two methods, the DSC was employed. Following the sequence depicted in Figure 2.10, from (a) to (f), the DSC values are 0.63, 0.71, 0.82, 0.85, 0.86, and 0.82. From the selected sections, an incremental increase in overlap between the two methods is evident, peaking at 0.86 before slightly decreasing.

Table 2.1 shows a comparison between the actual DSC and the lower bound of DSC for each layer. The lower bound of DSC values, ranging from 0.04 to 0.60, represent the theoretical DSC for uncorrelated images at each layer. As depth increases, particles that are initially scattered gradually fill the entire region, leading to an increase in the area of the cross-sections obtained by each method. This, in turn, raises the likelihood of correlation between the images being compared. Despite the increasing lower bound of DSC values, the actual DSC values remain significantly higher across all layers. The difference between the actual DSC and the lower bound is most pronounced in the shallow layers (e.g., Layer 1), where uncorrelated images would have minimal overlap, and less pronounced in deeper layers (e.g., Layer 6), where even uncorrelated images naturally have more overlap.This comparison confirms that the algorithm performs well, with the actual DSC values showing significant improvement over the lower bound, indicating strong object overlap and similarity between the cross-sections of the two methods.

Initially, lower overlap occurs due to irregularities on the particle surfaces, challenging their representation in the simulated ellipsoids. As the sections progress, the ellipsoids better emulate the internal particle distribution, maintaining an overlap of around 0.8. However, in deeper sections of the ellipsoids, a gradual appearance of blank spaces in the lower-left region is observed. This is attributed to the presence of numerous smaller particles in that area. In each layer of Figure 2.10, the rightmost image, show-

Table 2.1: DSC comparison with layers

| Layer | Depth (mm) | Actual DSC | Lower bound of DSC |
|---|---|---|---|
| Layer 1 | 2.0 | 0.63 | 0.04 |
| Layer 2 | 5.0 | 0.71 | 0.25 |
| Layer 3 | 8.0 | 0.82 | 0.43 |
| Layer 4 | 11.0 | 0.85 | 0.52 |
| Layer 5 | 14.0 | 0.86 | 0.55 |
| Layer 6 | 17.0 | 0.82 | 0.60 |



ing the overlapping cross-sections of the two methods, highlights examples with red and blue dashed boxes. The red dashed box illustrates cases where the algorithm performs well in fitting the particles across all layers. These particles tend to have a more regular shape and are larger in size compared to others. In contrast, the blue dashed box represents particles that the algorithm struggles to fit accurately. These particles are generally smaller and have irregular shapes. Due to the limited resolution of the Gocator, the algorithm cannot fit these particles well, and they can only be roughly indicated as present.

3D scanning only captures information from the top layer, hence forming a single layer of smaller ellipsoids. In contrast, X-ray tomography does not encounter this limitation, as additional particles fill the same location, preventing the appearance of blanks.

This comparative analysis further validates the reliability of surface-based PSD measurement techniques. Consequently, the Gocator 3D scanning can be employed for a quick and convenient estimation of PSD.

### 2.3.2. CONTAMINANT DETECTION

This study aimed to evaluate the performance differences of the LIBS sensor in capturing spectra from objects under varying environmental conditions. The focus was on assessing its ability to adapt to new data to maintain model accuracy and relevance in dynamic spectroscopic analysis. Additionally, the study aimed to understand how the movement of the conveyor belt might affect the effectiveness of the system's reflective mirrors. Spectral measurements from a wide range of materials were recorded under two conditions: while the conveyor belt was running and while it was stationary.

Figure 2.11 provides a visual representation of the findings. The results reveal minimal variation in the spectra from the materials, regardless of the conveyor belt's motion. The minor differences in spectra observed between the moving and stationary states of the conveyor belt do not significantly impact the overall system performance. This uniformity demonstrates the reliability and effectiveness of the system's design.

Despite the general consistency, there were slight spectral differences noted between the moving and stationary states of the conveyor belt. These differences, though minor, could lead to errors when classifying materials with similar chemical compositions, such as RCP, RFA, RCA, and others. These subtle variations, although not significantly

affecting overall system performance, must be considered in detailed analyses to avoid misclassification and ensure accurate results.

The observed differences between spectra collected from a static and moving belt can likely be attributed to several factors. One key reason may be variations in ambient conditions, such as the presence of dust or mechanical vibrations, which can cause slight disturbances in the measurements (Gaft et al., 2007; Mateo et al., 2007). These impurities can cause the LIBS signal to fluctuate depending on the specific point where the laser irradiates the sample. The impact of these environmental changes can be exacerbated by the movement of the sample, as the motion introduces additional variability in the signal (H. Kim et al., 2021). Matrix effects and interferences arising from the surface shape and condition also play a significant role in these differences. Changes in surface roughness, curvature, or material composition may alter how the laser interacts with the surface, further complicating the consistency of spectral data (Cabalín et al., 2010; Mateo et al., 2007). Finally, the speed of the belt can directly influence the spectrometer's ability to capture data accurately. Faster-moving belts may reduce the spectrometer's ability to fully detect and analyze the emitted signal due to shorter interaction times (Cabalín et al., 2010). These factors, when combined, help explain the spectral differences observed between static and moving belt conditions, illustrating the complexities involved in real-time spectral analysis.

Furthermore, the results also support the system's ability to perform consistently under different operational scenarios. Its resilience under different operational conditions underscores its potential as a reliable tool for real-time industrial applications, ensuring consistent and accurate data acquisition regardless of conveyor belt activity. This is paramount for industries where conveyor belt speeds might vary, and where maintaining measurement consistency is critical.

After acquiring spectra from various materials, a systematic classification was conducted using a cluster-based identification algorithm enhanced by incremental learning techniques. This algorithm, recognized for its ability to group data by identifying inherent similarities, was applied to discern patterns within the updated spectral data. The model's performance underwent a thorough assessment to ensure its reliability for practical applications. Remarkably, the model showcased robust performance metrics for this new system: achieving an accuracy rate of 0.94, a weighted average precision of 0.95, a weighted average recall of 0.94, and an F1-score (weighted average) standing at 0.95 on the validation dataset.

However, while these performance metrics confirm the overall effectiveness of LIBS as an analytical tool for analyzing recycled concrete aggregates, they do not fully address the practical concerns of most users, particularly regarding the system's performance in detecting essential contaminants. To provide a clearer understanding of the system's practical applications, it is crucial to detail the specific contaminant detection limits that the system can reliably ascertain for each type of contaminant. By providing this information, users can better assess the system's ability to determine whether contaminant concentrations exceed or stay within quality limits, which is vital for ensuring the quality and safety of recycled materials in industrial contexts.

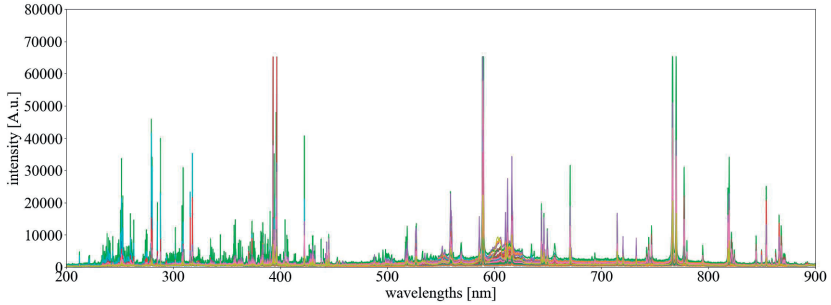


(i) Conveyor belt in the operational state

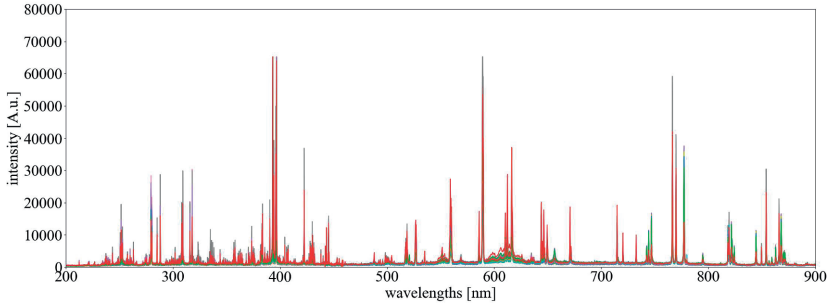


(ii) Conveyor belt in the stationary state

(a) Brick

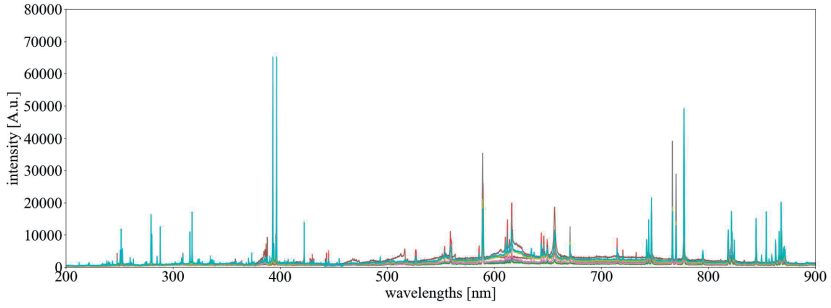


(i) Conveyor belt in the operational state

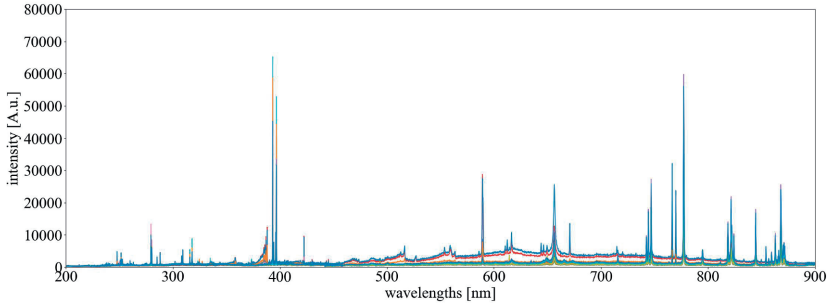


(ii) Conveyor belt in the stationary state

(b) Foam

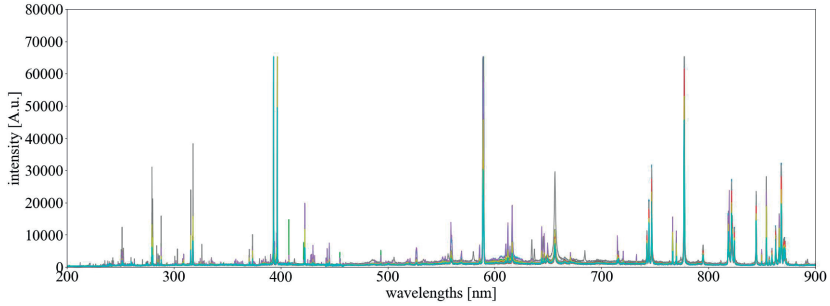


(i) Conveyor belt in the operational state

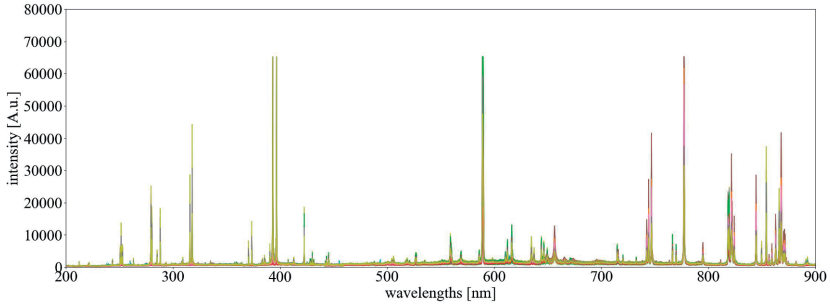


(ii) Conveyor belt in the stationary state

(c) Glass

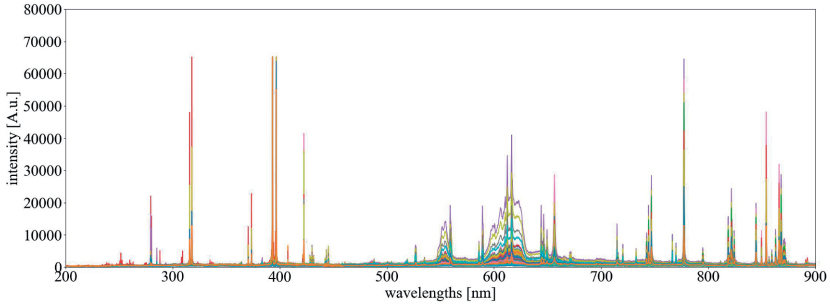


(i) Conveyor belt in the operational state

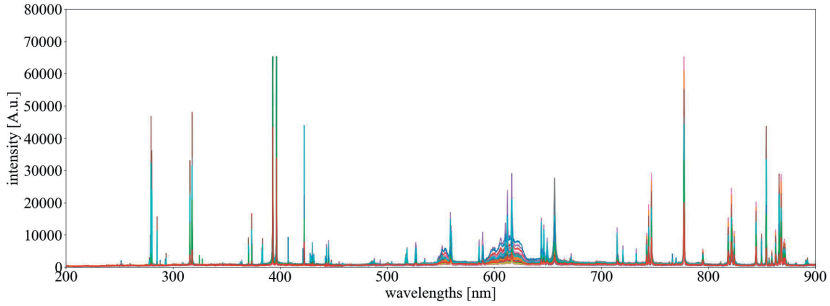


(ii) Conveyor belt in the stationary state

(d) Gypsum

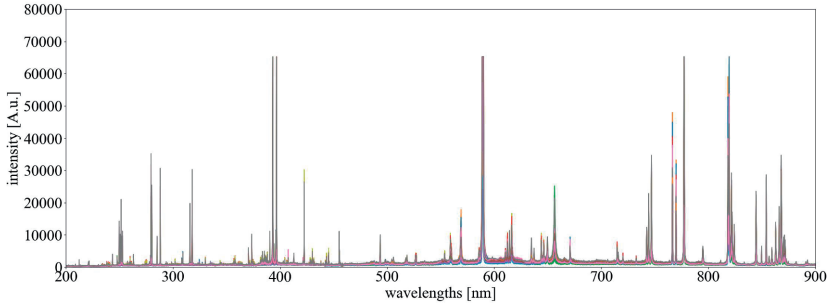


(i) Conveyor belt in the operational state

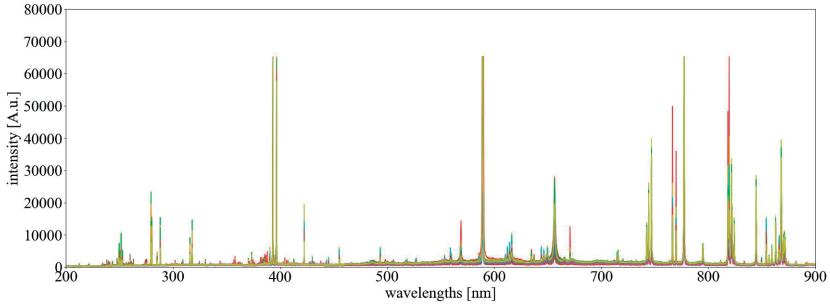


(ii) Conveyor belt in the stationary state

(e) Mineral fibers

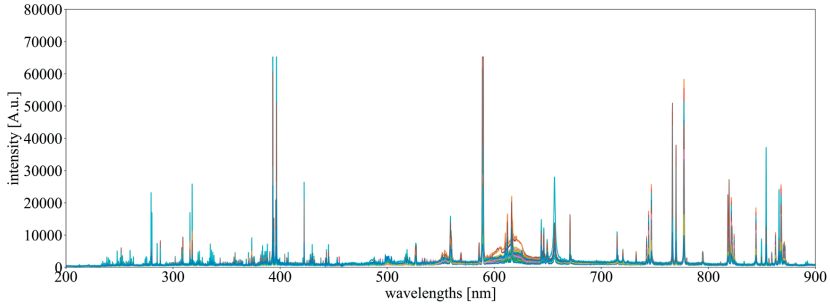


(i) Conveyor belt in the operational state

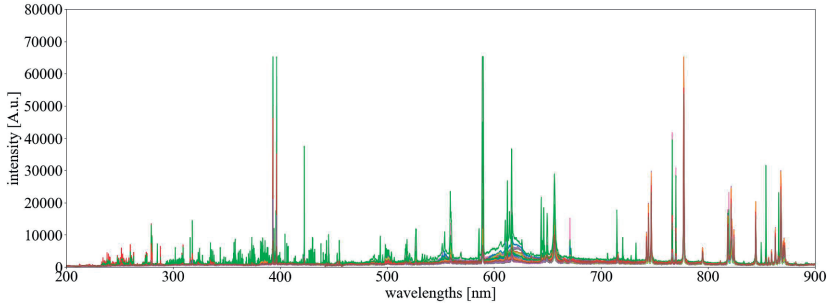


(ii) Conveyor belt in the stationary state

(f) Plastics

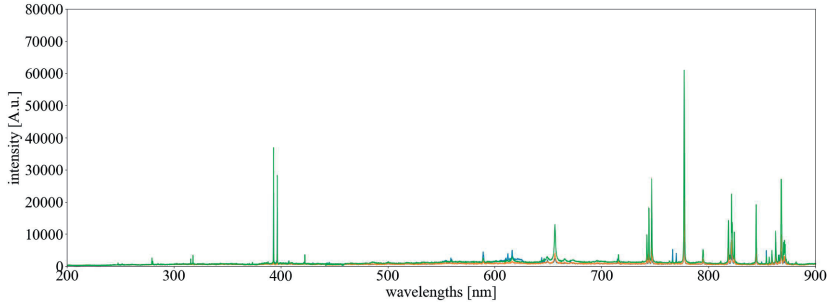


(i) Conveyor belt in the operational state

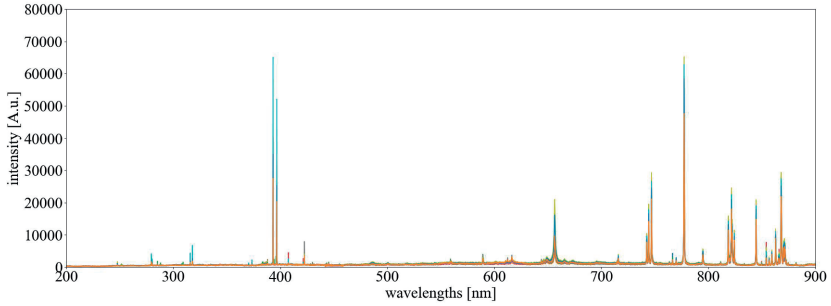


(ii) Conveyor belt in the stationary state

(g) Wood

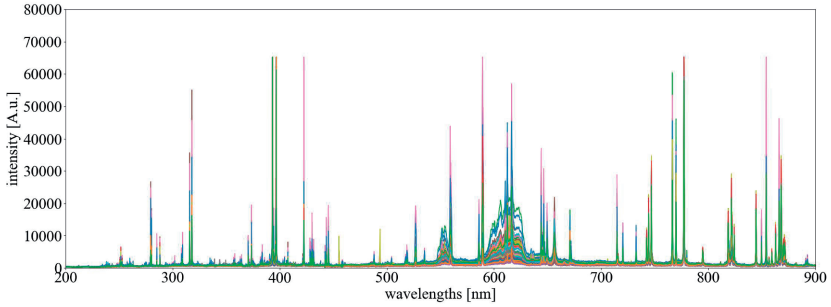


(i) Conveyor belt in the operational state

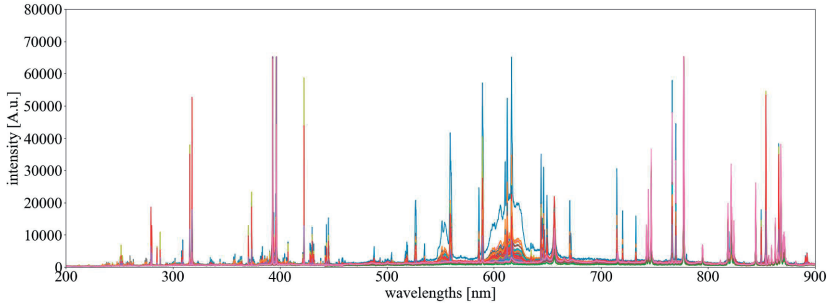


(ii) Conveyor belt in the stationary state

(h) Recycled cement paste powder (RCP)

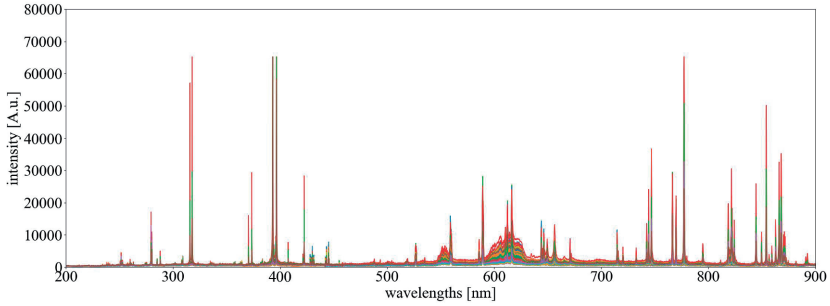


(i) Conveyor belt in the operational state

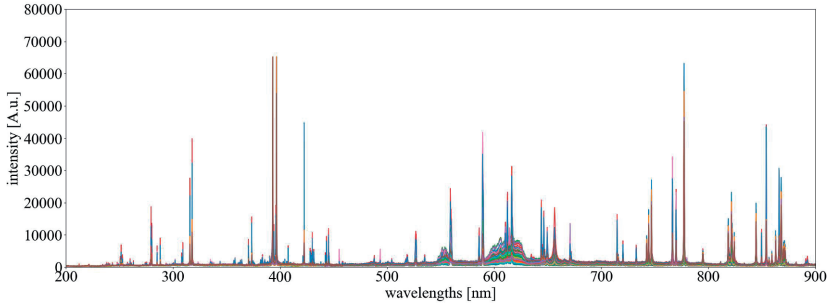


(ii) Conveyor belt in the stationary state

(i) Recycled fine aggregates (RFA)

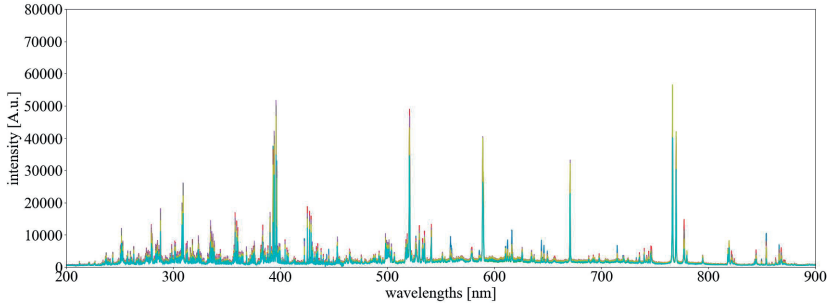


(i) Conveyor belt in the operational state

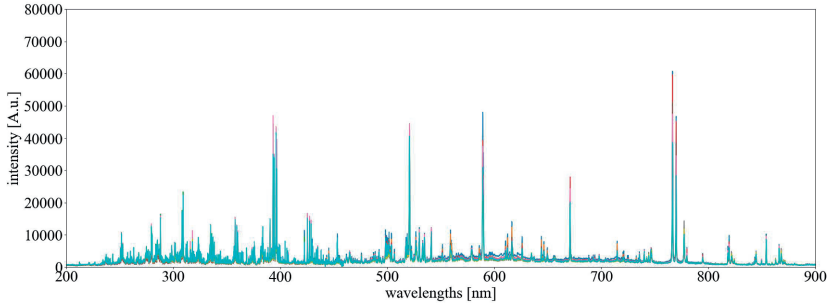


(ii) Conveyor belt in the stationary state

(j) RCA

Figure 2.11: Comparison of spectra of different materials in the operation and stationary states of the conveyor belt

Considering this, the system shows strong market potential. It can monitor RCA quality at a throughput of 50 tons per hour per conveyor, analyzing approximately 4,000 particles per ton of material. The system is capable of detecting critical contaminants at concentrations below 50 parts per million (ppm). For materials with strict content regulations, such as wood, the system meets the required limit of 0.2 $cm^3$/kg, which is equivalent to 0.08 g/kg or a mass concentration of 80 ppm. This detection limit is based on ensuring a false positive rate of less than 1 in 2000 for RCA being misinterpreted as wood, ensuring high confidence in material classification. This further highlights its reliability and effectiveness in industrial settings.

These metrics highlight LIBS's ability to deliver both accuracy and precision quickly, without compromising the quality of the outcomes. By adopting these advanced analytical techniques, industries can confidently make strides forward, optimizing the use of recycled materials and maintaining high-quality standards.

## 2.4. CONCLUSION

The increasing global focus on sustainable infrastructure development highlights the importance of efficiently using EoL materials. This study evaluates the potential of integrating advanced technologies to analyze and assess RCA obtained from demolition sites. The integration of a sensor-based quality inspection system within the C2CA technology framework represents progress in RCA assessment. Housed in a dedicated container, this sensor-based system showcases a blend of mobility, resilience, and accuracy crucial for on-site applications. This setup indicates scalability and adaptability, demonstrating the practicality of deploying such technologies across diverse demolition contexts.

The system's detailed granulometric analysis using the Gocator and the contaminant detection by the LIBS sensor provides a comprehensive evaluation of RCA quality. These analyses address PSD and contaminant content—key factors for material quality and compliance with industry standards. Additionally, the system's capability for real-time data capture and cloud-based storage represents a notable improvement in data management and accessibility. This supports informed decision-making processes and enhances quality control measures. Notably, the efficient monitoring of two conveyor belts using a single laser and spectrometer highlights the practicality and cost-effectiveness of this approach, rendering it a viable solution for industry requirements.

Furthermore, this approach avoids invasive and time-consuming sampling methods that could potentially affect the integrity of the RCA piles. By using non-destructive scanning techniques, we ensure the piles' structural and material integrity remains intact while providing valuable insights into their internal properties. The implementation of the Gocator yielded significant PSD data, aligning well with traditional manual sieving methods. This correlation emphasizes the potential of non-intrusive, technology-driven methodologies to streamline analysis, saving manual effort and time. It serves as a crucial link, connecting fundamental aggregate characteristics to concrete composite properties. PSD analysis offers essential insights into aggregate architecture, influencing concrete's performance, durability, and strength. It becomes a tool for informed decisions regarding concrete mix designs, modifications, and optimizations, contributing to better-quality infrastructure. Ultimately, the Gocator's application in assessing PSD for RCA piles represents progress in material characterization. It improves efficiency and accuracy while supporting sustainability principles and minimal environmental impact. This innovative approach could potentially influence PSD assessment standards, leading to more progressive applications in construction and demolition waste management.

In the realm of contaminant detection, the consistent spectral measurements acquired through the LIBS sensor, regardless of conveyor belt activity, establish a reliable foundation for the system. This reliability across diverse operational conditions has the potential to enhance industrial quality assessment practices. The use of the cluster-based identification algorithm further refines the system's precision, exhibiting commendable accuracy and metrics. By adopting incremental learning methods, researchers and practitioners can ensure their models remain current and effective in the face of ever-evolving data landscapes. The demonstrated consistency and accuracy in our results suggest the system's capability to significantly contribute to the quality assessment processes within the construction industry. As industries increasingly adopt

sustainable construction practices, leveraging such advanced analytical techniques becomes pivotal in maximizing the use of recycled materials without compromising quality standards. This research, therefore, stands as evidence of the effectiveness of our proposed system while highlighting the broader implications of integrating technology with sustainability for a more environmentally friendly future.



This research highlights the immense potential of integrating advanced technological frameworks into recycled concrete aggregate processing. This marriage of innovation and precision propels us toward a sustainable future where the quality of recycled materials is substantiated rather than speculated. The findings presented here demonstrate that with appropriate technological advancements, industries can harmonize efficiency with precision, advancing the sustainable agenda while upholding the highest quality standards. As we progress towards a world that emphasizes sustainability, studies such as this establish the essential foundation, guaranteeing that we revamp not only materials but also our outlook on quality and efficiency.

# BIBLIOGRAPHY


Abdelfattah, A., Costa, T., Dongarra, J., Gates, M., Haidar, A., Hammarling, S., Higham, N. J., Kurzak, J., Luszczek, P., Tomov, S., et al. (2021). A set of batched basic linear algebra subprograms and lapack routines. *ACM Transactions on Mathematical Software (TOMS)*, *47*(3), 1–23.

Akhtar, A., & Sarmah, A. K. (2018). Construction and demolition waste generation and properties of recycled aggregate concrete: A global perspective. *Journal of Cleaner Production*, *186*, 262–281.

Al Martini, S., Sabouni, R., Khartabil, A., Wakjira, T. G., & Alam, M. S. (2023). Development and strength prediction of sustainable concrete having binary and ternary cementitious blends and incorporating recycled aggregates from demolished uae buildings: Experimental and machine learning-based studies. *Construction and Building Materials*, *380*, 131278.

Alaejos, P., de Juan, M. S., Rueda, J., Drummond, R., & Valero, I. (2013). Quality assurance of recycled aggregates. In E. Vázquez (Ed.), *Progress of recycling in the built environment: Final report of the rilem technical committee 217-pre* (pp. 229–273). Springer Netherlands.

Aslam, M. S., Huang, B., & Cui, L. (2020). Review of construction and demolition waste management in china and usa. *Journal of environmental management*, *264*, 110445.

Barri, K., Jahangiri, B., Davami, O., Buttlar, W. G., & Alavi, A. H. (2020). Smartphone-based molecular sensing for advanced characterization of asphalt concrete materials. *Measurement*, *151*, 107212.

Basu, S., Kwee, T. C., Surti, S., Akin, E. A., Yoo, D., & Alavi, A. (2011). Fundamentals of pet and pet/ct imaging. *Annals of the New York Academy of Sciences*, *1228*(1), 1–18.

Bonifazi, G., Palmieri, R., & Serranti, S. (2018). Evaluation of attached mortar on recycled concrete aggregates by hyperspectral imaging. *Construction and Building Materials*, *169*, 835–842.

Braun, J., & Willett, S. D. (2013). A very efficient o(n), implicit and parallel method to solve the stream power equation governing fluvial incision and landscape evolution. *Geomorphology*, *180-181*, 170–179.

Cabalín, L., González, A., Ruiz, J., & Laserna, J. (2010). Assessment of statistical uncertainty in the quantitative analysis of solid samples in motion using laser-induced breakdown spectroscopy [A Selection of Papers Presented at the 5th Euro-Mediterranean Symposium on Laser Induced Breakdown Spectroscopy (EMSLIBS 2009)]. *Spectrochimica Acta Part B: Atomic Spectroscopy*, *65*(8), 680–687.

Cabral, J. S., Menegatti, C. R., & Nicolodelli, G. (2023). Laser-induced breakdown spectroscopy in cementitious materials: A chronological review of cement and concrete from the last 20 years. *TrAC Trends in Analytical Chemistry*, *160*, 116948.

Chang, C., Di Maio, F., Rem, P., Gebremariam, A. T., Mehari, F., & Xia, H. (2022). Cluster-based identification algorithm for in-line recycled concrete aggregates characterization using laser-induced breakdown spectroscopy (libs). *Resources, Conservation and Recycling*, *185*, 106507.

Chen, T., Zhang, T., & Li, H. (2020). Applications of laser-induced breakdown spectroscopy (libs) combined with machine learning in geochemical and environmental resources exploration. *TrAC Trends in Analytical Chemistry*, *133*, 116113.

Diaz-Chito, K., Ferri, F. J., & Hernández-Sabaté, A. (2018). An overview of incremental feature extraction methods based on linear subspaces. *Knowledge-Based Systems*, *145*, 219–235.

Dice, L. R. (1945). Measures of the amount of ecologic association between species. *Ecology*, *26*(3), 297–302.

Fajar, A., Sarno, R., Fatichah, C., & Fahmi, A. (2022). Reconstructing and resizing 3d images from dicom files. *Journal of King Saud University-Computer and Information Sciences*, *34*(6), 3517–3526.

Frison, G., Kouzoupis, D., Sartor, T., Zanelli, A., & Diehl, M. (2018). Blasfeo: Basic linear algebra subroutines for embedded optimization. *ACM Transactions on Mathematical Software (TOMS)*, *44*(4), 1–30.

Frison, G., Sartor, T., Zanelli, A., & Diehl, M. (2020). The blas api of blasfeo: Optimizing performance for small matrices. *ACM Transactions on Mathematical Software (TOMS)*, *46*(2), 1–36.

Gaft, M., Sapir-Sofer, I., Modiano, H., & Stana, R. (2007). Laser induced breakdown spectroscopy for bulk minerals online analyses [A Collection of Papers Presented at the 4th International Conference on Laser Induced Plasma Spectroscopy and Applications (LIBS 2006)]. *Spectrochimica Acta Part B: Atomic Spectroscopy*, *62*(12), 1496–1503.

Gálvez-Martos, J.-L., Styles, D., Schoenberger, H., & Zeschmar-Lahl, B. (2018). Construction and demolition waste best management practice in europe. *Resources, conservation and recycling*, *136*, 166–178.

Huda, W., & Slone, R. (1996). Review of radiologic physics. *Physics in Medicine and Biology*, *41*(12), 2807.

Kabirifar, K., Mojtahedi, M., Wang, C., & Tam, V. W. (2020). Construction and demolition waste management contributing factors coupled with reduce, reuse, and recycle strategies for effective waste management: A review. *Journal of cleaner production*, *263*, 121265.

Kim, H., Lee, J., Srivastava, E., Shin, S., Jeong, S., & Hwang, E. (2021). Front-end signal processing for metal scrap classification using online measurements based on laser-induced breakdown spectroscopy. *Spectrochimica Acta Part B: Atomic Spectroscopy*, *184*, 106282.

Kim, J. (2022). Influence of quality of recycled aggregates on the mechanical properties of recycled aggregate concretes: An overview. *Construction and Building Materials*, *328*, 127071.

Lederer, J., Gassner, A., Kleemann, F., & Fellner, J. (2020). Potentials for a circular economy of mineral construction materials and demolition waste in urban areas: A case study from vienna. *Resources, Conservation and Recycling*, *161*, 104942.

Lotfi, S., Di Maio, F., Xia, H., Serranti, S., Palmieri, R., Bonifazi, G., et al. (2015). Assessment of the contaminants level in recycled aggregates and alternative new technologies for contaminants recognition and removal. In *Emabm 2015. proceedings of the 15th euroseminar on microscopy applied to building materials* (pp. 319–331, Vol. 1). Delft University of Technology.

Marie, I., & Mujalli, R. (2019). Effect of design properties of parent concrete on the morphological properties of recycled concrete aggregates. *Engineering Science and Technology, an International Journal*, *22*(1), 334–345.

Marín-Cortés, S., Fernández-Álvarez, M., Enríquez, E., & Fernández, J. F. (2024). Experimental characterization data on aggregates from construction and demolition wastes for the assistance in sorting and recycling practices. *Construction and Building Materials*, *435*, 136798.

Marique, A.-F., & Rossi, B. (2018). Cradle-to-grave life-cycle assessment within the built environment: Comparison between the refurbishment and the complete reconstruction of an office building in belgium. *Journal of environmental management*, *224*, 396–405.

Mateo, M., Nicolas, G., & Yanez, A. (2007). Characterization of inorganic species in coal by laser-induced breakdown spectroscopy using uv and ir radiations. *Applied Surface Science*, *254*(4), 868–872.

Nalon, G. H., Santos, R. F., de Lima, G. E. S., Andrade, I. K. R., Pedroti, L. G., Ribeiro, J. C. L., & de Carvalho, J. M. F. (2022). Recycling waste materials to produce self-sensing concretes for smart and sustainable structures: A review. *Construction and Building Materials*, *325*, 126658.

Oyama, T., Karungaru, S., Tsuge, S., Mitsukura, Y., & Fukumi, M. (2008). Incremental learning method of simple-pca. In I. Lovrek, R. J. Howlett, & L. C. Jain (Eds.), *Knowledge-based intelligent information and engineering systems* (pp. 403–410). Springer Berlin Heidelberg.

Ozawa, S., Pang, S., & Kasabov, N. (2006). An incremental principal component analysis for chunk data. *2006 IEEE International Conference on Fuzzy Systems*, 2278–2285.

Pelc, N. J. (2014). Recent and future directions in ct imaging. *Annals of biomedical engineering*, *42*, 260–268.

Poon, C.-S., & Chan, D. (2007). Effects of contaminants on the properties of concrete paving blocks prepared with recycled concrete aggregates. *Construction and Building Materials*, *21*(1), 164–175.

Psarras, C., Barthels, H., & Bientinesi, P. (2022). The linear algebra mapping problem. current state of linear algebra languages and libraries. *ACM Transactions on Mathematical Software (TOMS)*, *48*(3), 1–30.

Sorensen, T. (1948). A method of establishing groups of equal amplitude in plant sociology based on similarity of species content and its application to analyses of the vegetation on danish commons. *Biologiske skrifter*, *5*, 1–34.

Soto-Paz, J., Arroyo, O., Torres-Guevara, L. E., Parra-Orobio, B. A., & Casallas-Ojeda, M. (2023). The circular economy in the construction and demolition waste management: A comparative analysis in emerging and developed countries. *Journal of Building Engineering*, 107724.

Steer, P., Guerit, L., Lague, D., Crave, A., & Gourdon, A. (2022). Size, shape and orientation matter: Fast and semi-automatic measurement of grain geometries from 3d point clouds. *Earth Surface Dynamics*, *10*(6), 1211–1232.

Trivedi, S. S., Snehal, K., Das, B., & Barbhuiya, S. (2023). A comprehensive review towards sustainable approaches on the processing and treatment of construction and demolition waste. *Construction and Building Materials*, *393*, 132125.

Trotta, O., Bonifazi, G., Capobianco, G., & Serranti, S. (2021). Recycling-oriented characterization of post-earthquake building waste by different sensing techniques. *Journal of imaging*, *7*(9), 182.

Tuan, N. M., Kim, Y., Lee, J.-Y., & Chin, S. (2022). Automatic stereo vision-based inspection system for particle shape analysis of coarse aggregates. *Journal of Computing in Civil Engineering*, *36*(2), 04021034.

Vegas, I., Broos, K., Nielsen, P., Lambertz, O., & Lisbona, A. (2015). Upgrading the quality of mixed recycled aggregates from construction and demolition waste by using near-infrared sorting technology. *Construction and Building Materials*, *75*, 121–128.

Wang, Z., Afgan, M. S., Gu, W., Song, Y., Wang, Y., Hou, Z., Song, W., & Li, Z. (2021). Recent advances in laser-induced breakdown spectroscopy quantification: From fundamental understanding to data processing. *TrAC Trends in Analytical Chemistry*, *143*, 116385.

Wu, H., Liang, C., Zhang, Z., Yao, P., Wang, C., & Ma, Z. (2023). Utilizing heat treatment for making low-quality recycled aggregate into enhanced recycled aggregate, recycled cement and their fully recycled concrete. *Construction and Building Materials*, *394*, 132126.

Wu, L., Sun, Z., & Cao, Y. (2024). Modification of recycled aggregate and conservation and application of recycled aggregate concrete: A review. *Construction and Building Materials*, *431*, 136567.

Xia, H., & Bakker, M. (2014). Reliable classification of moving waste materials with libs in concrete recycling. *Talanta*, *120*, 239–247.

Yamazaki, I., Kurzak, J., Wu, P., Zounon, M., & Dongarra, J. (2018). Symmetric indefinite linear solver using openmp task on multicore architectures. *IEEE Transactions on Parallel and Distributed Systems*, *29*(8), 1879–1892.

Zhang, C., Hu, M., Di Maio, F., Sprecher, B., Yang, X., & Tukker, A. (2022). An overview of the waste hierarchy framework for analyzing the circularity in construction and demolition waste management in europe. *Science of the Total Environment*, *803*, 149892.

# 3

# In-line Recycled Coarse Aggregates Characterization Using Laser-Induced Breakdown Spectroscopy

*To upcycle End-of-Life (EoL) concrete from demolished buildings, it is essential to efficiently identify the different materials that may contaminate it. The precise identification and classification of materials and contaminants are vital processes for in-line quality inspection of recycled concrete aggregates transported on a conveyor belt. In this study, a total of eight potential contaminants are considered as target contaminant materials in the streams made of coarse and fine aggregates resulting from the upcycling of EoL concrete. These contaminants degrade the quality of the aggregates even at low concentrations, so it is essential to identify the presence of such contaminants along with the main products of recycling which are recycled coarse aggregates (RCA) and recycled fine aggregates (RFA). An efficient method is proposed to identify and classify EoL concrete waste along with RCA and RFA in motion on conveyor belts via laser-induced breakdown spectroscopy (LIBS) coupled with a cluster-based identification algorithm. The model is verified with an accuracy of 0.97, a precision (weighted average) of 0.98, a recall (weighted average) of 0.97, and an F1-score (weighted average) of 0.98 for the validation set, under the optimal conditions. This study suggests that LIBS may be well suited for fast and in-line analysis of recycled concrete aggregates in industrial applications. This approach presents an innovative approach for the quality characterization of secondary materials produced from EoL concrete being transported on conveyor belts, and therefore can be of great value for the processing and high-end utilization of EoL concrete.*

Apart from minor updates, this chapter has been published in Chang et al., 2022.

## 3.1. Introduction

Concrete has long been one of the most popular manufactured construction materials. In the conventional production process, the concrete is usually made using cement and natural aggregates that have well-defined and predictable properties. Therefore, it is possible to foresee the mechanical and durability properties of the produced concrete. In contrast, when concrete is made using recycled aggregates, it is impossible to predict the resulting concrete's mechanical and durability properties because recycled aggregates have variable properties. That is why it is challenging to upcycle End-of-Life (EoL) concrete and close the material loop. Because recycled aggregates are often blended with other construction waste materials, it commonly serves for low-level construction, for example, embankment, sub-base, and leveling of roads (Vegas et al., 2015).

A significant amount of construction work carried out in the 1950s during the post-World War II economic boom is reaching life expectancy in the next few decades, which will lead to a rapid increase in construction and demolition wastes (C&DW), particularly in Europe. A large amount of C&DW cannot be efficiently recycled and is even dumped directly in landfills, causing environmental pollution (Kabirifar et al., 2021; Nanda and Berruti, 2021). Meanwhile, it is expected that the demand for concrete will rise in the coming years, particularly in developing countries (Bonifazi et al., 2018). The gap between supply and demand for concrete will lead to the consumption of large amounts of resources, and the over-mining of raw materials for concrete also adds to the damage to the environment. EoL concrete accounts for the vast majority of C&DW (Lotfi and Rem, 2016), and the most viable solution for EoL concrete is recycling or upcycling. The conventional linear approach to recycling needs to be upgraded to a circular process, that is, secondary raw materials are obtained from EoL concrete for a green and sustainable solution (Mining, 2015). At present, one of the most popular methods for high-grade concrete recycling is the wet process, which produces clean concrete aggregates by washing coarse aggregates but also produces sludge that needs to be disposed of (Zhang et al., 2019). In addition, an innovation project called C2CA (Concrete to Cement and Aggregate, "C2CA Technology", 2024), funded by the European Commission (EC), proposes a dry alternative to the existing wet process by offering an innovative solution called Advanced Dry Recovery (ADR) (Gebremariam et al., 2020). This solution significantly reduces the cost of processing the coarse fraction of high-grade recycled EoL concrete. The complete recycling of EoL concrete can close the building and demolition lifecycle and is of great benefit to the environment in terms of reducing the depletion of natural resources, noise pollution, energy consumption, and dust and gases emissions (Di Maria et al., 2016).

EoL concrete is a material with a highly variable composition. Its composition results from the original application and recipe of primary concrete, how the materials are connected to the building, and the care and measures are taken when the structure is disassembled and dismantled. The main challenge is safeguarding the quality of the secondary aggregates resulting from the recycling of the EoL concrete. It is challenging to keep the demolished concrete as pure material, and it is usually mixed with other building materials such as bricks, cement paste, foam, glass, gypsum, mineral fibers, plastics, and wood, all of which are considered waste and can have impacts on the quality of the resulting recycled concrete. This implies that special technical and organizational

means are required to ensure that the recycled concrete has the same quality as primary concrete, despite the problems mentioned above.

Recycled aggregates are a promising alternative to “Virgin Aggregates”. And one of the main challenging problems affecting the quality of recycled concrete is the presence of different contaminant particles (i.e., bricks, gypsum, wood, plastic, etc.) (Bonifazi et al., 2018) that can severely reduce the strength of the resulting concrete (Silva et al., 2014). When embedded in concrete, organic substances such as wood are unstable when subjected to dry-wet and freeze-thaw cycles (Hansen, 1992). Water-soluble sulfates present in substances such as gypsum can react and may cause expansive reactions (Alexander and Mindess, 2005). In general, the use of crushed waste glass as coarse aggregates leads to a decrease in the mechanical properties of concrete, primarily due to its irregular shape, poor surface characteristics, and high friability (Harrison et al., 2020; Silva et al., 2014). The density of glass is similar to that of stone and bricks, thus complicating its separation, and in addition, non-crystalline metastable silica may undergo alkali-silica reactions (Hansen, 1992). Therefore, when contaminants normally present in EoL concrete waste are absent or below the limits demanded by market standards, the recycled aggregate may be considered "clean" (Lotfi and Rem, 2016; Lotfi et al., 2014; Serranti et al., 2015) so that EoL concrete can be recycled into clean aggregates to close the materials’ loop in the construction sector. To upcycle EoL concrete, contaminants must be identified, monitored, and minimized. It is essential to identify pollutants in secondary materials produced from EoL concrete to signal exceptions in input quality and recycling process conditions and guarantee clean recycled aggregate products, which requires the establishment of an effective classification and quality control system. It is crucial to exploit efficient, reliable, non-destructive, cost-effective sensing technologies to identify contaminants automatically. Also, to facilitate the broader use of recycled aggregates as construction material, it is essential to create transparency on the quality of recycled aggregates through the value chain.

For the recycling process, an important step is the rapid identification of contaminants in EoL concrete waste. Under cumbersome industrial circumstances, this task can be challenging, particularly at high conveyor belt speeds. Nevertheless, given the significance of improving the quality of secondary materials produced from EoL concrete and reducing the contaminants therein, different technologies and procedural systems have been developed to offer unique and feasible approaches. A hyperspectral imaging (HSI) system in the near-infrared range (Serranti et al., 2012) was applied for quality control to recognize the recycled aggregates from different contaminants (Serranti et al., 2015). However, HSI is still not robust enough under harsh industrial conditions. A classification method based on the integration of the laser-induced breakdown spectroscopy (LIBS) spectral emissions (Lotfi et al., 2015; Xia and Bakker, 2014) was proposed for in-line quality inspection, the success of which relies on the quality of the training set and the possibly remaining false positives.

Recently, the use of LIBS has gained more attention in the field of resource recovery. As a simple, rapid, and efficient analytical technique without sampling requirements, LIBS only samples tiny fractions from a target material’s surface by generating a high power density beam using an ultra-short pulse laser (Cremers and Radziemski, 2006; Xia and Bakker, 2014). As the sampled material is ablated, a plasma is formed, result-

ing in the emission of an observable spectrum. A spectrometer can detect or analyze to acquire information on the composition of the molecules and atoms of the raw material (Lasheras et al., 2011; Xia, 2021). Additionally, the advantages of LIBS include the removal of impurities from the sample surface by laser ablation, which decreases their influence on the results; the low cost of analyzing samples compared to other traditional analytical techniques (Yan et al., 2021); the relative simplicity and ease of use of the instrument (Hussain and Gondal, 2013); and the ability to analyze a large number of samples simultaneously in a short time and to detect a wide range of elements (Fernandes Andrade et al., 2021). Consequently, LIBS has been widely applied in the areas of elemental detection (Godoi et al., 2011; Hussain and Gondal, 2013), substance identification (Gondal and Siddiqui, 2007; Völker et al., 2020), and material classification (Castro and Pereira-Filho, 2016; Gottlieb et al., 2017).

Furthermore, there are many studies on combining LIBS and various algorithms for identification and classification, including principal component analysis (PCA) (Junjuri and Gundawar, 2020), scaled conjugate gradient (SCG) (Yang et al., 2020), classification and regression tree (CART) (Moncayo et al., 2015), k nearest neighbor (kNN) (Costa et al., 2017), soft independent modeling of class analogy (SIMCA) (Pease and Tchakerian, 2014), linear discriminant analysis (LDA) (Gaudiuso et al., 2018), partial least squares for discriminant analysis (PLS-DA)(Xia and Bakker, 2014), support vector machine (SVM) (Li et al., 2018), factorial discriminant analysis (FDA) (Baskali-Bouregaa et al., 2020), artificial neural networks (ANN) (Junjuri et al., 2020), and convolutional neural network (CNN) (He et al., 2020). Nevertheless, it is still necessary to increase the precision and sensitivity of this technique. To make algorithms based on LIBS widely available in terms of efficiency and detection limits, several methodological improvements remain to be made.

In this study, an EoL concrete waste identification system based on LIBS was developed, which targeted the precise and automated identification of contaminants. The system emulated the actual industrial situation as much as possible, with each material passing underneath LIBS through a conveyor belt. The LIBS single-shot spectra of each constituent of EoL concrete were collected. Based on these spectral data, a cluster-based classification algorithm was used to create separate spectral databases for each material, allowing for precise identification of the constituents according to a single-shot spectrum. In addition, the effects of different data pre-processing methods and parameters were investigated.

## 3.2. Chemometric Methods

In this research, the chemometric methods combining principal component analysis and chi-square distribution are used as a classification model (Figure 3.1) for evaluating single-shot spectral data. Their rationales are introduced in detail herewith.

### 3.2.1. Principal Component Analysis

As an unsupervised dimensionality reduction method, PCA used for data visualization and pattern detection of raw data, is the most widely used multivariate data analysis algorithm in the LIBS community (Pořízka et al., 2018). Although the thousands of di-

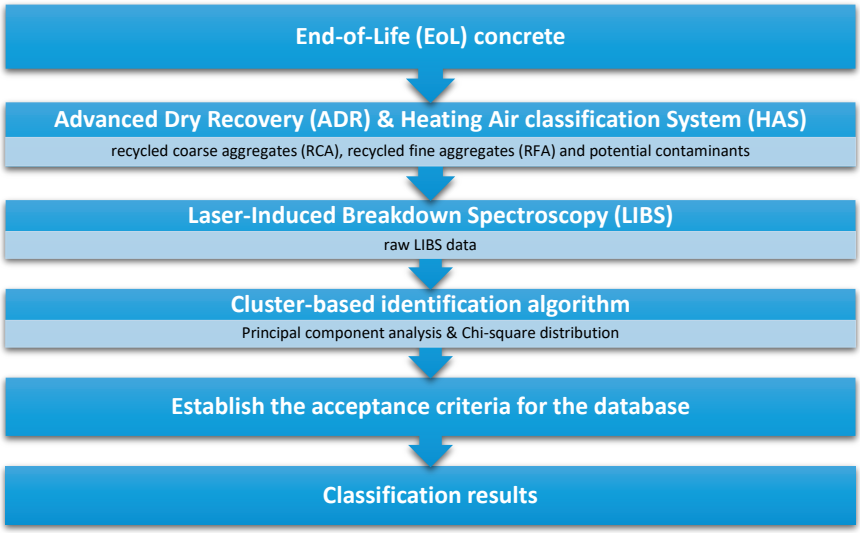


Figure 3.1: Scheme for establishing the cluster-based identification model



mensions of the raw spectral data preserve all the information simultaneously, much noise is also retained along with it, resulting in data redundancy and leading to an increased computational effort. Therefore, the high-dimensional raw spectral data needs to be dimensionally reduced.

A database $x[s] = (x_1, x_2, \ldots, x_N)\,[s]; (s = 1, 2, \ldots, S)$ Laser shot of $S$ emission spectra for a specific material $X$ is generated, where $x_i\,(i = 1, \ldots, N)$ is the intensity of plasma emission at a wavelength $\lambda_i\,(i = 1, 2, \ldots, N)$, $N$ is the number of spectral wavelengths recorded by the spectrometer. Thus, each spectrum can be considered as a point in an $N$-dimensional space. In this case, the thousands of emission spectra of material $X$ form a cloud in this space that resembles a multi-dimensional ellipsoid. Different materials appear as different clouds of points. For a new spectrum of an unknown material, the classification challenge is to locate the cloud to which it belongs or mark it as unrecognizable if it is too far away from any documented cloud in the database.

Due to a significant amount of variation in particle properties or plasma formation conditions, each spectrum $x[s]$ of material $X$ differs from the centroid $\bar{x}$ of the cluster, then the spectral cloud as a whole represents a multi-dimensional distribution with the centroid $\bar{x}$ as the mean. There is always the possibility to scale (transform) and rotate the axes of the coordinate system, aiming for a simpler multi-dimensional normal distribution of the points in the cluster. Notably, it is always possible to have a new, rotated orthonormal coordinate system with axes aligned along $N$ unit vectors: $e_k = (e_{k1}, e_{k2}, \ldots, e_{kN})\,; (k = 1, 2, \ldots, N)$. Then, in this new coordinate system, the multi-dimensional normal distribution is equivalent to $N$ independent one-dimensional normal distributions, one for each new axis. Consequently, the spectrum of material $X$ in the database has been transformed into the new coordinate system:

$$\xi[s] = (\xi_1, \xi_2, \ldots, \xi_N)[s] = (x[s] \cdot e_1, x[s] \cdot e_2, \ldots, x[s] \cdot e_N) \tag{3.1}$$

Then the center point or average of the spectra of material $X$ is:

$$\bar{\xi} = \left(\overline{\xi_1}, \overline{\xi_2}, \ldots, \overline{\xi_N}\right) = (\bar{x} \cdot e_1, \bar{x} \cdot e_2, \ldots, \bar{x} \cdot e_N) \tag{3.2}$$

And the deviations of the spectra concerning the center point in the new system are:



$$\Delta\xi[s] = (\Delta\xi_1, \Delta\xi_2, \ldots, \Delta\xi_N)[s] = ((x[s] - \bar{x}) \cdot e_1, (x[s] - \bar{x}) \cdot e_2, \ldots, (x[s] - \bar{x}) \cdot e_N) \tag{3.3}$$

Thus, the components $\Delta\xi_g[s]\,(g = 1, 2, \ldots, N)$ and $\Delta\xi_l[s]\,(l = 1, 2, \ldots, N)$ of the set of spectral deviations along these new axes are mutually uncorrelated with the centroids, shown in Eq. 3.4:

$$\frac{1}{S}\sum_{1}^{S} \Delta\xi_g[s]\Delta\xi_l[s] = \begin{cases} \overline{\Delta\xi_g^2} & \text{if } g = l \\ 0 & \text{if } g \neq l \end{cases} \tag{3.4}$$

Moving back to the original coordinate system, Eq. 3.4 turns into Eq. 3.5:

$$\frac{1}{S}\sum_{1}^{S} \left[(x[s] - \bar{x}) \cdot e_g\right][(x[s] - \bar{x}) \cdot e_l] = \overline{\Delta\xi_g^2}\,\delta_{gl} \tag{3.5}$$

Eq. 3.5 is used to find the appropriate set of new unit vectors $e_k$. The new axes are chosen in such an order that the variances $\overline{\Delta\xi_g^2}$ of the multi-dimensional normal distribution along the new axes go from high to low values, so that the first one, $e_1$, coincides with the maximum variance $\overline{\Delta\xi_1^2}$, etc. It is worth noting that not all of these N dimensions are essential for the subsequent categorization process. Only a much lower number $n$ of dimensions needs to be considered. This entails that information from parts of the emission spectra that do not have a large impact (are zero or have little variation except for noise) is omitted. In contrast, the potentially interesting information is presented in the preceding dimensions of the new coordinate system. The significant information is filtered out by projecting the raw spectral data into a low-dimensional space. It is worth mentioning that the value of $n$ will have a substantial impact on the classification accuracy. Therefore, after PCA, the spectral database of S emission spectra for material $X$ will record a number $n[X]$, a set of unit vectors $e_m[X]\,(m = 1, 2, \ldots, n[X])$, a set of vectors of principal components $(\xi_1, \xi_2, \ldots, \xi_{n[X]})[s]$, and a center point or average $\left(\overline{\xi_1}, \overline{\xi_2}, \ldots, \overline{\xi_{n[X]}}\right)$ along with variances $\overline{\Delta\xi_m^2}$, to describe the multi-dimensional normal distribution of the S spectra in the database.

### 3.2.2. CHI-SQUARE DISTRIBUTION

If $Z_1, Z_2, \ldots, Z_j$ are $j$ independent standard normal distribution $N(0,1)$ random variables, then the sum of their squares $W_j = Z_1^2 + Z_2^2 + \cdots + Z_j^2$ is said to have a chi-square $(\chi^2)$ distribution with $j$ degrees of freedom, which is often expressed as $W_j \sim \chi^2(j)$ or $W_j \sim \chi_j^2$ (Lancaster and Seneta, 2005). The obtained principal components after data

processing can be regarded as chi-square distributions, and then a cluster-based identification algorithm will be established accordingly.

After transforming the spectrum of material $X$ to the new set of coordinates and restricting to the first $n[X]$ dimensions, $(\xi_1, \xi_2, \ldots, \xi_{n[X]})[s]$ is a realization of the multi-dimensional normal distribution for the principal components of spectra of material $X$. This means that each component $\xi_m$ is normally distributed with mean $\overline{\xi_m}$ and variance $\overline{\Delta\xi_m^2}$. Therefore, after $z$-score standardization, each value:

$$Z_m = \frac{\xi_m - \overline{\xi_m}}{\sqrt{\overline{\Delta\xi_m^2}}} \tag{3.6}$$



is normally distributed with a mean of 0 and a variance of 1. This implies that if it is not known which material was hit by the laser, then the spectrum $x[s]$ can be accepted as originating from material $X$ in case it is highly probable that the set of values $Z_m$ result from $n[X]$ independent standard normal distributions. According to the chi-square distribution, the value:

$$\chi^2[s] = \sum_1^{n[X]} Z_m^2 = \sum_1^{n[X]} \frac{(\xi_m - \overline{\xi_m})^2}{\overline{\Delta\xi_m^2}} \tag{3.7}$$

is used to check whether it is small enough to come from the $\chi^2_{n[X]}$-distribution. Each $\chi^2[s]$ can be translated into the probability $P$-value which is the $p[s]$ of $\chi^2_{n[X]}$-distribution. The larger the $\chi^2[s]$, the smaller the $P$-value $p[s]$, the higher the confidence level. $P$-values lower than the selected significance level indicate statistical significance. By setting the significance level for material $X$ as acceptance criteria, which can be determined according to the $P$-value $p[X]$ and the associated value of $\chi^2[X]$ for material $X$, the fraction of all spectra with $P$-value $p[s]$ greater than $p[X]$ or $\chi^2[s]$ less than $\chi^2[X]$ will be considered as deriving from particles of material $X$. A small value of the threshold $P$-value $p[X]$ indicates that most or nearly all spectra from material $X$ will be accepted, but it is also possible that spectra from other materials will be misclassified as material $X$. A large value of the threshold $P$-value $p[X]$ implies that many spectra will be classified as not accepted, so these spectra do not contribute to the quality analysis. The issue is to find a good compromise.

## 3.3. EXPERIMENT AND DATA PRE-PROCESSING

### 3.3.1. EXPERIMENTAL SETUP

As shown in Figure 3.2, the LIBS system consisted of a laboratory-scale conveyor belt, a compact optical module, and an Nd : YAG nanosecond pulse laser for the present study. The Nd : YAG nanosecond pulse laser (TRLi DPSS Series) emitted at a wavelength of 1064 nm, a pulse width of 8-10 ns, a frequency of 100 Hz, and laser energy of 170 mJ per pulse. With a 300 mm focal length lens, the laser was focused vertically onto the sample surface to produce laser-induced plasma. The focusing lens collected the plasma emission spectra and then coupled them to an optical fiber attached to a spectrometer (SPECTRAL Industries, Iris Echelle spectrometer). A delay time of 1.5 $\mu$s was employed for the


Figure 3.2: LIBS system

acquisition of the spectra to avoid interference from continuous laser-induced plasma radiation. The timing of the LIBS experiment was triggered with a digital delay pulse generator (Quantum Composers). The experiments were performed under atmospheric conditions. The speed of the conveyor belt was variable and could reach a maximum speed of 50 cm/s. Samples were moved at a constant speed of 20 cm/s to simulate the transport of materials on a typical feed conveyor belt. At 100 Hz, the laser shoots every 2 mm on the sample stream.

### 3.3.2. EOL CONCRETE SAMPLES

Several samples of demolition wastes were collected from demolition sites in the Netherlands. Due to selective demolition, the resulting EoL concrete was clean. Other demolition wastes such as bricks and glasses were separately handpicked from demolition sites. The coarse and fine recycled aggregates were processed by using C2CA technologies (Gebremariam et al., 2020), where the crushed 0-16 mm was treated with ADR and classified as the recycled coarse aggregates (RCA) (4-16 mm), and the fine fraction (0-4 mm). The fine fraction of recycled aggregates was further treated with Heating Air classification System (HAS) to produce the recycled fine aggregates (RFA) and recycled cement paste-rich powder. Recycled mineral fibers were collected from demolition sites and mechanically ground. The flat glass was also collected from demolition sites and broken into pieces. Recycled gypsum was also in its ground form, while representative forms of foam, wood, and plastics were used.

### 3.3.3. DATA PRE-PROCESSING

In general, appropriate pre-processing methods can improve models' classification results by reducing the spectral fluctuations between various measurements (Zeaiter et

al., 2006). This research performed no spectral background subtraction or additional spectral filtering methods on the raw spectral data. This is to avoid losing the spectral information of the laser-induced plasma emission after 1.5 $\mu$s since the laser incidence. There were a total of 2,400 single-shot spectra per material at the wavelength range from 179.4 nm to 1199.4 nm with a total of 11790 intensity values per shot. To reduce the accidental error, the average of every adjacent 5 intensity values (Averaged by 5) and the average of every adjacent 10 intensity values (Averaged by 10) were calculated, compared, and evaluated. In addition, Box-Cox transformation was performed to make the intensity values converge to normal distributions. The spectral dataset for each material was divided into training and validation (ratio 9:1): 240 single-shot spectra were randomly selected from each material and combined into a dataset of 2400 single-shot spectra for validation. The remaining 2160 single-shot spectra per material were used for training to build a standard library for each material.



## 3.4. RESULTS AND DISCUSSION

### 3.4.1. OPTIMIZATION OF PRE-PROCESSING METHODS

Taking the spectral data of bricks as an example, the spectral data using five pre-processing methods (Box-Cox transformation, Averaged by 5, Averaged by 10, Averaged by 5 & Box-Cox transformation, and Averaged by 10 & Box-Cox transformation) were subjected to PCA and compared with the processing methods of the original spectral data. After PCA dimensionality reduction of the brick spectral data, their cumulative explained variance is calculated. The various pre-processing methods increased the explained variance of the first principal component to different degrees. Among the effects resulting from the single-step pre-processing methods, the Box-Cox transformation method showed the most significant improvement compared to the two averaging methods. The difference between the impacts caused by the two averaging methods was not significant. The superimposed pre-processing methods had a greater influence than the single-step pre-processing methods, but the differences between them were not significant. As for the cumulative explained variance, the first 10 principal components of all pre-processing methods could represent almost all information of the spectra. The cumulative explained variance of the first 50 principal components of all pre-processing methods was greater than 0.999, indicating that these principal components were sufficient to cover most of the brick spectra information. The Box-Cox transformation method had a negative impact compared to the original spectral data, while both averaging techniques improved the impact. The averaging methods combined with the Box-Cox transformation method had a negative effect. However, the two superimposed pre-processing methods did not differ much from each other.

It is worth mentioning that, in contrast to the conventional spectral analysis models, this identification model is not mainly dependent on the wave peaks in the LIBS spectra but the overall distribution of the spectra. Therefore, the wave peaks are not analyzed in detail in this paper.

The training set of bricks was used to build its unique database, and the classification results with different pre-processing methods are compared. Because only the spectra of bricks were used as a training data set, ideally, all spectra should be identified as coming

from bricks. However, because a uniform p-value was set (for comparison purposes), some spectra were identified as outliers i.e. not coming from bricks. Although the averaging of the raw spectral data could effectively improve the explained variance, it did not affect the discrimination of the training set. In contrast, the Box-Cox transformation method could slightly increase the classification accuracy of the training set.

Furthermore, the validation set of all materials was used to compare the pre-processing methods. When identifying whether a shot was from bricks, there was little difference between the identification results of each pre-processing method, with the Box-Cox transformation method being slightly better. And when identifying whether a shot was from the outliers, the Box-Cox transformation method improved the identification accuracy significantly. In contrast, the technique that averaged every five intensity values was slightly better than the method that averaged every ten intensity values.



Based on the classification results of the validation set, the impact of each pre-processing method on the final results of the model is evaluated. Using the raw spectral data, the model showed the worst accuracy, while the model using Box-Cox transformation and Averaged by 5 & Box-Cox transformation methods showed the best accuracy, precision (weighted average), recall (weighted average), and F1-score (weighted average) all reaching 0.99. Overall, the Averaged by 5 & Box-Cox transformation pre-processing method was selected to reduce the number of computer operations while achieving better accuracy.

### 3.4.2. Optimization of Acceptance Criteria

As previously mentioned, the number of principal components is the main parameter that affected the final classification accuracy of the model. Combining the training and validation sets, 3D plots of the first three principal components for each material are shown in Figure 3.2. Each point represents a single-shot spectrum. Red dots indicate single-shot spectra of certain material in the training set, green dots indicate single-shot spectra of nine materials other than that material in the validation set, and black dots indicate single-shot spectra of that material in the validation set. There were significant differences in the results between the different materials, and it was feasible to differentiate the single-shot spectra from various materials based on the transformed principal components. Different single-shot spectra of the same type of material appeared clustered. For the remaining nine materials, the data points distributed in space were more or less mixed. So each material could create its own exclusive database separately using the red dots and identify and classify other materials accordingly. However, choosing too few principal components may result in a poorly differentiated database, with overlap between different materials. And choosing too many may result in a classification model with a too high threshold that excludes too many points that should have belonged to that material. Thereby, the optimum number of principal components for each material needed to be selected.

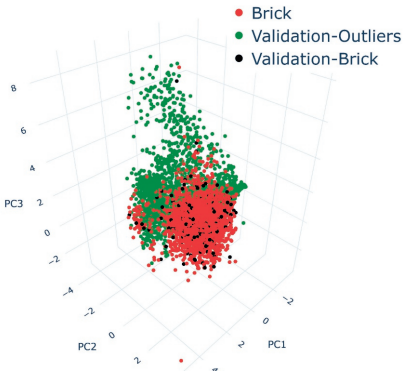


(a) Brick

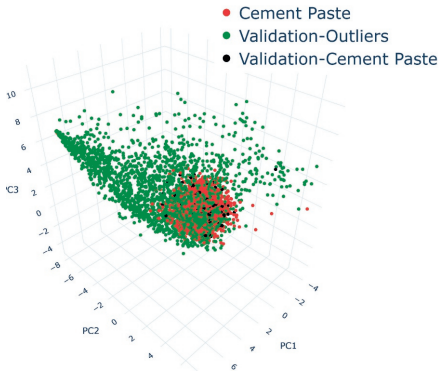


(b) Cement Paste

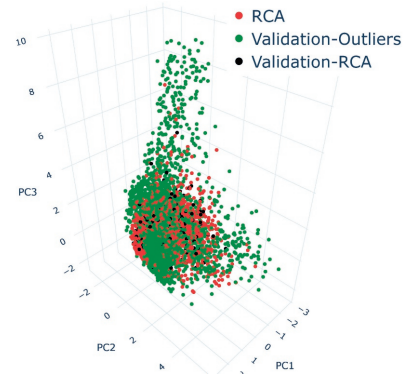


(c) RCA

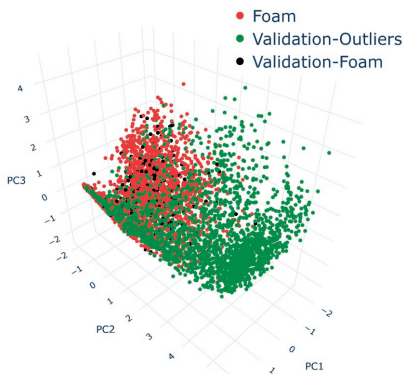


(d) Foam

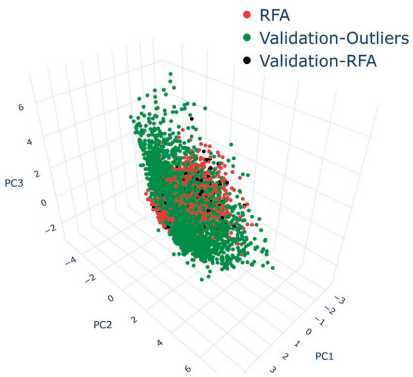


(e) RFA

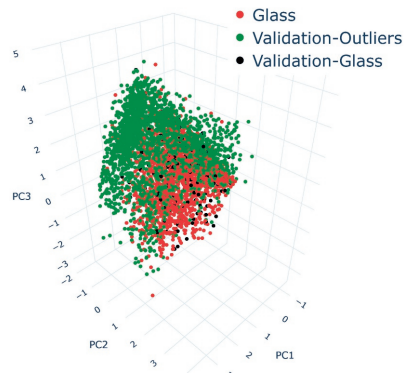


(f) Glass

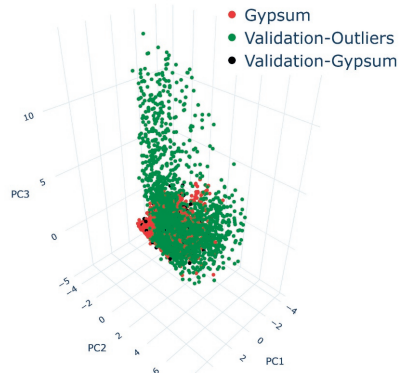


(g) Gypsum

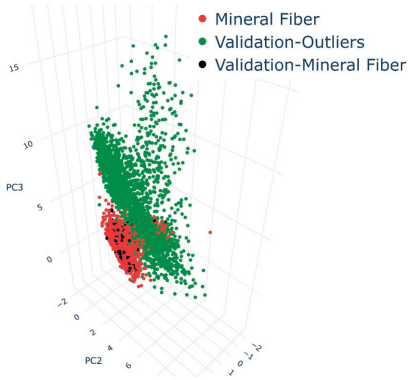


(h) Mineral Fibers

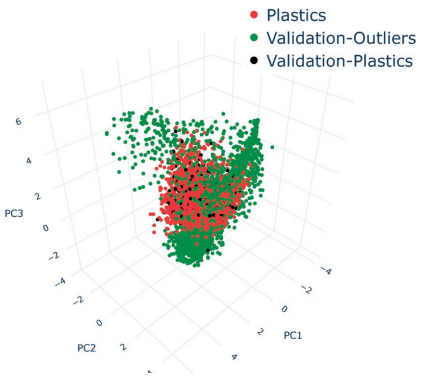


(i) Plastics

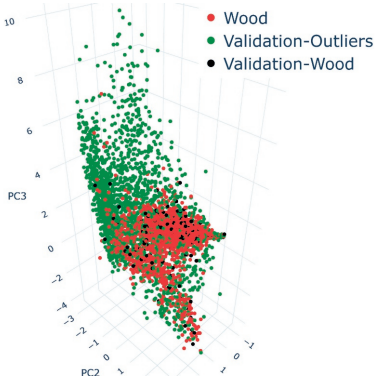


(j) Wood

Figure 3.2: 3D plots of the first three principal components for each material

In addition, the probability $P$-value of the chi-square distribution also played an essential role in the accuracy of the final model. Thus, combining the number of principal components and the final P-value was necessary to extract the optimal pairing. After several rounds of attempts, the best matches for different materials are selected.

### 3.4.3. DISCUSSION ON FURTHER OPTIMIZATION OF THE ALGORITHM

Once the acceptance criteria and databases for each material were created, the validation data set was used to check the accuracy of the entire package of models. When comparing the validation data set with the established material databases, it could be found that some single-shot spectra were accepted by two or even three material databases. Thus, resulting in overlaps for which the belongings of these spectra could not be determined. Among them, the highest number of overlaps was between cement paste and RCA, with the number reaching 50. This was due to the presence of adhering cement

paste on the surface of the RCA, which made it difficult to distinguish between the two. To determine the final attribution of the overlapping spectra, their P-values could be made use of. In this case, the P-values of each spectrum obtained in the overlapped material databases should be compared, and the material database corresponding to the maximum P-value is the one to which the spectrum belonged.

Moreover, after evaluating all spectra in the validation set through all material databases, some single-shot spectra were rejected by all material databases. As a result, the belongings of these spectra could not be determined. In this case, an optional method is to compare the *P*-values. Each of these spectra could obtain a corresponding P-value from each of the ten material databases. The spectrum was then classified into a material database corresponding to the largest P-value by comparing the magnitude of the ten P-values for each spectrum. However, among these spectra, some spectra remained with a P-value of 0 in all ten material databases and could not be classified according to their P-values. Eventually, these spectra were classified as unrecognizable spectra.



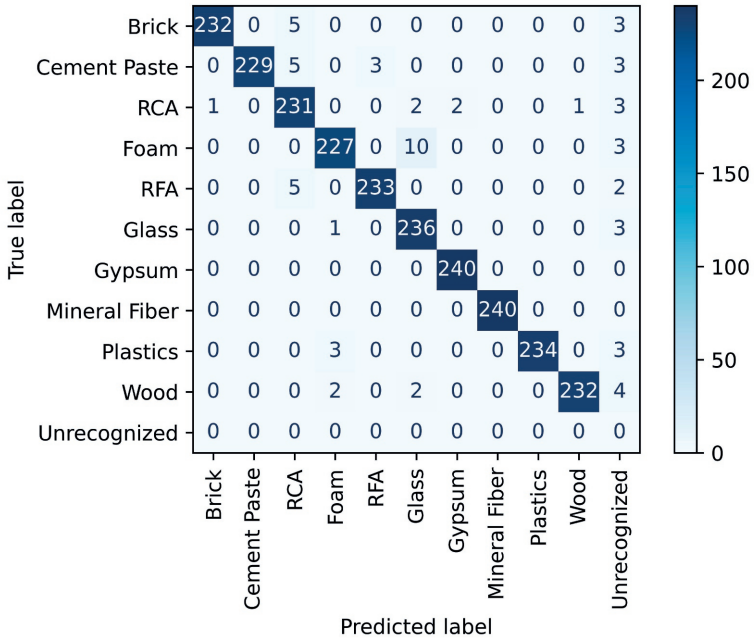


Figure 3.3: Confusion matrix of the validation set

The final classification results are shown in Figure 3.3. There were still 0-4 single-shot spectra of each material that could not be distinguished. Foam and glass were misidentified the most, with up to 10 single-shot spectra of foam being mistaken for glass, which mainly resulted in a precision of 0.94 for glass. The classification report of the validation set is shown in Table 3.1. An increase in the value of accuracy, precision, or recall indicated that the model had a better classification performance. Wherein the F1 score is the

harmonic mean of the precision and recall, which are mutually constrained. The higher the value of the F1 score is close to 1, the better the model's classification performance is. The accuracy of the whole model reached 0.97, with the precision (weighted average) of 0.98, the recall (weighted average) of 0.97, and the F1-score (weighted average) of 0.98.

Table 3.1: Classification report of the validation set

| | **Precision** | **Recall** | **F1-score** | **Support** |
|---|---|---|---|---|
| Brick | 1.00 | 0.97 | 0.98 | 240 |
| Cement Paste | 1.00 | 0.95 | 0.98 | 240 |
| RCA | 0.94 | 0.96 | 0.95 | 240 |
| Foam | 0.97 | 0.95 | 0.96 | 240 |
| RFA | 0.99 | 0.97 | 0.98 | 240 |
| Glass | 0.94 | 0.98 | 0.96 | 240 |
| Gypsum | 0.99 | 1.00 | 1.00 | 240 |
| Mineral Fibers | 1.00 | 1.00 | 1.00 | 240 |
| Plastics | 1.00 | 0.97 | 0.99 | 240 |
| Wood | 1.00 | 0.97 | 0.98 | 240 |
| Unrecognized | 0.00 | 0.00 | 0.00 | 0 |
| weighted avg | 0.98 | 0.97 | 0.98 | 240 |

The results indicated that the combination of LIBS and cluster-based identification algorithm enabled the precise identification of contaminants in secondary materials produced from EoL concrete. Materials with similar appearance and composition could be distinguished almost completely. The graded materials could be used in different classes of construction work to improve their utilization.

Taking bricks as an example, the raw spectral data of the validation set were classified as bricks, unrecognized, and misclassified spectra, respectively. From Figure 3.4, it could be found that the unrecognized spectra were usually caused by the presence of certain peaks much more significant than typical values (pink lines). In contrast, the misclassified spectra had an overall scale much smaller than typical values and were hidden below the typical values. Thus, when translating a spectrum to a point in multi-dimensional space, the point from the unrecognized spectrum was usually kept away from the ellipsoid of the brick database, while the point from the misclassified spectrum was contained within the ellipsoid of the brick database. This explains why these spectra were classified as unrecognized spectra and misclassified spectra.

There are also a few recommendations for this identification model. Before using the model for identification, it should be calibrated. Seasonal variations and slow, device-related changes over a long time can produce a drift in the database center point itself.

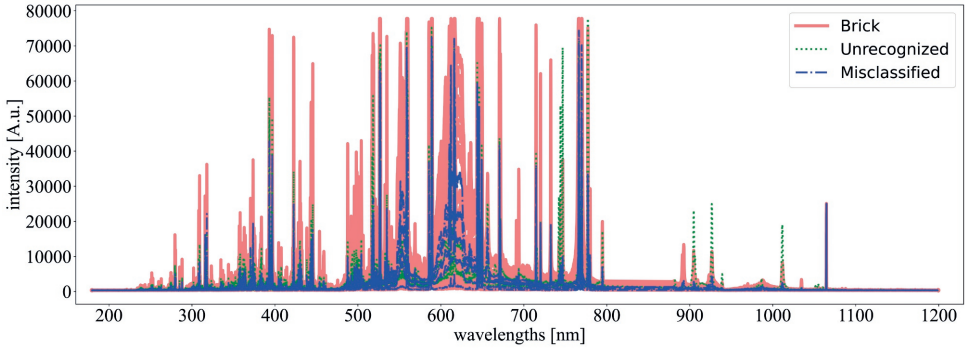


Figure 3.4: The raw spectral data of the validation set with classification results

This part of the calibration must be done continuously while the LIBS system is operating.

## 3.5. CONCLUSION

Proposed was a reliable identification technique based on the LIBS spectral emissions for secondary materials produced from EoL concrete in motion. Object material sourced from concrete demolition waste was sampled with a laser in the air. Particular attention was paid to reproducing the working conditions that the feed was experiencing moving on a conveyor belt in recycling practice as closely as possible. An investigation of the method was carried out to analyze the technique's ability to categorize spectra. Firstly different pre-processing methods were used, out of which the Averaged by 5 & Box-Cox transformation method reached the most reliable results. To avoid losing any information, no spectral background subtraction or other sorts of spectral filtering was applied to the raw spectral data. Then, the study of the best match between the number of principal components and P-values for each material was initiated, leading to the creation of a database for each material. The overall accuracy of the model reached 0.97 according to the results of the validation set classification. This approach has excellent accuracy for single-shot LIBS spectra of material in motion compared to conventional qualitative LIBS techniques. Moreover, the proposed methodology does not require the characterization of individual wave peaks appearing in the LIBS spectra. Although the proposed model is sensitive to drift and computationally intensive, it is still worth trying because it is highly reliable in identifying the correct material. Besides, it can be corrected relatively easily for slowly changing conditions. It works better in a reduced dimensional space of variables, reflecting that most of the thousands of spectral data do not contain essential information.

The achieved results demonstrate that the cluster-based classification algorithm is a practical technique for the rapid and online analysis of EoL concrete in motion and can serve as a new method and technique for the industrial selection and quality control of secondary materials produced from EoL concrete. Although only single material streams are sampled to test the quality characterization model in this research, this val-

idates the feasibility of employing the technique to identify contaminants in secondary materials and provides the basis for future tests of mixed product-waste streams. The ultimate goal of the recycled aggregate quality assessment is to provide users with sufficient information about the quality of the product and how to use the material in the best way for a particular application. It is also worth noting that further studies on the levels and grain size distribution of contaminants are needed, which requires finding a good technique to measure and calculate them directly or indirectly.

# BIBLIOGRAPHY


Alexander, M., & Mindess, S. (2005). *Aggregates in concrete*. CRC Press.

Baskali-Bouregaa, N., Milliand, M.-L., Mauffrey, S., Chabert, E., Forrestier, M., & Gilon, N. (2020). Tea geographical origin explained by libs elemental profile combined to isotopic information. *Talanta*, *211*, 120674.

Bonifazi, G., Palmieri, R., & Serranti, S. (2018). Evaluation of attached mortar on recycled concrete aggregates by hyperspectral imaging. *Construction and Building Materials*, *169*, 835–842.

*C2ca technology* [Accessed: 2024-08-11]. (2024). https://www.c2ca.tech/

Castro, J. P., & Pereira-Filho, E. R. (2016). Twelve different types of data normalization for the proposition of classification, univariate and multivariate regression models for the direct analyses of alloys by laser-induced breakdown spectroscopy (libs). *Journal of Analytical Atomic Spectrometry*, *31*(10), 2005–2014.

Chang, C., Di Maio, F., Rem, P., Gebremariam, A. T., Mehari, F., & Xia, H. (2022). Cluster-based identification algorithm for in-line recycled concrete aggregates characterization using laser-induced breakdown spectroscopy (libs). *Resources, Conservation and Recycling*, *185*, 106507.

Costa, V. C., Aquino, F. W. B., Paranhos, C. M., & Pereira-Filho, E. R. (2017). Identification and classification of polymer e-waste using laser-induced breakdown spectroscopy (libs) and chemometric tools. *Polymer Testing*, *59*, 390–395.

Cremers, D. A., & Radziemski, L. J. (2006). History and fundamentals of libs. *Laser Induced Breakdown Spectroscopy: Fundamentals and Applications*, 9–16.

Di Maria, F., Bianconi, F., Micale, C., Baglioni, S., & Marionni, M. (2016). Quality assessment for recycling aggregates from construction and demolition waste: An image-based approach for particle size estimation. *Waste management*, *48*, 344–352.

Fernandes Andrade, D., Pereira-Filho, E. R., & Amarasiriwardena, D. (2021). Current trends in laser-induced breakdown spectroscopy: A tutorial review. *Applied Spectroscopy Reviews*, *56*(2), 98–114.

Gaudiuso, R., Ewusi-Annan, E., Melikechi, N., Sun, X., Liu, B., Campesato, L. F., & Merghoub, T. (2018). Using libs to diagnose melanoma in biomedical fluids deposited on solid substrates: Limits of direct spectral analysis and capability of machine learning. *Spectrochimica Acta Part B: Atomic Spectroscopy*, *146*, 106–114.

Gebremariam, A. T., Di Maio, F., Vahidi, A., & Rem, P. (2020). Innovative technologies for recycling end-of-life concrete waste in the built environment. *Resources, Conservation and Recycling*, *163*, 104911.

Godoi, Q., Leme, F. O., Trevizan, L. C., Pereira Filho, E. R., Rufini, I. A., Santos Jr, D., & Krug, F. J. (2011). Laser-induced breakdown spectroscopy and chemometrics

for classification of toys relying on toxic elements. *Spectrochimica Acta Part B: Atomic Spectroscopy*, *66*(2), 138–143.

Gondal, M. A., & Siddiqui, M. N. (2007). Identification of different kinds of plastics using laser-induced breakdown spectroscopy for waste management. *Journal of Environmental Science and Health Part A*, *42*(13), 1989–1997.

Gottlieb, C., Millar, S., Grothe, S., & Wilsch, G. (2017). 2d evaluation of spectral libs data derived from heterogeneous materials using cluster algorithm. *Spectrochimica Acta Part B: Atomic Spectroscopy*, *134*, 58–68.

Hansen, T. C. (1992). *Recycling of demolished concrete and masonry*. CRC Press.

Harrison, E., Berenjian, A., & Seifan, M. (2020). Recycling of waste glass as aggregate in cement-based materials. *Environmental Science and Ecotechnology*, *4*, 100064.

He, Y., Zhao, Y., Zhang, C., Li, Y., Bao, Y., & Liu, F. (2020). Discrimination of grape seeds using laser-induced breakdown spectroscopy in combination with region selection and supervised classification methods. *Foods*, *9*(2), 199.

Hussain, T., & Gondal, M. (2013). Laser induced breakdown spectroscopy (libs) as a rapid tool for material analysis. *Journal of Physics: Conference Series*, *439*(1), 012050.

Junjuri, R., Gummadi, A. P., & Gundawar, M. K. (2020). Single-shot compact spectrometer based standoff libs configuration for explosive detection using artificial neural networks. *Optik*, *204*, 163946.

Junjuri, R., & Gundawar, M. K. (2020). A low-cost libs detection system combined with chemometrics for rapid identification of plastic waste. *Waste Management*, *117*, 48–57.

Kabirifar, K., Mojtahedi, M., Wang, C. C., & Tam, V. W. (2021). Effective construction and demolition waste management assessment through waste management hierarchy; a case of australian large construction companies. *Journal of cleaner production*, *312*, 127790.

Lancaster, H. O., & Seneta, E. (2005). Chi-square distribution. *Encyclopedia of biostatistics*, *2*.

Lasheras, R., Bello-Galvez, C., Rodriguez-Celis, E., & Anzano, J. (2011). Discrimination of organic solid materials by libs using methods of correlation and normalized coordinates. *Journal of hazardous materials*, *192*(2), 704–713.

Li, X., Yang, S., Fan, R., Yu, X., & Chen, D. (2018). Discrimination of soft tissues using laser-induced breakdown spectroscopy in combination with k nearest neighbors (knn) and support vector machine (svm) classifiers. *Optics & laser technology*, *102*, 233–239.

Lotfi, S., Deja, J., Rem, P., Mróz, R., van Roekel, E., & van der Stelt, H. (2014). Mechanical recycling of eol concrete into high-grade aggregates. *Resources, conservation and Recycling*, *87*, 117–125.

Lotfi, S., & Rem, P. (2016). Recycling of end of life concrete fines into hardened cement and clean sand. *Journal of Environmental Protection*, *7*(6), 934–950.

Lotfi, S., Di Maio, F., Xia, H., Serranti, S., Palmieri, R., Bonifazi, G., et al. (2015). Assessment of the contaminants level in recycled aggregates and alternative new technologies for contaminants recognition and removal. In *Emabm 2015. proceedings of the 15th euroseminar on microscopy applied to building materials* (pp. 319–331, Vol. 1). Delft University of Technology.

Mining, U. (2015). Urban mining: Concepts, terminology, challenges. *Waste Manag*, *45*, 1–3.

Moncayo, S., Manzoor, S., Navarro-Villoslada, F., & Caceres, J. (2015). Evaluation of supervised chemometric methods for sample classification by laser induced breakdown spectroscopy. *Chemometrics and Intelligent Laboratory Systems*, *146*, 354–364.

Nanda, S., & Berruti, F. (2021). Municipal solid waste management and landfilling technologies: A review. *Environmental chemistry letters*, *19*(2), 1433–1456.

Pease, P., & Tchakerian, V. (2014). Source provenance of carbonate grains in the wahiba sand sea, oman, using a new libs method. *Aeolian Research*, *15*, 203–216.

Pořízka, P., Klus, J., Képeš, E., Prochazka, D., Hahn, D. W., & Kaiser, J. (2018). On the utilization of principal component analysis in laser-induced breakdown spectroscopy data analysis, a review. *Spectrochimica Acta Part B: Atomic Spectroscopy*, *148*, 65–82.

Serranti, S., Gargiulo, A., & Bonifazi, G. (2012). Classification of polyolefins from building and construction waste using nir hyperspectral imaging system. *Resources, Conservation and Recycling*, *61*, 52–58.

Serranti, S., Palmieri, R., Bonifazi, G., et al. (2015). Quality control of recycled aggregates from demolition waste by advanced sensing technology. *SARDINIA...*

Silva, R., De Brito, J., & Dhir, R. (2014). Properties and composition of recycled aggregates from construction and demolition waste suitable for concrete production. *Construction and Building Materials*, *65*, 201–217.

Vegas, I., Broos, K., Nielsen, P., Lambertz, O., & Lisbona, A. (2015). Upgrading the quality of mixed recycled aggregates from construction and demolition waste by using near-infrared sorting technology. *Construction and Building Materials*, *75*, 121–128.

Völker, T., Millar, S., Strangfeld, C., & Wilsch, G. (2020). Identification of type of cement through laser-induced breakdown spectroscopy. *Construction and Building Materials*, *258*, 120345.

Xia, H. (2021). Sensor-based quality inspection of secondary resources: Laser-induced breakdown spectroscopy.

Xia, H., & Bakker, M. (2014). Reliable classification of moving waste materials with libs in concrete recycling. *Talanta*, *120*, 239–247.

Yan, B., Liang, R., Li, B., Tao, J., Chen, G., Cheng, Z., Zhu, Z., & Li, X. (2021). Fast identification and characterization of residual wastes via laser-induced breakdown spectroscopy and machine learning. *Resources, Conservation and Recycling*, *174*, 105851.

Yang, Y., Li, C., Liu, S., Min, H., Yan, C., Yang, M., & Yu, J. (2020). Classification and identification of brands of iron ores using laser-induced breakdown spectroscopy combined with principal component analysis and artificial neural networks. *Analytical Methods*, *12*(10), 1316–1323.

Zhang, C., Hu, M., Dong, L., Gebremariam, A., Miranda-Xicotencatl, B., Di Maio, F., & Tukker, A. (2019). Eco-efficiency assessment of technological innovations in high-grade concrete recycling. *Resources, Conservation and Recycling*, *149*, 649–663.

# 4

# 3D Surface Analysis to Assess Particle Size Distribution in Unscreened Recycled Coarse Aggregates for Quality Assurance

*Efficiently measuring and optimizing the particle size distribution (PSD) of recycled coarse aggregates (RCA) is essential for ensuring their consistent quality and usability in high-performance concrete production. Unlike primary coarse aggregates, which exhibit minimal quality fluctuation over extended periods and require infrequent testing, RCA quality varies significantly within shorter intervals (hourly or per truckload). This variation necessitates a precise and automated method for quality assessment, traditionally absent in primary aggregate processing, thus limiting RCA's broader adoption. This study introduces a rapid, automated, and non-contact 3D surface analysis technology to assess and optimize the PSD of unscreened RCA as they move along a conveyor belt. The RCA particles, ranging from 4.0 to 16.0 mm, exhibit different shapes. Most particles bulge outward, forming convex structures, while a smaller portion curves inward, creating concave shapes. A specially designed conical feeder and splitter ensure that RCA particles are deposited in continuous, symmetric triangular piles on the conveyor belt. This allows for representative PSD measurements by analyzing only a strip taken at one side of the pile, in the studied case located at one-third distance from the pile's top. The technology employs a high-resolution 3D point cloud for surface analysis. It directs each point towards the nearest steepest ascent based on the watershed segmentation algorithm. This gradient-based approach enables the system to efficiently map the surface topography by tracing*

Apart from minor updates, this chapter has been submitted for publication.

*paths from lower points to local summits. This algorithm facilitates rapid and parallel data processing, significantly reducing computation time. This technology supports real-time, accurate PSD analysis of large volumes (minimum 50 tons per hour) without halting the conveyor, achieving a Root Mean Square Error (RMSE) between 4.69% and 6.09%. Using an optimization method based on the cumulative percentage retained curves, the technology enhances the quality of unscreened RCA and streamlines the recycling process, ensuring a stable and high-quality RCA supply to facilities. This advancement provides essential data for informed decision-making in RCA management and supports the production of high-quality RCA, contributing to sustainable resource utilization and waste reduction in the construction industry.*

## 4.1. INTRODUCTION

RECYCLED coarse aggregates (RCA) derived from demolition wastes have gained significant attention in sustainable construction practices due to their potential for reducing environmental impact and conserving natural resources (Han and Thakur, 2015; Mohammadinia et al., 2017; Sinoh et al., 2023). One major challenge in using RCA is the frequent and substantial fluctuation in quality (Brand et al., 2015; Khoury et al., 2018). Unlike primary aggregates, which are typically sourced from relatively consistent geological formations and therefore exhibit stable quality over extended periods (months), RCA quality can vary dramatically within much shorter timescales, often as brief as an hour or per truckload. This is primarily due to the heterogeneous nature of demolition waste, which can include materials from different parts of buildings or various demolition sites (Ibrahim, 2016; Mollaei et al., 2023). It can also result from differences in recycling processes (Ibrahim, 2016; Mollaei et al., 2023). Consequently, the variability in the composition and properties of the incoming demolition waste directly affects the consistency of the RCA produced (Jayasuriya et al., 2018; Pacheco et al., 2019).



The inconsistency in RCA quality can lead to challenges in meeting the stringent specifications required for high-performance concrete applications. Construction projects often have precise requirements for aggregate quality to ensure the safety and longevity of structures (Etxeberria, 2020). The inability to consistently meet these requirements with RCA can limit its use in critical applications, despite its environmental benefits. This variability necessitates more frequent and rigorous testing to ensure that each batch of RCA meets the necessary standards, adding to the operational costs and complexity (Kou and Poon, 2015; Lotfy and Al-Fayez, 2015). Additionally, the fluctuating quality of RCA can impact the efficiency of the recycling process itself. When the quality of the input materials varies significantly, it can be difficult to optimize the recycling process parameters (Pedro et al., 2017), such as sorting mechanisms. This can lead to inefficiencies, increased wear and tear on equipment, and higher energy consumption. In the worst cases, it might even necessitate reprocessing of batches that fail to meet any quality standard, further driving up costs and resource use.

To address these challenges, it is crucial to implement a highly automated and real-time quality assessment process for RCA. However, assessing the physical properties of recycled aggregates poses challenges in terms of accuracy, efficiency, and real-time monitoring. Extensive research (Al-Bayati et al., 2016; Chang et al., 2022; Evangelista et al., 2015; B. Wang et al., 2021) has been conducted in this area to address these challenges. Among the various properties of recycled aggregates, one crucial factor is the particle size distribution (PSD) of RCA. The PSD plays a significant role in determining the workability and strength of the final concrete product (Meddah et al., 2010; Siregar et al., 2017; J. Wu et al., 2018). A batch of RCA with a higher proportion of fine particles can lead to a concrete mix that is too cohesive and difficult to work with, while a batch with too many coarse particles may result in a mix that lacks sufficient cohesiveness and strength. These fluctuations can compromise the structural integrity and durability of the final concrete product. Therefore, the accurate determination of PSD is essential for evaluating its performance and ensuring its suitability for optimal utilization in various applications, with a particular emphasis on industrial-scale implementation. This necessity underscores the importance of optimal PSD in enhancing the overall perfor-

mance and sustainability of high-performance concrete production.

To determine the PSD of RCA, traditional methods involve manual sampling and laboratory testing (Nedeljković et al., 2021; Yoshida et al., 2014). However, these methods have several limitations, including being expensive, offline, late, and susceptible to human errors (Florea and Brouwers, 2013). Such methods cannot provide timely feedback to the operator of the recycling plant, essential for detecting off-spec production and ensuring stable and guaranteed quality to facilities (C.-R. Wu et al., 2020). The practice of sampling the plant stream, conducting sieving tests in the laboratory, and then incorporating the results back into the plant control system often introduces a significant lag time. This lag time can delay decision-making processes and hinder the optimization of recycling operations (Mazhoud et al., 2022). The use of online automated non-contact measurement techniques for real-time PSD analysis can help mitigate this issue by providing immediate feedback on the PSD, enabling timely adjustments and optimization of the recycling process. Online automated PSD measurement delivers a digital result, and so it is an essential component of digital recycling plants, which offer a further cost reduction for sustainable concrete production.



Over the past few decades, the use of image-based PSD analysis has gained significant attention due to the progress in computer vision and digital image processing (Akashi et al., 2010; Al-Thyabat and Miles, 2006; Gao et al., 2024; Sun et al., 2017; Zhou et al., 2023). However, conventional image-based (Zeng et al., 2022; Zhou et al., 2023) systems used for PSD analysis have several limitations that need to be addressed. One significant limitation is the susceptibility of these systems to surrounding conditions (Chatterjee et al., 2010; Tafesse et al., 2012). The properties of the material surfaces being analyzed also pose challenges (Bai et al., 2021; Tessier et al., 2007). Different materials may reflect or absorb light differently, leading to variations in the captured images. Acquiring information about particles located beneath the surface is another obstacle in traditional imaging techniques (Hamzeloo et al., 2014; X. Wu et al., 2019). Additionally, distinguishing between superimposed and non-superimposed particles presents a challenge in image-based PSD analysis (Hamzeloo et al., 2014; Kistner et al., 2013). Errors in PSD analysis mainly stem from the analysis methods or algorithms employed (Bamford et al., 2021; Olivier et al., 2020; Yaghoobi et al., 2019; Zhang et al., 2012). If these methods are not properly validated or optimized, they can contribute to errors such as over-segmentation and under-segmentation (Engin and Maerz, 2019; Zhang et al., 2020).

In recent years, advancements in 3D scanning technology have revolutionized the field of object measurement (Bi and Wang, 2010; Moon et al., 2019; Y. Wang et al., 2022). This technology enables the capturing of detailed geometric information of aggregate piles on conveyor belts, effectively overcoming challenges related to color or illumination variations (Thurley, 2011). However, the application of 3D scanners for PSD analysis of aggregate piles on conveyor belts presents unique challenges. One such challenge is the high-speed movement of the material on the conveyor belts. As the aggregate piles are transported rapidly, the particles should move as little as possible and the 3D scanner must capture precise measurements within a short period. This necessitates the development of robust transportation methods, efficient scanning techniques, and hardware capable of acquiring accurate data in real time. Moreover, handling the large volume of data generated by the 3D scanner presents a data processing challenge. To achieve

real-time analysis, sophisticated algorithms are required to efficiently process and analyze the acquired data. These algorithms should be capable of handling the high data throughput and extracting meaningful information about the PSD from the scanned data. Another challenge is the presence of segregation and grouping errors (Thurley, 2011), which refers to the tendency of larger particles to rise to the surface of the pile, while smaller particles tend to settle at the bottom. This uneven distribution can introduce errors in the PSD analysis. Currently, the analysis of particle piles on conveyor belts has received less attention in the literature compared to single-layer particle analysis (Engin and Maerz, 2019; Galdames et al., 2017). Nonetheless, ongoing research is being conducted to address these challenges and explore new methodologies for analyzing particle piles on conveyor belts. By developing innovative approaches and algorithms, researchers aim to improve the accuracy and efficiency of PSD analysis using 3D scanning technology.



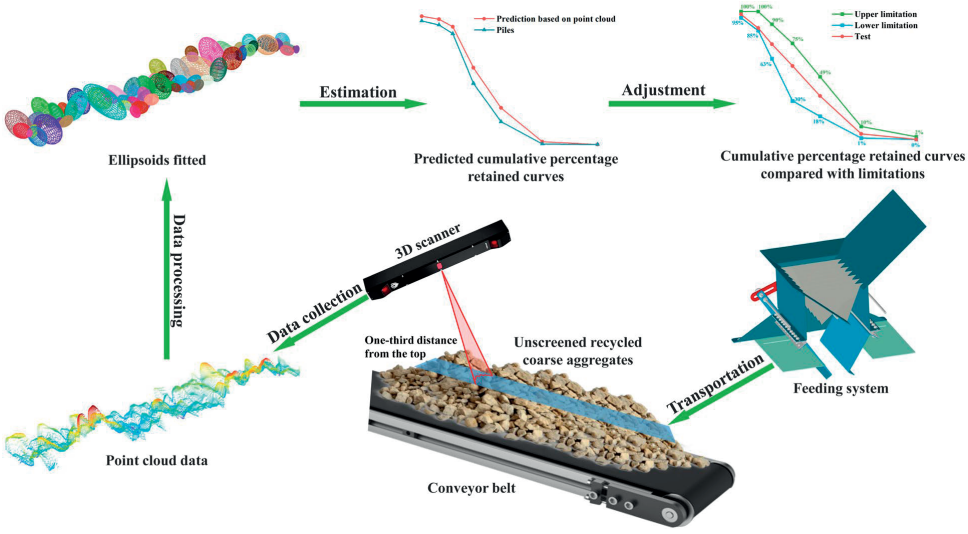


Figure 4.1: Schematic of industrial-scale implementation for intelligent PSD optimization

This study employs 3D surface analysis to efficiently monitor and improve the PSD of unscreened RCA to achieve optimal PSD for high-performance concrete. This research involves several key components: a specially designed feeding system for creating stable triangular piles, a straightforward sampling method for representative surface measurements, a 3D data processing method based on the actual morphological characteristics of RCA particles for accurate PSD estimation, and an intelligent design of PSD optimization. The results and discussion section explores the representativeness of the sampled areas, the corrections applied to the data, and the performance of the 3D point cloud processing method in predicting the PSD. The findings contribute to enhancing the understanding of RCA characterization and provide valuable insights for its efficient utilization in construction applications. Experimental validation and comparison with traditional manual methods are conducted to evaluate the accuracy and reliability of the

proposed method. Figure 4.1 illustrates the procedural flowchart, offering a visual summary of the methodological sequence employed in this study.

## 4.2. Experimental and Methods

### 4.2.1. Materials

In this study, RCA samples were obtained by implementing C2CA (Concrete to Cement and Aggregate) technologies to batches of End-of-life concrete from dismantled construction (Gebremariam et al., 2020). Multiple samples of recycled aggregates sourced from demolition wastes were acquired from different demolition sites across the Netherlands. These recycled aggregate samples then underwent a series of processing steps using the C2CA technologies to generate coarse and fine recycled aggregates. More specifically, the crushed particles ranging from 0 to 16.0 mm were subjected to treatment using Advanced Dry Recovery (ADR) (Gebremariam et al., 2020). As a result of this treatment, the particles were categorized as the RCA with the typical sizes between 4.0 and 16.0 mm. Additionally, the fine fraction measuring 0 to 4.0 mm was separated as a distinct product during the processing steps.



### 4.2.2. Equipment

#### Feeding system

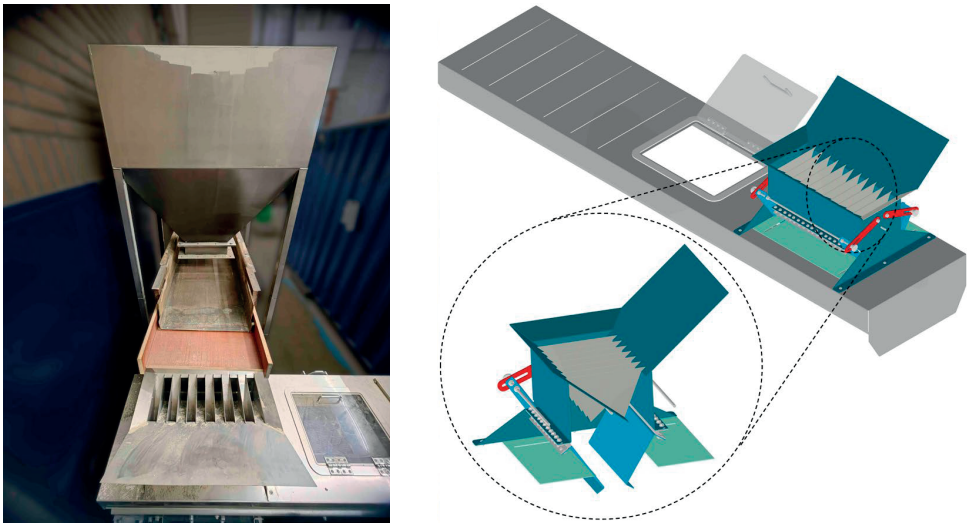

(a) Conical feeder and splitter

(b) Cross-sectional view of the splitter

Figure 4.2: Feeding system

The feeding system to the conveyor belt of the 3D scanning system (Figure 4.2) consists of two main components: the conical feeder and the splitter. The purpose of this feeding system is to maintain a consistent flow of the RCA and create stable and symmetric triangular piles on the conveyor belt for further analysis. The process starts by

introducing the RCA at the upper section of the conical feeder, ensuring a smooth and controlled feeding mechanism. From there, the RCA are conveyed seamlessly into the splitter, maintaining a consistent flow under the effect of applied vibration. The vibration frequency was set to 30 Hz, and the magnitude of the vibration was regulated by the input voltage provided by the controller. The splitter, a crucial element of the system, is equipped with two sets of symmetrically distributed triangular slots. These slots are specifically designed to enhance the precise and equal division of the incoming RCA into two streams. As the RCA entered the splitter (Figure 4.3 illustrates three different scenarios, with the dashed lines representing the trajectories of the RCA particles), they either fell directly or experienced several reflections off the splitter walls. Eventually, they descended through the bottom slot of the splitter and accumulated on the conveyor belt.



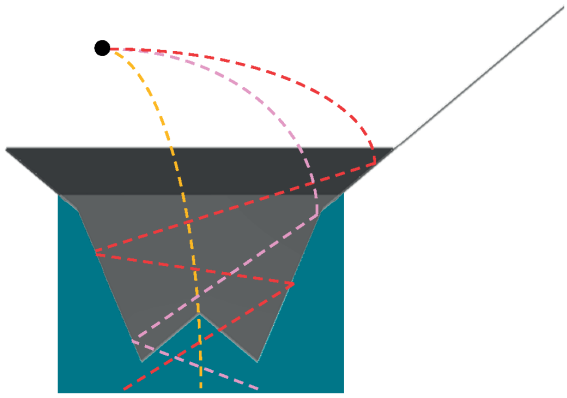

Figure 4.3: Schematic cross-sectional diagram for RCA entering the splitter

This process aims to achieve a symmetrical distribution of RCA particles within each layer and, by extension, each half-layer of the piles formed on the conveyor belt (Figure 4.4). The design of the conical feeder and the symmetric splitter is intended to ensure that each type of particle would have an equal probability of being distributed across the width of the feeder's rim. This setup aims to maintain uniform distribution within each half-layer of consistent thickness in the pile, which is formed at a continuous critical slope. However, it is important to note that the actual PSD and composition across the pile are not entirely uniform, as demonstrated by subsequent experiments. The PSD and composition still vary along the slope of the pile.

After conducting several experiments, it was observed that when the conveyor belt was operating at a speed of 0.529 m/s, the triangular piles featured a base edge of 37.0 cm and a height of $9.0 \pm 0.5$ cm. According to this, it can be calculated that a single conveyor belt can process at least 50 tons of RCA per hour. The stability and uniform distribution of the triangular piles are essential for subsequent analysis and measurement of the PSD. This feeding system ensures a controlled and consistent flow of the RCA, enabling accurate and reliable analysis of the RCA piles on the conveyor belt.

The even distribution and formation of stable triangular piles of RCA on the conveyor belt can be explained scientifically by considering the physical properties of the

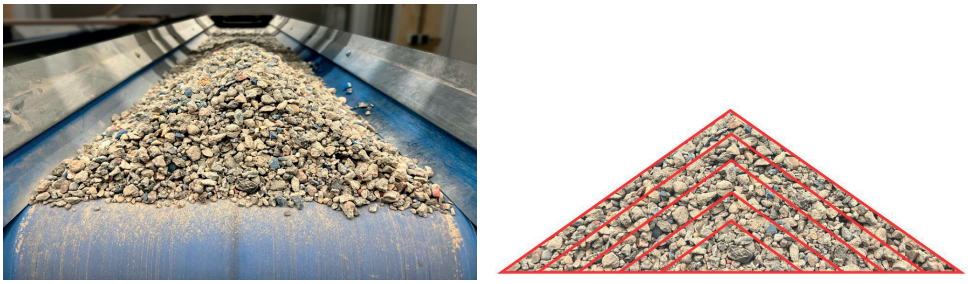

(a) Cross-sectional view (b) Layered formation

Figure 4.4: RCA piles



materials and the mechanics of the feeder and the splitter.

**(1) Shape and size of RCA** The physical properties, like the shape and size of the RCA, influence how the material flows and piles up. Compared to primary aggregates, RCA has more angular shapes and includes both convex and concave hull formations. Irregularly shaped and sized particles tend to interlock and stabilize more quickly, forming distinct piles.

**(2) Feeder design** The conical feeder design helps in the controlled and uniform flow of RCA. The shape of the feeder, along with its vibration frequency and magnitude, ensures that the RCA is released evenly across the entire width of the splitter.

**(3) Splitter configuration** The splitter with symmetrically distributed triangular slots is designed to divide the flow of RCA evenly. This results in two streams that form stable piles due to the consistent and symmetric division of materials.

**(4) Vibrational mechanics** The vibration of the system is key. By adjusting the vibration frequency and magnitude, the RCA is encouraged to move and settle in a uniform manner, reducing the likelihood of clumping or uneven distribution.

**(5) Conveyor belt** The movement of the conveyor belt also influences the pile formation. The speed of the belt needs to be synchronized with the rate of material flow from the splitter to ensure that the RCA is deposited evenly and forms stable piles.

**(6) Gravity and friction** Gravity ensures the downward movement of RCA, while frictional forces between the particles and between the particles and the conveyor belt influence how the piles form and stabilize.

In summary, the even distribution and formation of stable triangular piles are due to the interplay of material properties, the mechanical design of the feeder and splitter, vibrational dynamics, and the physics of motion and friction. The result is a pile in which

each half-layer, as shown in Figure 4.4 (b), and particularly the top layer, is representative in terms of PSD and composition for the flow as a whole.

### 3D SCANNING SYSTEM

During the transportation of the RCA on the conveyor belt, the 3D scanner Gocator (Figure 4.5) was employed to capture 3D point clouds of the RCA piles. The Gocator was positioned directly above the conveyor belt, situated a quarter of the belt width horizontally from the edge of the conveyor belt. This positioning allowed for optimal access to scan the data from one side of the RCA piles.

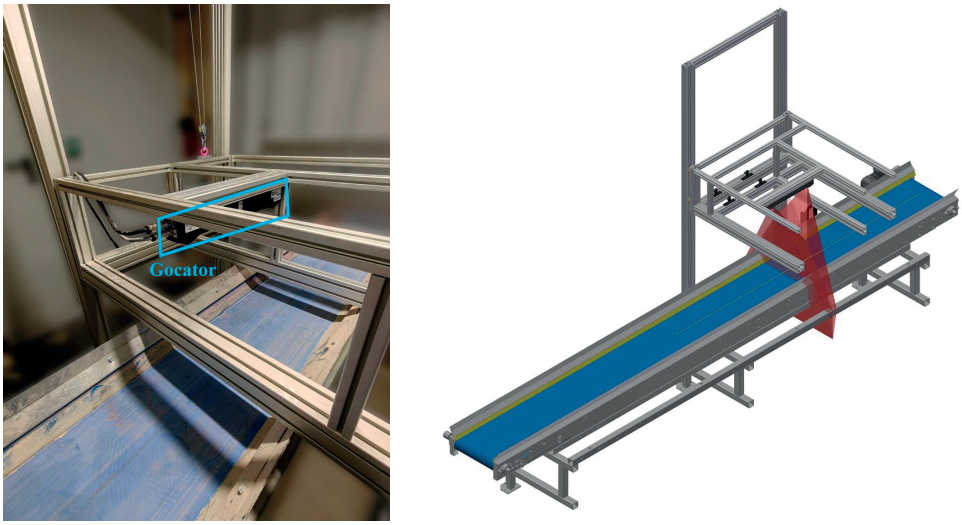


(a) Close view (b) 3D view

Figure 4.5: 3D scanning system

The resolution of the point clouds varied in different directions. Specifically, the resolution along the conveyor belt of the obtained point clouds was influenced by two main factors: the conveyor belt speed and the Gocator's encoder resolution. The conveyor belt speed was regulated by adjusting the rotational speed of the motor drive, which could be varied within an adjustable range by modifying the output frequency and the number of poles. For this study, the output frequency of the motor drive was set to 50 Hz, with 4 poles, resulting in a rotational speed of 1500 rpm. Considering a gearbox ratio of 19 and a wheel perimeter of 402.116 mm, the conveyor belt speed was calculated to be 0.529 m/s. In terms of the Gocator's encoder resolution, it was set to 1024 ticks per revolution, which yielded a calculated resolution of 0.393 mm for the point clouds along the conveyor belt. Across the conveyor belt, the resolution ranged from 0.375 to 1.100 mm, depending on the field of view. For this study, the resolution across the conveyor belt was determined to be 0.378 mm. For the resolution along the height of the RCA piles, the Gocator system was set to a constant resolution of 0.083 mm along the height axis.

### 4.2.3. Sampling Methods

To enhance the efficiency and accuracy of PSD measurements using the 3D scanner Gocator, an approach was developed to estimate the PSD of the entire RCA piles based on analyzing a single part of their surface. This approach requires careful consideration of representative sampling for 3D surface analysis.

It is essential to examine the formation characteristics of the material flow. The conical outlet of the silo (Figure 4.2 (a)) generates a radially outward flow of materials, designed so that each type of particle has the same probability to end up anywhere across the edge of the vibrating feeder, and so, after the splitter, in any of the layers, on each side of the pile. Since the pile is always at the critical angle, this means that a one-sided top layer of a given thickness contains the centers of mass of a representative sample of particles. However, due to the phenomenon of segregation, it is to be expected that the composition and PSD of particles vary within such a layer from the top of the pile to the bottom. Besides, the fact that the one-sided layer is representative does not mean that the particles of which a substantial fraction of the top surface is visible are also representative for the volume of the layer, and so for the overall particle flow as a whole.

Therefore, for industrial sampling, it is a pragmatic solution to investigate if there happens to be a range of positions along the side of the pile where these largely visible particles provide a representative sample. The following steps were undertaken to achieve this:

**(1) Assessing the representativeness of PSD** The PSD of the full side surface of the RCA piles was carefully examined and compared with the overall PSD of the piles. This analysis provided valuable insights into the relationship between the PSD of the surface and the entire RCA piles, ensuring representative sampling.

**(2) Improving particle sampling accuracy** To improve the accuracy of particle sampling on the surface, the sampling area was sprayed with paint (Figure 4.6). Only particles with at least seventy percent paint coverage as viewed from one side were selected for sieving. This measure enabled clear distinction from the rest of the RCA piles, facilitating more precise sampling of the designated area.

**(3) Selecting sampling strips** To reduce the amount of data to be processed, 20 mm wide strips were selected for sampling at specific areas, including one-third and two-thirds distance from the top, as well as the top and middle portions. The bottom part of the side surface, which contained scattered small particles and was considered non-representative, was excluded from the sampling process.

**(4) Sieving for comparison** Manual sieving using circular sieves was performed on both the sampled portions and the entire RCA piles to determine their respective PSD. This involved separating the particles into different size fractions through a series of sieves and measuring the weight of particles retained on each sieve.

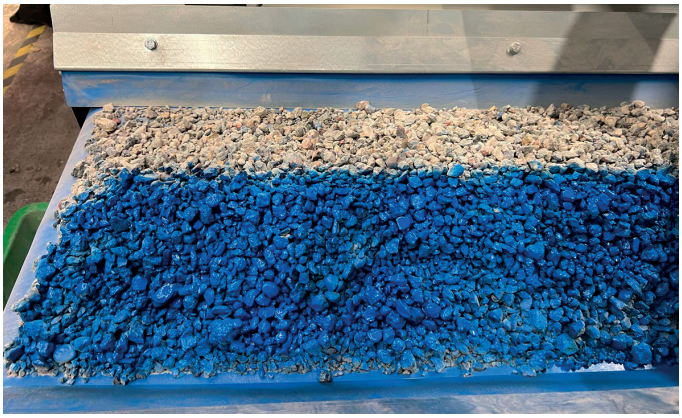

(a) Full side surface



(b) One-third and two-thirds distance from the top

(c) top of the side

Figure 4.6: Sampling from the side surface of the RCA piles

**(5) Identifying representative sampling area** The most representative sampling area was identified by comparing the PSD of the sampled areas with the entire RCA piles. This step ensured that the chosen area closely reflected the overall PSD.

**(6) Establishing a numerical relationship** A numerical relationship was established between the PSD of the specific sampling area and the overall PSD of the RCA piles. This relationship allowed for the estimation of the entire PSD based on the analysis of the selected area, providing a reliable method for PSD determination.

### 4.2.4. Analysis Methods

#### 3D Point Cloud Data Processing

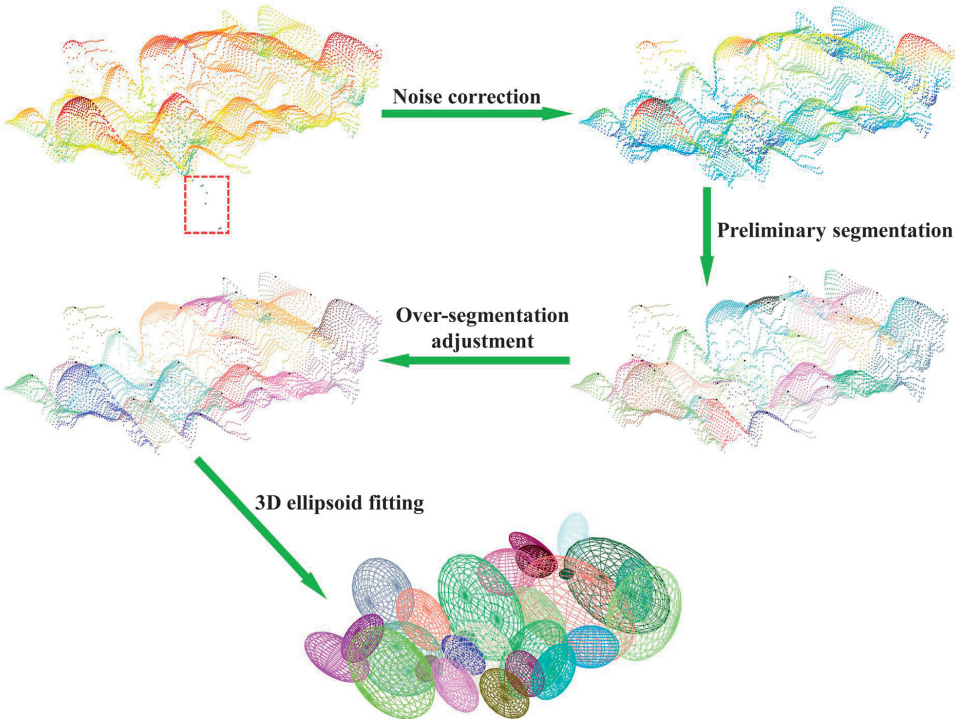


Figure 4.7: 3D point cloud data processing

To gather detailed morphological information from the designated sampling area, the 3D scanner Gocator is used to generate 3D point cloud data of the surface. This research adopts and improves the single flow algorithm (O'Callaghan and Mark, 1984; Wilson and Gallant, 2000) by adapting it to the actual morphological characteristics of RCA particles. The single flow algorithm is a commonly used method in terrain analysis for hydrological modeling. The enhancements made in this study enable a rapid and efficient 3D surface analysis of the 3D point cloud data. This method assumes the path of the steepest slope for point direction and records these directional paths as topologically ordered vectors of indices. The objective is to extract the size information of each particle by applying a parallel watershed segmentation (Braun and Willett, 2013; Steer et al., 2022) to the obtained 3D point clouds. This segmentation process separates the 3D point clouds into distinct regions, each representing an individual particle, or, if the particle is not strictly convex, a part of a particle. Over-segmentation is corrected based on proximity, neighbor relations, and surface orientation similarity. The regions corresponding to a single particle are then modeled with ellipsoids to create a representation of the particle that is suitable for estimating its shape factor, screen size, and volume. Fitting ellipsoids allow for a quantitative description of particle morphology. The length

of the second shortest axis of the fitted ellipsoid is adopted as the gradation parameter for the particles. This parameter provides a measure of particle size, which is crucial for constructing the PSD. The process, illustrated in Figure 4.7, involves several key steps.

The watershed segmentation method distinguishes itself from the local maxima-based method, which relies only on identifying the highest neighboring points, by incorporating gradient information and global topological data. This combination leads to more accurate and robust segmentation results. Although both methods initiate from local extrema, the watershed segmentation method shows better performance, particularly in areas with complex topologies. The key distinctions between the two methods can be explained through the following aspects:

**(1) Segmentation foundation** The watershed segmentation method adopts a global approach by considering not only local extrema but also the overall gradient and flow direction of the particles. It simulates water rising from local minima, effectively "flooding" the entire region. This approach takes into account the entire topological structure of particles from the beginning, ensuring that segmentation is influenced by the overall shape and characteristics of the particles, rather than just local features. This allows it to form regions that are topologically coherent and consistent with the overall shape of the particles. The local maxima-based method identifies local peaks in the dataset and uses these peaks as the starting point for segmentation. However, when applied to complex topologies, it often misses important details, especially when dealing with irregularly shaped particles. The reliance on only local features limits its ability to accurately segment more intricate datasets.



**(2) Boundary formation** Since the watershed segmentation method is driven by water flow paths based on gradient information, the segmentation boundaries form naturally at points where the flow from different basins converges (i.e., along the watershed lines). This boundary formation mechanism ensures that the segmentation respects the overall structure of the particles, resulting in smooth and natural boundaries. In contrast, local maxima methods may produce irregular or jagged boundaries, particularly when dealing with complex regions.

By integrating global topological information and gradient-based flow, the watershed segmentation method provides a more robust and accurate segmentation process, especially in complex environments where the local maxima-based method might struggle to deliver precise results.

**Noise Correction**

In 3D point cloud data analysis, the precision and consistency of the data are critical. Noise and outliers often lead to measurement errors, which significantly affect the analysis results. For instance, when measuring gaps between particles, the Gocator might capture lower reflectivity, leading to unusual values (as shown within the red dashed box in Figure 4.7). These errors not only impact the assessment of particle size and distribution but also interfere with the analysis of other geometric properties. To improve the reliability and consistency of the results, it is essential to apply preprocessing methods

such as noise filtering and data smoothing. These methods help refine the data, making it both more accurate and consistent.

It is important to note beforehand that handling these noise and outliers is crucial during the initial segmentation process, as it ensures a smoother workflow. However, in the later stage of over-segmentation adjustment, the actual values of the data become essential. They represent the physical gaps between two particles, helping to accurately differentiate between a concave hull, as shown in Figure 4.10 (b), and the case of two adjacent particles. This distinction reduces the likelihood of incorrect merging.

The base surface of the entire point cloud needs to be horizontally aligned beforehand. Since the slope angles of the generated RCA piles are relatively consistent, this characteristic can be leveraged to reorient the base surface of the point cloud easily. This process ensures that the base surface is perfectly horizontal, with its normal vector pointing vertically upwards.



In the context of 3D point cloud data collected by the Gocator, the x and y coordinates form a structured grid while the $z$-axis represents varying height or depth measurements. Typically, noise and outliers stem from abnormal $z$-axis values. Managing these erroneous $z$-values is critical for maintaining the integrity and utility of the data. To address this issue, linear interpolation is employed across the grid to estimate abnormal $z$-values based on their spatial arrangement and adjacent data points. This method is well-suited for the data's structured nature, characterized by regular spatial intervals.

The process of interpolating abnormal $z$-values accounts for both horizontal and vertical spatial relationships to preserve the integrity of the data's surface geometry. For each missing or negative $z$-value, interpolation is performed by forming a plane defined by at least three surrounding points that are not collinear. The interpolated $z$-value at any given point $P_i(x_i, y_i, z_i)$ on the grid is then calculated using the formula derived from the plane equation:

$$z = a_p + b_p x + c_p y \tag{4.1}$$

where $a_p$, $b_p$, and $c_p$ are coefficients determined by the known $z$-values of the neighboring points. This strategy ensures that the interpolation considers the gradient changes both along $x$ and $y$ axes, providing a smooth transition across the grid. To ensure completeness, any remaining points with abnormal values at the boundaries or within the dataset, which could not be interpolated due to lack of neighboring data points, are addressed by backward and forward filling methods.

This interpolation method guarantees that all data points are filled and positive, reflecting plausible physical measurements. The use of linear interpolation offers a straightforward and computationally efficient approach to handling missing or erroneous data points. It also preserves the geometrical and topological consistency of the dataset, which is imperative for subsequent analytical tasks such as surface reconstruction, volumetric analysis, and visualization.

**Preliminary Segmentation**

The objective of preliminary segmentation is to rapidly divide the 3D point clouds into different areas by sequentially adding points to the local highest point. Each area includes a local highest point, facilitating the establishment of computational orders for

the points that represent the shape of particles. The segmentation creates a structured dataset with particles represented by local high points and their associated downhill points. The preliminary segmentation process can be broken down into several key conceptual steps:

- (1) Identification of local highest points: This step involves identifying the local highest points within the 3D point cloud. These local highest points act as the starting points for defining individual particle segments.
- (2) Calculation of steepest ascent path: For each point in the 3D point cloud, the path of steepest ascent towards the nearest local highest point is calculated. This determines the grouping of points into potential particle segments.
- (3) Segment formation: Based on the paths of the steepest ascent, points are grouped into segments that are associated with the local highest points identified earlier.



**(1) Identification of local highest points**

Using the coordinates of each point $P_i$, the algorithm scans the surrounding points to identify the highest elevation within the defined $k_p$ neighborhood. This local maximum $TP_i$ is designated as the highest point for that region.

Each point on the surface of the particles is denoted by its coordinates $P_i(x_i, y_i, z_i)$. For every point $P_i$, there is a corresponding particle, denoted as a set of points $N(P_i)$, which contains the total number of $n_p$ points. Among these, $TP_i$ is identified as the local highest point. To Identify local highest points, it is important to determine the uphill point for each point $P_i$.

Uphill point, $UP_i$: For each point $P_i$, the uphill point is the neighboring point where the point path direction goes to, identified by the steepest ascent from $P_i$.

The steepest ascent to a neighboring point $P_j(x_j, y_j, z_j) \in N(P_i)$ is calculated using the gradient formula (Kelley, 1962):

$$d_{ij} = \sqrt{(x_j - x_i)^2 + (y_j - y_i)^2 + (z_j - z_i)^2} \tag{4.2}$$

$$\Delta z_{ij} = \frac{z_j - z_i}{d_{ij}} \tag{4.3}$$

where $d_{ij}$ is the Euclidean distance between points $P_i$ and $P_j$. Each point $P_i$ evaluates its neighboring points to determine its uphill point based on the steepest ascent:

$$UP_i = \arg \max_{p_j \in N(P_i)} \Delta z_{ij} \tag{4.4}$$

The point with the highest positive gradient value $\Delta z_{ij}$ represents the steepest ascent from $P_i$.

By calculating the steepest ascent for each point $P_i$ to its $k_p$ nearest neighbors, particles are initially segmented based on the local highest point representing their summits. Given that a small amount of fine material (2.0–4.0 mm) will be present in the targeted RCA product, the minimum visible surface area for a single particle should be around 3.1

$mm^2$. The Gocator sensor has a resolution of 0.393 mm and 0.378 mm in the horizontal plane, respectively. To establish a clear lower size limit for the visible particle area during segmentation, and considering that not all measurement points will precisely align with the particle surface—resulting in a slightly smaller area than 3.1 $mm^2$—the minimum $k_p$ value is set at 20. This value covers an area of 2.971 $mm^2$, preventing the misinterpretation of larger particles as multiple smaller ones.

**(2) Calculation of steepest ascent path**

Once the local highest points are identified, the next step is to calculate the steepest ascent path for each point in the 3D point cloud. This path determines the direction in which each point will "climb" towards its nearest local highest point. In this step, the dataset is organized into a structured format that allows for efficient access and manipulation. The sorting operation arranges the particles based on their spatial properties, preparing them for the segmentation algorithm. Additionally, an array, denoted as $D$, will be created to store all the downhill point information.

To perform this operation, the process assumes that the path direction goes uphill, following the path of the steepest ascent. For each point $P_i$, it is necessary to identify its downhill point set.

Downhill point set $DP_{i,d}$: For each point $P_i$, the downhill point set includes all points where their steepest ascent path direction goes to the point $P_i$. Here, $d = 1, \cdots, ND_i$, where $ND_i$ is the total number of points, whose steepest ascent pathways converge at point $P_i$. Essentially, $DP_{i,d}$ comprises all points that consider $P_i$ as their uphill point, as illustrated in equations 4.5 and 4.6:

$$UP_{DP_{i,d}} = P_i \tag{4.5}$$

$$DP_{i,d} = \{P_j \mid UP_j = P_i\} \tag{4.6}$$

For each point $P_i$, initialize $ND_i$ values to zero. This count will later be incremented based on the point path directions determined by the topology. Using the uphill point $UP_i$ information, which specifies where each point $P_i$'s next direction goes to, the downhill point counts $ND_{UP_i}$ for $UP_i$ are then updated. Specifically, for each point $P_i$, once its uphill point $UP_i$ is determined, the count of downhill points for $UP_i$ is increased by 1. Specifically, $ND_{UP_i}$ is incremented as follows:

$$ND_{UP_i} = ND_{UP_i} + 1 \tag{4.7}$$

This procedure is demonstrated using a single example consisting of nine points, as depicted in Figure 4.8 and Table 4.1. Black dots represent the points in the 3D point cloud. Black dotted lines show all potential connections between neighboring points. Blue solid lines indicate the connections made according to the steepest ascent hypothesis (as shown by the arrows) used to construct the topology. Point 9 is assumed to be the local highest point in the area.

Then, transform the list $ND_i$ into an index array $\Psi$, which contains the location of where the list of downhill points to point $P_i$ is stored. The index array $\Psi$ is constructed to facilitate quick access to the starting point of each point $P_i$'s downhill point list within

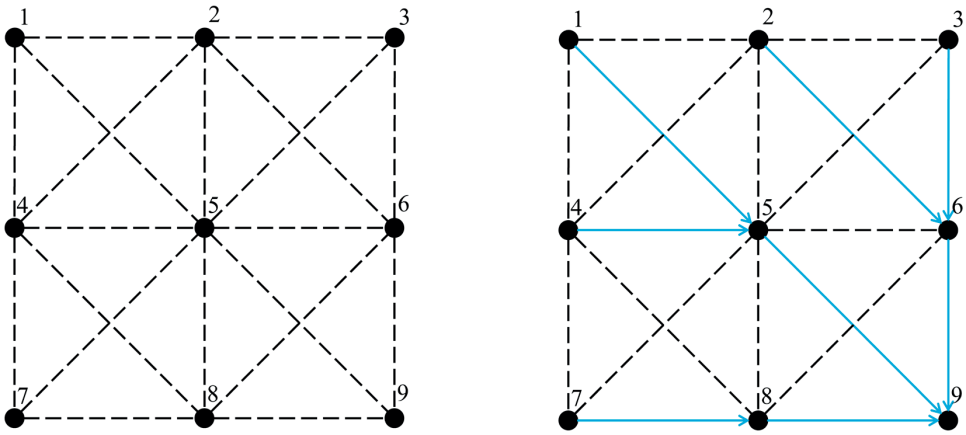


(a) Possible path directions

(b) Steepest ascent path directions

Figure 4.8: Top-down view of a 3D point cloud

Table 4.1: Calculation of relevant parameters in Figure 7

| $P_i$ | 1 | 2 | 3 | 4 | 5 | 6 | 7 | 8 | 9 |
|---|---|---|---|---|---|---|---|---|---|
| $UP_i$ | 5 | 6 | 6 | 5 | 9 | 9 | 8 | 9 | 9 |
| $DP_{i,j}$ | / | / | / | / | 1 | 2 | / | 7 | 5 |
| | / | / | / | / | 4 | 3 | / | / | 6 |
| | / | / | / | / | / | / | / | / | 8 |
| | / | / | / | / | / | / | / | / | 9 |
| $ND_i$ | 0 | 0 | 0 | 0 | 2 | 2 | 0 | 1 | 4 |
| $\Psi_i$ | 1 | 1 | 1 | 1 | 1 | 3 | 5 | 5 | 6 |

a global list array $D$. The single dimension array $D$ is used to store all the downhill point information $DP_{i,d}$. The array $\Psi$ is built in reverse order, starting from the last point and moving to the first. The specific steps are as follows:

$$\Psi_{n_p} = n_p + 1 - ND_{n_p} \tag{4.8}$$

$$\Psi_{i-1} = \Psi_i - ND_{i-1} \quad \text{for } i = n_p, \cdots, 2 \tag{4.9}$$

This ensures that each point $P_i$'s downhill point set in D can be accessed using $\Psi_i$, as the starting index. The initialization and updating of downhill point counts are operations that scale linearly with the number of points, making the algorithm efficient for large-scale models.

Store the count of how many times each point has been designated as the uphill point into an integer array $\Phi$. Initialize this integer array $\Phi$ with all elements set to zero. For each point $P_i$, identify its corresponding uphill point $UP_i$. Once identifying $UP_i$, update $D$ and $\Phi$, and populate the downhill point list using:

$$D(\Psi_{UP_i} + \Phi_{UP_i}) = i \tag{4.10}$$

$$\Phi_{UP_i} = \Phi_{UP_i} + 1 \tag{4.11}$$

Here, $\Psi_{UP_i}$ indicates the start of the downhill point in array $D$ for the uphill point $UP_i$. This step effectively adds a point $P_i$ to the list $D$ of its uphill point $UP_i$ and increments the count of downhill points for $UP_i$. Once all points have been processed, downhill point information of each point $P_i$ can be retrieved using:

$$DP_{i,d} = D(\Psi_i + \alpha) \text{ for } \alpha = 0, \cdots, \Psi_{i+1} - 1 \tag{4.12}$$

Here, $\Psi_i$ is the index in $D$ where the downhill point list for point $P_i$ starts, allowing sequential access to all downhill points of the point $P_i$.

**(3) Segmentation formation**

In this step, points are grouped into segments based on the paths of the steepest ascent calculated in the previous step. Each segment corresponds to a particle, with points being grouped around their respective local highest points. The use of stacks and index arrays facilitates the efficient management of these groupings, allowing for rapid computation even with large datasets. The goal is to build a stack $S$ that arranges points from the lowest point to the highest based on their dependencies in the point network. The stack helps to ensure that each point is processed in the correct order.

Initialize a stack $S$ and set global variable index $\beta$ initialized to 1. This index $\beta$ will be used to track the current position in the stack $S$ where points are added. For each top point $TP_\lambda$, $\lambda = 1, \cdots, n_\lambda$, initialize $\beta$ to 1 and invoke the stack addition procedure for each downhill point of $TP_\lambda$ using the list from the downhill point array $D$. Initiate the stacking process, this is done recursively:

$$add\_to\_stack(L_D, \beta) \text{ for } L_D = D\left(\Psi_{\tau_{P\lambda}}, \Psi_{\tau_{P\lambda}+1}, \cdots, \Psi_{\tau_{P\lambda+1}-1}\right) \tag{4.13}$$

where $\lambda$ starts from each top point, and $\beta$ is incremented within the *add_to_stack* function, which recursively adds points to the stack. The *add_to_stack* function is recursive, ensuring all points contributing to a top point are included before moving to points contributing to its downhill points, thus effectively creating a well-ordered process for boundary calculations.

Define and use the function $add\_to\_stack(L_D, \beta)$ to recursively add points to the stack:

$$S(\beta) = L_D \tag{4.14}$$

Continue adding downhill points of $L_D$ recursively:

$$add\_to\_stack(\Upsilon, \beta) \text{ for } \Upsilon = D(\Psi_{L_D}, \Psi_{L_D} + 1, \cdots, \Psi_{L_{D+1}} - 1) \tag{4.15}$$

This recursion continues until a point is reached that has no downhill points.

This process builds the stack by ensuring that all points are added following their steepest ascent path directions, maintaining a natural order from downstream to upstream contributors. This process is recursive, meaning that whenever a point is added to the stack, all its downhill points are also added to the stack until no more downhill points can be added. Points without downhill points do not initiate further recursive calls, preventing unnecessary stack operations and ensuring the recursion remains bounded.

The stack stores the sequence of all points from 1 to $n_p$. Points are added to the stack in a specific order that reflects the physical shape of the particles. Importantly, the structure of the stack ensures that each point is visited exactly once, and the length of the stack is equivalent to $n_p$. The stack-building process can be parallelized by distributing the local highest points among multiple processors. Each processor constructs a segment of the stack independently.

The arrangement of the stack is displayed in Figure 4.9 (a) according to the scenario depicted in Figure 4.8. From this example, it is evident that inverting the order of the points on the stack results in a reversed configuration (Figure 4.9 (b)).

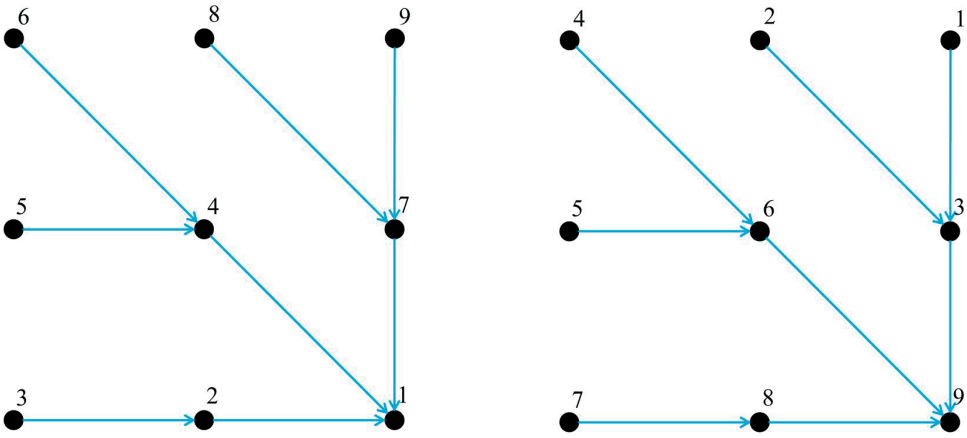


(a) Stack (b) Inverted stack

Figure 4.9: Stack and inverted stack order

By inverting the order of points in the stack, starting from points without downhill points (bottom points) and moving uphill, the computation can systematically handle each particle area. At each junction of the paths, if the junction includes uphill points, the inverted stack moves to the bottom of each lower branch. This allows for a systematic and step-by-step calculation of points from the lower areas before continuing past the junction. If there are no uphill points at the junction, the inverted stack moves to the bottom of another particle. This approach ensures that each point and its downhill points are calculated before moving upstream, enhancing the accuracy of the model. Equation

4.16 represents the stack where points are stored in a specific order to be processed from the bottom points upward through the network.

$$S(i) \text{ for } i = n_p, \cdots, 1 \tag{4.16}$$

The $n_p$ points are processed in an order that is appropriate to classify each point to the particle area. The inverted stack begins at the bottom points and proceeds uphill, following the steepest ascent path. These operations are performed in parallel, ensuring efficiency even for large datasets. Once completed, a total of $n_\lambda$ particles are segmented.

The preliminary segmentation uses the steepest ascent algorithm to rapidly and efficiently segment 3D point clouds. By calculating the uphill and downhill paths for each point, the structure enables the creation of particle areas in an organized, computationally efficient manner. The stack construction ensures that points are processed in a logical order from bottom to top, facilitating large-scale model processing.



**Over-segmentation Adjustment**

Figure 4.10 illustrates cross-sectional views of point clouds obtained by scanning particles in two different states using the Gocator. In the diagram, the vertical gray lines represent the structured spacing formed by the Gocator during the scan along the x-axis, while the red and blue dots depict points captured on the surface of the particles. In Figure 4.10 (a), the shape described is a convex hull, which is round and smooth. In contrast, Figure 4.10 (b) shows a concave hull, characterized by indentations or inward curves.

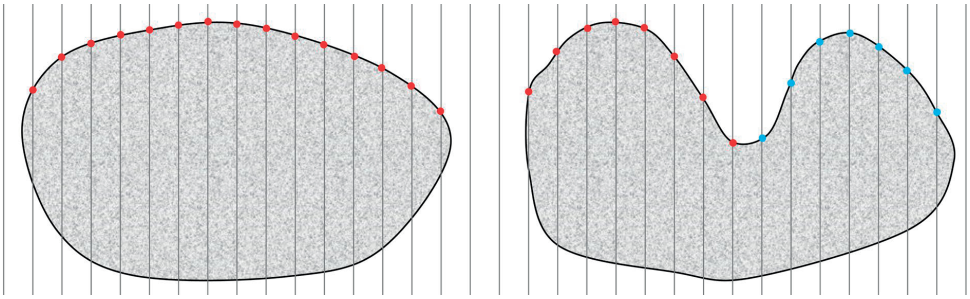

(a) Convex hull (b) Concave hull

Figure 4.10: Schematic cross-sectional diagram for 3D scanning of particles

During the preliminary segmentation process, particles with convex hull shapes are easily identified as a single particle due to their smooth and unbroken outlines. However, particles with concave hull shapes present challenges; when attempting to extract local highest points, these shapes are prone to being mistakenly divided into separate segments, as shown in Figure 4.10 (b) with red and blue sections, resulting in the erroneous division into two particles. This leads to over-segmentation. To address this issue, it is essential to merge adjacent segments that originally belong to the same particle to ensure accurate recognition and analysis.

To address the common issue of over-segmentation resulting from the initial watershed segmentation, particles are merged based on proximity, neighbor relations, and surface orientation similarity. Two neighboring particles are merged if they share a border, and the boundary points between them are continuous. This step ensures that particles over-segmented due to local topographic maxima or noise are accurately merged.

It is worth reiterating that, in this process, the previously smoothed values obtained using the interpolation method will no longer be used. Instead, the original values will be applied. This adjustment allows for more accurate identification of neighboring particles, preventing incorrect merging. Additionally, it helps to differentiate the concave hull scenario in 4.10 (b).

After preliminary segmentation, two adjacent particles, designated as $PA_u$ and $PA_v$ ($u, v \in \{1, \cdots, n_\lambda\}$), to be merged into a single particle, they must meet the following proximity and continuity conditions: The distance between the boundary points of the two particles must be sufficiently small to ensure that the two particles share a border. Additionally, the average absolute difference in the local curvature at these boundary points should be below a certain threshold to maintain the continuity of the boundary.



When assessing the proximity and continuity between the boundary points of two adjacent particles $PA_u$ and $PA_v$, merging is considered if the distance between the two particles' boundary points is less than 0.6 mm, which is derived from the Gocator's resolutions of 0.378 mm, 0.393 mm, and 0.083 mm. These values suggest that the maximum distance between two adjacent points in space is approximately 0.6 mm. Additionally, the boundary points of the two particles should have nearly identical local curvatures to ensure continuity.

Define $BP_u$ as the set of boundary points in particle $PA_u$, similarly, define $BP_v$ as the set of boundary points in $PA_v$. Let $bP_{iu}$ be a subset of points in $BP_u$ and $bP_{iv}$ be a subset of points in $BP_v$ that satisfy the following conditions: For each boundary point $bP_{iu} \in BP_u$, there exists a boundary point $bP_{iv} \in BP_v$ such that $\|bP_{iu} - bP_{iv}\| \leq 0.6\,\text{mm}$; Each $bP_{iu}$ uniquely corresponds to the nearest boundary point $bP_{iv}$. This implies that $bP_{iu}$ and $bP_{iv}$ should appear in pairs. Define $n_{iu}$ as the number of boundary points $bP_{iu}$ in $BP_u$ that meet these conditions, and $n_{iv}$ as the number of boundary points $bP_{iv}$ in $BP_v$ that meet these conditions. Thus, we have:

$$n_b = n_{iu} = n_{iv} \tag{4.17}$$

Where $n_b$ is the number of boundary points satisfying the conditions.

To calculate the local curvature at the point $bP_{iu}$, it's necessary to approximate the local surface using points in its vicinity. This involves using a spatial data structure, such as a KD-tree, to efficiently locate the $k_b$ nearest neighbors of each point $bP_{iu}$. For this calculation, each point's neighborhood $N(bP_{iu})$ comprises the $k_b = 9$ nearest neighbors.

To model the local surface around each point $bP_{iu}$, an optimal quadratic polynomial is fitted using the least squares method, which is a technique that minimizes the sum of the squared differences between the observed values and the values predicted by the model. The general form of the polynomial is:

$$z = a_b x^2 + b_b y^2 + c_b xy + d_b x + e_b y + f_b \tag{4.18}$$

The coefficients $a_b$, $b_b$, $c_b$, $d_b$, $e_b$, $f_b$ are determined to minimize the squared error sum:

$$\sum_{ju=1}^{k_b} \left[ z_{ju} - \left( a_b x_{ju}^2 + b_b y_{ju}^2 + c_b x_{ju} y_{ju} + d_b x_{ju} + e_b y_{ju} + f_b \right) \right]^2 \rightarrow \min \tag{4.19}$$

where $(x_{ju}, y_{ju}, z_{ju})$ are the coordinates of the points in the neighborhood $N(bP_{iu})$.

Once the surface is fitted, the first and second derivatives at each point are calculated to determine the local curvature. These derivatives are given by:

$$f_x = 2a_b x + c_b y + d_b \tag{4.20}$$

$$f_y = 2b_b x + c_b x + e_b \tag{4.21}$$

$$f_{xx} = 2a_b \tag{4.22}$$

$$f_{yy} = 2b_b \tag{4.23}$$

$$f_{xy} = c_b \tag{4.24}$$

The local curvature $\kappa$ at each point can be estimated using the following formula:

$$\kappa = \frac{f_{xx}(1 + f_y^2) - 2f_{xy}f_x f_y + f_{yy}(1 + f_x^2)}{2(1 + f_x^2 + f_y^2)^{\frac{3}{2}}} \tag{4.25}$$

Calculate the local curvature for all points $bP_{iu}$ and $bP_{iv}$ and compare these values. If the average absolute difference in local curvature is minimal, it is likely that the two particles are geometrically continuous and might belong to the same particle. The average absolute difference in local curvature $\Delta\kappa$ is defined as:

$$\Delta\kappa = \frac{1}{n_b} \sum_{iu,iv=1}^{n_b} |\kappa_{iu} - \kappa_{iv}| \tag{4.26}$$

If $\Delta\kappa$ is below a certain threshold (in this case, 3 $mm^{-1}$), the particles s are considered geometrically similar and may be candidates for merging. These procedures effectively assess and resolve merging challenges in the 3D point cloud data of the RCA surface.

It is important to note that this algorithm is not designed to offer a highly detailed and precise point cloud segmentation method. Instead, its primary purpose is to enable fast segmentation of the point cloud. In certain exceptional cases, such as the one shown in Figure 4.11, the initial segmentation may mistakenly identify two separate parts as red and blue, even though they should be classified as one. A and B represent two vertices that have been identified as separate parts. Clearly, these two parts do not satisfy the proximity and continuity conditions. As a result, they remain separated during the over-segmentation adjustment phase. We are currently unable to effectively merge these types of particles into a single entity based on the aforementioned criteria. However, it is worth noting that such particle shapes are relatively rare in RCA, and this scenario

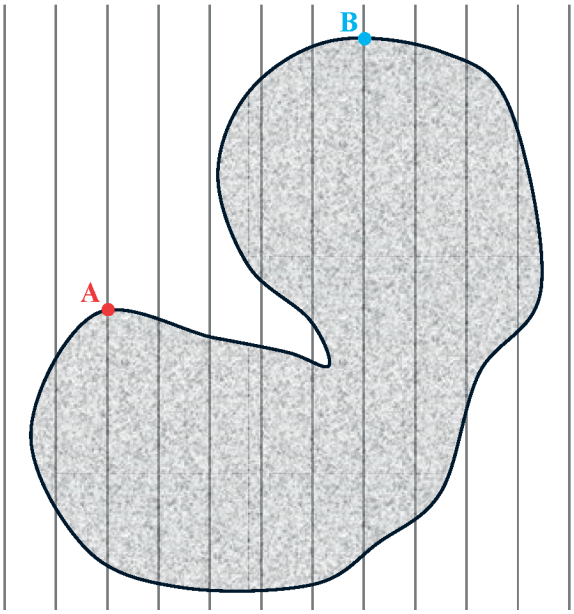


Figure 4.11: Schematic cross-sectional diagram for the special case



occurs only under a specific condition—such as when the particles are in a unique upright position with no other particles obstructing the view during the Gocator scanning. Given the infrequency and specific nature of these cases, their impact on the final results is minimal, and it is therefore reasonable to disregard them.

**3D Ellipsoid Fitting**

Following segmentation, each particle's morphology is determined by fitting a 3D ellipsoid to describe the geometry of the particle. The optimal fit is achieved by minimizing the sum of squared distances from the points to the ellipsoid's surface, under constraints ensuring the surface represents an ellipsoid. The ellipsoid is defined by the equation:

$$a_e x^2 + b_e y^2 + c_e z^2 + 2f_e yz + 2g_e xz + 2h_e xy + 2p_e x + 2q_e y + 2r_e z + d_e = 0 \qquad (4.27)$$

where $x$, $y$, and $z$ are the relative coordinates to the center of the area being fitted, and $a_e$, $b_e$,$c_e$, $f_e$, $g_e$, $h_e$, $p_e$,$q_e$, $r_e$, and $d_e$ are the parameters that define the ellipsoid's shape, orientation, and position in the space. This fitting process involves a direct least-square fitting method and provides crucial morphological parameters such as the diameters of the major, intermediate, and short axes.

In ellipsoid fitting, flat or nearly flat surfaces tend to introduce greater uncertainty in the estimated parameters. To address this issue, if the calculated ellipsoid parameters, specifically the lengths of the three axes, significantly deviate from a reasonable range (with an upper limit of 22.4 mm), the result should be considered an outlier and filtered

out. This process helps ensure that uncertainties in flat regions do not excessively impact the final ellipsoid parameters.

Finally, the cumulative percentage retained graph was plotted based on the volume of the fitted ellipsoid and the apparent density of the RCA. This graph depicted the PSD within the specific sampling area, which also represented the estimation of the overall PSD of the RCA piles.

### PSD Optimization

The European Standard (Standard, 2002) establishes criteria for the use of recycled aggregates in concrete production. As depicted in Figure 4.12, the standard sets forth both upper and lower percentage limits for each particle size interval. When the cumulative percentage retained curve falls within these specified limits, there is no need to adjust the PSD of the RCA. However, should the RCA sample's PSD necessitate an adjustment to meet these specified cumulative percentage thresholds, with material addition being a permissible efficient method—due to the labor-intensive nature of extracting particles by specific particle size—a linear programming model can be employed to streamline this adjustment. The objective is to increment the least possible weight to each particle size category to comply with cumulative percentage retained curve restrictions. The following outlines the linear programming methodology for addressing this challenge:

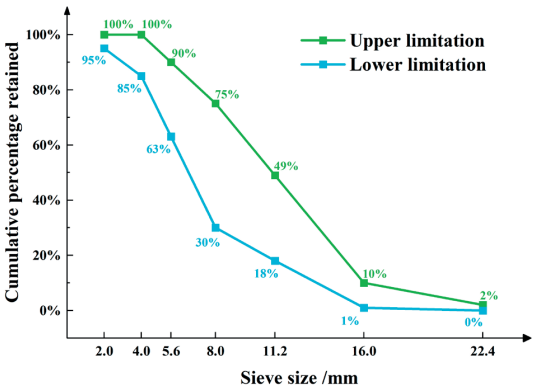


Figure 4.12: Standard for cumulative percentage retained curves

**Variable Definition**

For a defined set of particle size intervals $in(in = 1,\cdots,8)$, we categorize the particle sizes into distinct intervals based on their diameter. Specifically: Interval 1 is defined for particle diameters greater than 22.4 mm. Interval 2 is defined for particle diameters from 16.0 mm to 22.4 mm. Interval 3 is defined for particle diameters from 11.2 mm to 16.0 mm. Interval 4 is defined for particle diameters from 8.0 mm to 11.2 mm. Interval 5 is defined for particle diameters from 5.6 mm to 8.0 mm. Interval 6 is defined for particle diameters from 4.0 mm to 5.6 mm. Interval 7 is defined for particle diameters from 2.0 mm to 4.0 mm. Interval 8 is defined for particle diameters less than 2.0 mm. Within

each interval $in$, the variable $w_{in}$ denotes the total weight of particles present within. A decision variable $aw_{in}$ is defined to represent the weight of particles to be added to particle size interval $in$.

**Objective Function**

The primary goal of the objective function is to minimize the total additional weight across all particle size intervals. The formulation of the optimal function is articulated as follows:

$$\text{Minimize} \sum_{in=1}^{tn} aw_{in} \tag{4.28}$$

subject to

$$W_{in} = \sum_{m=1}^{in} w_m + \sum_{m=1}^{in} aw_m \tag{4.29}$$

$$W_T = \sum_{jn=1}^{tn} w_{jn} + \sum_{jn=1}^{tn} aw_{jn} \tag{4.30}$$

$$CP_{\text{in}} = \frac{W_{\text{in}}}{W_T} \times 100 \text{ for in } = 1, \cdots, 7 \tag{4.31}$$

$$L_{in} \leq CP_{in} \leq U_{in} \tag{4.32}$$

$$aw_{\text{in}} \geq 0, \forall \text{ in} \tag{4.33}$$

where $tn$ is the total number of particle size intervals. Constraints 4.28 to 4.33 ensure that, for each particle size interval $in$, the current weight of particles $w_{in}$, $in$ addition to the particles added through the variable $aw_{in}$, satisfies the cumulative percentage lower limit $L_{in}$ and upper limit $U_{in}$. Here, $W_{in}$ signifies the total weight of particles across intervals 1 to $in$, while $W_T$ represents the weight of all particles combined. $CP_{in}$ denotes the cumulative percentage for interval $in$.

## 4.3. RESULTS AND DISCUSSION

### 4.3.1. SAMPLING DATA ANALYSIS

#### REPRESENTATIVE SAMPLING AREA IDENTIFICATION

In the initial analysis, the PSD measured by manual sieving of particles with more than 70% paint on the full side surface was compared and analyzed with the overall PSD of the RCA piles. Multiple experiments were performed on different batches of RCA to ensure reliable and representative results. The findings obtained from Figure 4.13 (a) demonstrated that there was no significant distinction between the two PSDs. Notably, the calculated root mean square errors (RMSE) for both tests were remarkably low, measuring only 2.05% and 4.46%, which indicated a high level of similarity. These outcomes strongly supported the conclusion that the PSD data acquired from measuring a single

side of the triangular RCA piles could effectively represent the PSD of the entire RCA piles. Consequently, the observed consistency between the PSDs further consolidated the credibility and feasibility of inferring the PSD of the entire RCA piles based on the PSD measured at a specific area on the surface of the piles.

Analyzing the full side surface by point cloud analysis is computation-intensive, and therefore, it is attractive to consider a well-chosen strip of a limited width. After comparing and analyzing the PSD of different sampling areas on the side surface of various batches of RCA piles, it was observed from Figure 4.13 (b)-(e) that 20 mm wide strips taken at different positions - one-third distance from the top, two-thirds distance from the top, the top of the side, and the middle of the side - exhibited varying degrees of representativeness when compared to the overall PSD of the RCA piles.



It was evident that the PSD of the sampling areas tended to be overestimated when compared to the PSD of the entire pile. This discrepancy arose due to the behavior of the particles during the feeding process. Specifically, smaller particles have a tendency to roll down to the bottom of the pile, resulting in a higher concentration of particles in the 2.0-4.0 mm size range at the bottom section. As a result, there are relatively fewer 2.0-4.0 mm size particles in other regions of the pile's side surface. This uneven distribution of particles leads to a small percentage of mass in the 2.0-4.0 mm size range at most of the selected sampling areas. Consequently, when constructing the cumulative percentage retained curves, there is an overestimation of the PSD in this range.

Among these different sampling areas, the strips taken at the one-third distance from the top demonstrated the highest level of representativeness. The calculated RMSE for these strips was 4.10% and 2.48%, respectively. These values indicated a comparably minimal level of discrepancy between the PSD of the selected strips and the overall PSD of the RCA piles.

While the strips taken at the one-third distance from the top provided the most accurate representation of the overall PSD, it is important to note that there was still a certain degree of deviation between the curves of the selected strips and the overall PSD. This deviation, especially in the 2.0-5.6 mm particle size range, was particularly pronounced. Therefore, additional experiments were conducted to make necessary corrections and refine the accuracy of the obtained PSD data.

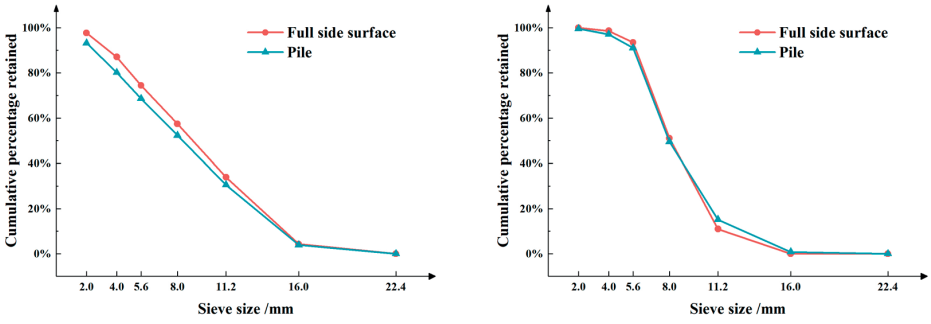


(a) Full side surface

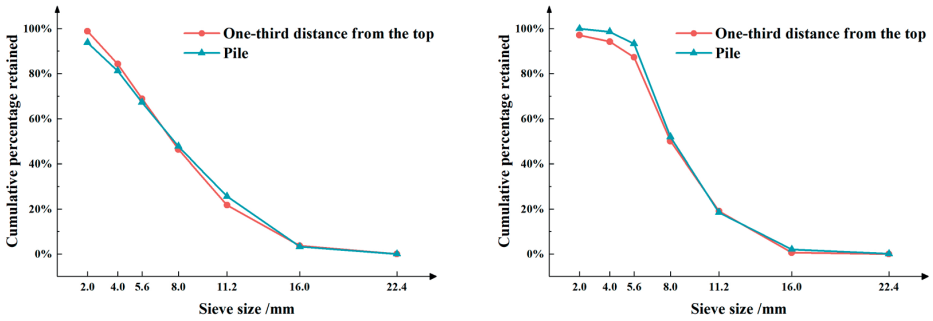


(b) One-third distance from the top



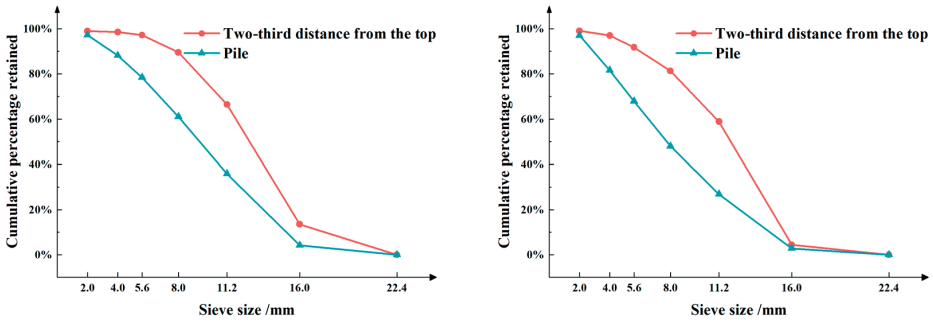


(c) Two-thirds distance from the top

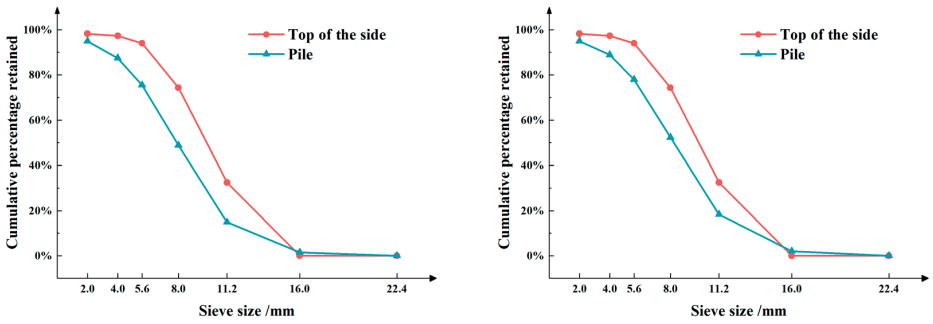


(d) Top of the side

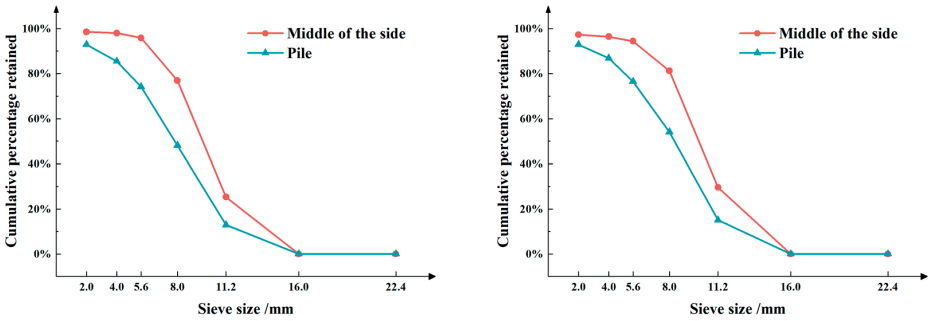


(e) Middle of the side

Figure 4.13: Cumulative percentage retained at different sampling areas

The observed results can be attributed to the utilization of the feeding system, which facilitates a uniform mixing and output of the RCA. As the RCA are transported onto the conveyor belt, it forms a triangular pile (Figure 4.4 (b)) that is generated layer by layer symmetrically and uniformly, starting from the inside and progressing toward the outside. This process allows for the deduction of the overall PSD by analyzing the PSD of a single full side surface of the outermost layer.

However, it is important to note that within each layer, there may be uneven separation, leading to variations in the PSD of different areas. Consequently, the PSD is not identical across different areas within each layer. More generally, when a different material is used or the same material is in different states (e.g., varying humidity levels), the PSD of the full side surface tends to be representative when employing this feeding method. In contrast, the areas of representative strips on the surface may not always be consistent, necessitating further experimentation for comprehensive analysis. In the present study, the RCA used were treated with the C2CA technique, ensuring a constant material state and allowing for consistent conclusions to be drawn.

### Numerical Relationship Establishment

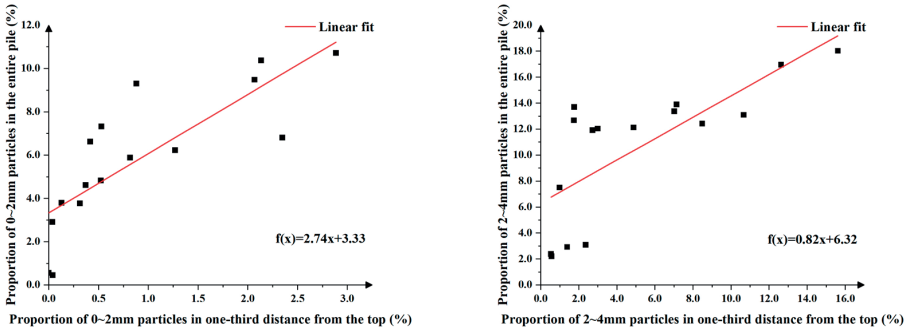


(a) 0-2.0 mm

(b) 2.0-4.0 mm

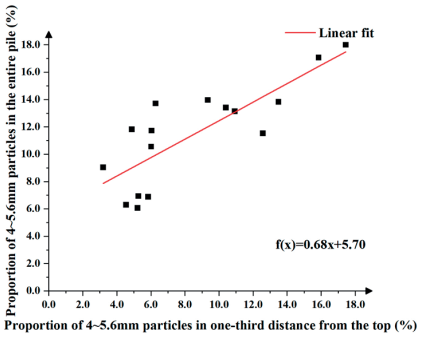


(c) 4.0-5.6 mm

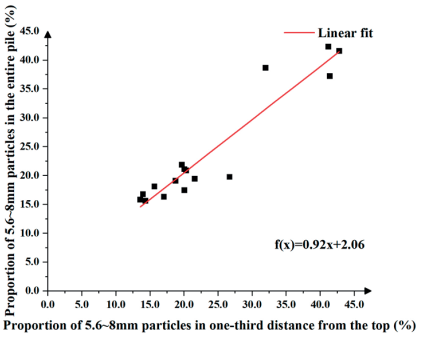


(d) 5.6-8.0 mm

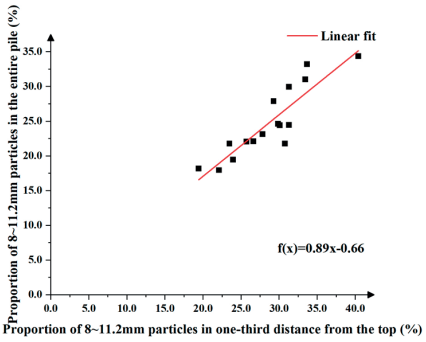


(e) 8.0-11.2 mm

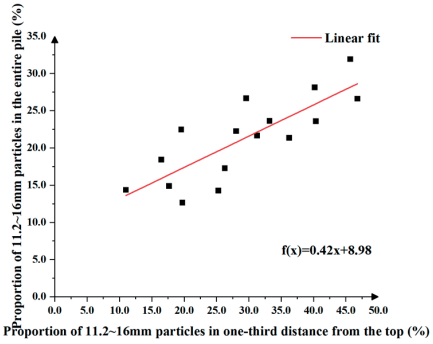


(f) 11.2-16.0 mm

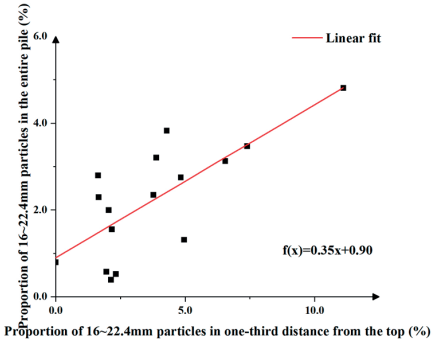


(g) 16.0-22.4 mm

Figure 4.14: The linear fit between the proportion of different-sized particles in one-third distance from the top and the entire pile

A total of sixteen sets of experiments were conducted using different batches of RCA, with samples taken at the one-third distance from the top of the RCA piles, marked and identified using paint to ensure consistent sampling. These samples, as well as the entire RCA piles, underwent manual sieving to obtain mass percentage data for different particle size ranges. The collected data of the sampled areas were then compared and matched with the corresponding data from the entire RCA piles, and the results were visualized in Figure 4.14.

Table 4.2: The comparison of root mean square errors (RMSE) before and after the adjustment

| **Root Mean Square Errors (wt%)** | **Before adjustment (wt%)** | **After adjustment (wt%)** |
|---|---|---|
| Test 1 | 4.10 | 3.25 |
| Test 2 | 4.57 | 3.97 |
| Test 3 | 2.63 | 2.48 |
| Test 4 | 4.41 | 1.63 |
| Test 5 | 5.73 | 2.32 |
| Test 6 | 5.68 | 2.13 |
| Test 7 | 5.37 | 1.14 |
| Test 8 | 5.50 | 1.43 |
| Test 9 | 10.04 | 3.29 |
| Test 10 | 3.46 | 1.63 |
| Test 11 | 2.79 | 2.77 |
| Test 12 | 6.54 | 0.54 |
| Test 13 | 2.79 | 2.37 |
| Test 14 | 7.01 | 1.45 |
| Test 15 | 8.30 | 2.37 |
| Test 16 | 8.14 | 5.48 |

Additionally, a linear fitting was applied to establish a relationship between the sampled data and the overall data. Taking into account experimental errors and the impact of manual sieving, it can be observed that a certain linear relationship existed between the sampled data and the overall data within each particle size range. Leveraging the obtained linear relationship, each mass percentage data of sampled areas was corrected accordingly. However, due to the corrections made, the sum of percentages for each particle size range no longer added up to 100%. Therefore, it was necessary to recalculate the percentage for each particle size range to ensure consistency. Table 4.2 provides

a comparison of the results before and after the correction process. The comparison demonstrates a decrease in the RMSE for the curves representing the cumulative percentage retained of the sampled areas and the entire RCA piles. This reduction in RMSE values is particularly significant in cases where the initial RMSE was high, indicating a substantial improvement in the alignment between the curves. However, in cases where the initial RMSE was already low, the effect of the correction is relatively minor.

These findings highlight the importance of considering experimental errors and applying appropriate corrections to accurately represent the PSD of RCA piles. By refining the data through the analysis and correction process, the reliability and accuracy of the obtained results are enhanced.

### 4.3.2. PSD ESTIMATION



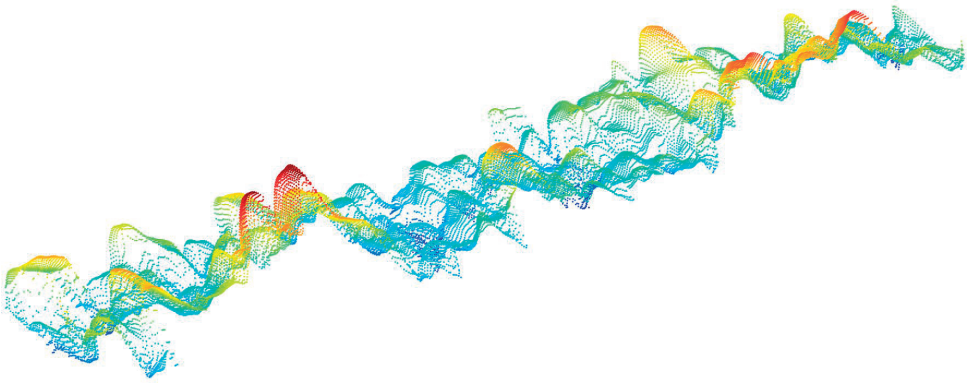

(a) 3D view of the 3D point cloud data

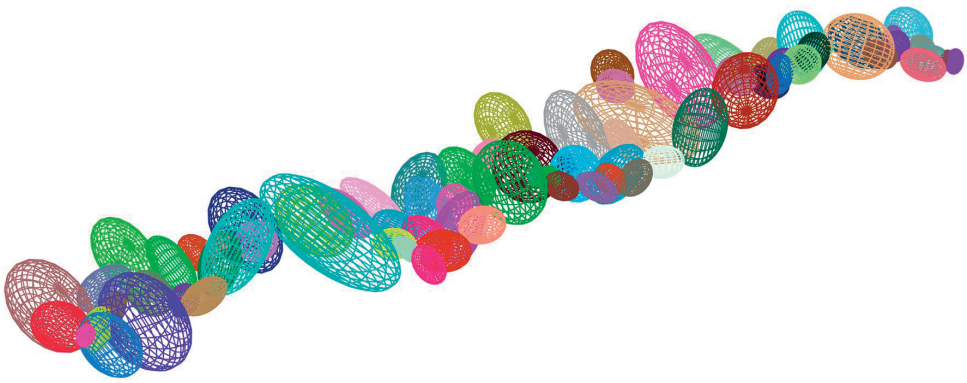

(b) Ellipsoids fitted to each particle

Figure 4.15: 3D point cloud data processing

Figure 4.15 (a) presents the 3D point cloud data obtained from the 20 mm-wide strip

located at the one-third distance from the top on the side surface of the RCA piles using the 3D scanner Gocator. To analyze the data, ellipsoids were fitted to the 3D point cloud data (Figure 4.15 (b)). The parameters of the fitted ellipsoids, specifically the lengths of three axes, were statistically analyzed. Among these parameters, the second shortest axis length was selected as the particle size parameter for particle counting. This selection was made to replicate the manual sieving process using circular sieves. By utilizing the second shortest axis length, the methodology aims to approximate the PSD in a manner consistent with traditional manual sieving techniques.



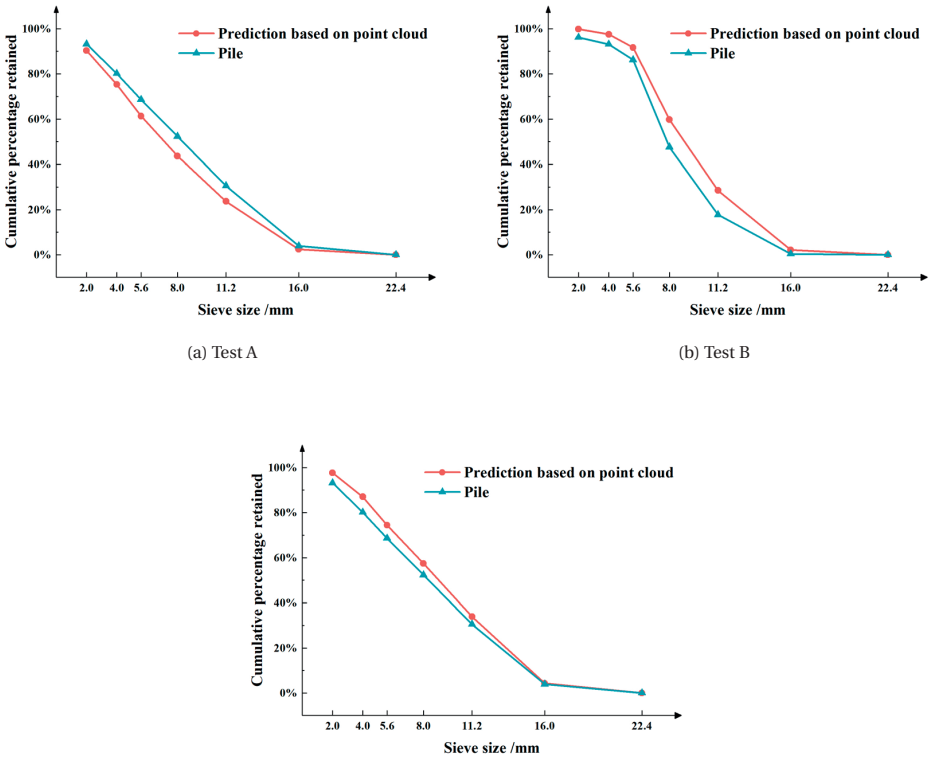


(a) Test A

(b) Test B

(c) Test C

Figure 4.16: Cumulative percentage retained curves

To obtain the cumulative percentage retained curves, it was necessary to determine the mass of each particle size range. The mass was estimated by calculating the volume and apparent density of each particle separately. The volume of each particle was estimated based on the volume of the fitted ellipsoids. Notably, during the estimation of particle mass, it was observed that smaller RCA particle sizes corresponded to higher apparent densities. To address this observation, a correction was applied to the mass of particles in different particle size ranges. By employing the correction method mentioned in the previous section, the mass percentages of each particle size range were

adjusted accordingly. This adjustment facilitated the generation of the final cumulative percentage retained curves.

Figure 4.16 shows the comparison between the cumulative percentage retained curves predicted by the 3D point cloud data and those obtained by manual sieving, according to the results of three different pilot implementation scanning experiments. To evaluate the performance of the prediction method, the RMSE between the predicted values and the manually measured values were calculated for each experiment, yielding values of 5.26%, 6.09%, and 4.69%, respectively. These RMSE values indicated the good performance and accuracy of the method in predicting the PSD of RCA piles on a conveyor belt.

### 4.3.3. ADJUSTMENT FOR OPTIMAL PSD



The above-mentioned predictions of the cumulative percentage retained curves are compared against the European Standard. From Figure 4.17 (a)(i), (b)(i), and (c), it is evident that among the three tests, the PSD in Test C meets the upper and lower limits of the EU standards, eliminating the need for additional adjustments. In contrast, Tests A and B fall short of these standards, necessitating the incorporation of RCA of varied particle sizes to achieve the required PSD, as delineated in 4.2.4 PSD Optimization.

Quantitative adjustments for Test A specify that for every 100.0 kg, an addition of 22.3 kg of aggregate is required in the 4.0 to 5.6 mm range, 18.9 kg in the 5.6 to 8.0 mm range, 18.9 kg in the 8.0 to 11.2 mm range, and 18.9 kg in the 11.2 to 16.0 mm range to meet the desired standards. It is important to note that the ADR coarse product is wind-sifted in the final step of the ADR process. If the airflow of the wind sifter is too mild, or if the ADR is operated at too high a feed rate, too much fine material (2.0-4.0 mm) will end up in the coarse product. This situation necessitates the addition of a significant amount of coarser particles to correct the PSD, as seen in Test A, where approximately 80 kg of additional material per 100 kg is required. However, the technology described in this study could generate a signal that automatically adjusts the wind-sifting airflow to higher levels, thereby reducing the amount of fines in the coarse product and potentially eliminating the need for additional material correction.

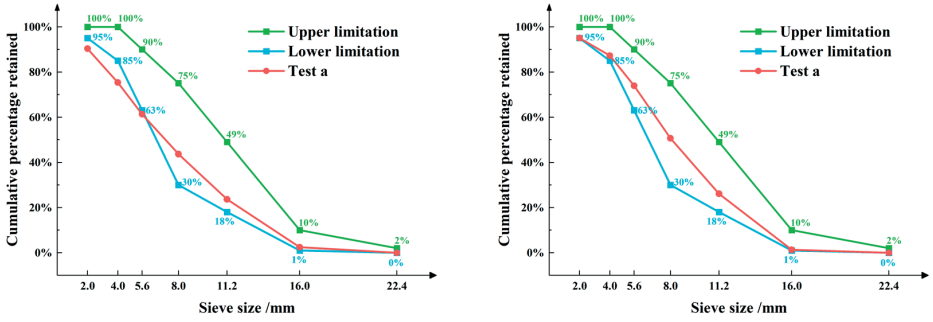


(i) Predicted by 3D point cloud data

(ii) Adjusted for optimal PSD

(a) Test A

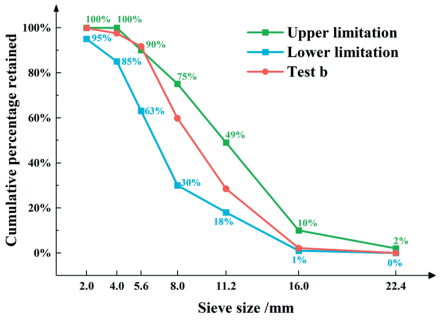


(i) Predicted by 3D point cloud data

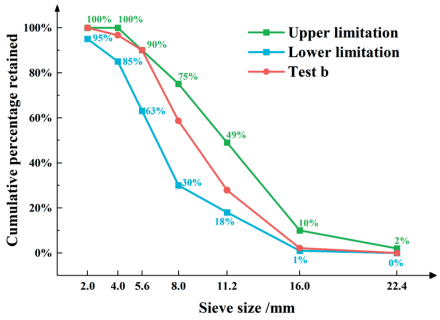


(ii) Adjusted for optimal PSD

(b) Test B

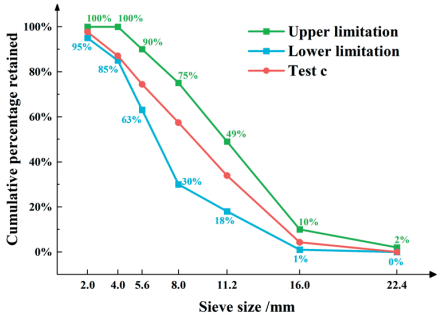


(c) Test C

Figure 4.17: Comparison before and after optimization

Conversely, Test B necessitates a notably lesser augmentation, with only 0.7 kg of aggregate required in both the 2.0 to 4.0 mm and 4.0 to 5.6 mm ranges per 100 kg. Illustrated in Figure 4.17 (a)(ii) and (b)(ii), are the cumulative percentage retained curves post-aggregate addition, which successfully achieved optimal PSD.

## 4.4. Conclusion

The proposed system introduces a reliable and efficient technology for the intelligent design of optimal PSD with unscreened RCA, consisting of the following steps: a) feeding RCA onto the conveyor belt; b) sampling a target area using the 3D scanner Gocator; c) employing the 3D surface analysis for PSD estimation; d) correcting deviations, and e) adjusting for optimal PSD by mixing in specific particle sizes or changing the parameters of the RCA production process. This technology improves PSD by assessing RCA piles on a conveyor belt using 3D scanning technology. Continuous measurements can be obtained without interrupting the material flow, facilitating the effective utilization of RCA in concrete aggregate recycling. The developed approach allows for the estimation

of the entire PSD based on the analysis of the PSD data obtained from measuring a 20 mm-wide strip located at the one-third distance from the top of the single side surface of the triangular RCA piles. It is important to emphasize the significance of this finding, as there was basically no guarantee that the analysis of a small part of the pile side would give such a good representation of the overall PSD. The analysis and correction process further improves the accuracy of the obtained PSD data. The 3D surface analysis demonstrates good performance and accuracy in predicting the PSD of RCA piles, as evidenced by the low RMSE obtained when compared to manually measured values.

This study contributes valuable insights to the field of RCA analysis and provides a solid foundation for accurate characterization and assessment of the RCA properties. Additionally, it enhances the efficiency and accuracy of RCA analysis, enabling researchers and practitioners to obtain reliable PSD information with minimal effort. The demonstrated effectiveness of inferring the overall PSD from a single measured part expands the possibilities for efficient and cost-effective analysis of RCA piles, benefiting both researchers and industry professionals in their pursuit of sustainable construction practices. This timely information empowers decision-makers with the necessary knowledge to make informed choices regarding the utilization, processing, and management of RCA in concrete aggregate recycling. It enhances efficiency and effectiveness in the recycling process, contributing to sustainable practices and resource optimization. Moreover, the proposed system offers several advantages over conventional methods:



**(1)Non-contact measurement** The non-contact nature of the measurement ensures that the aggregate piles remain undisturbed during the transportation process on the conveyor belt, preserving their natural arrangement and characteristics. This non-contact approach contributes to maintaining the integrity of the triangular piles and minimizes the potential for bias and human error in the assessment of RCA properties.

**(2)Simplified data acquisition** The system simplifies the data acquisition process by reducing the number of required measurements, improving efficiency while maintaining accuracy. It eliminates the need for manual sampling, thereby reducing labor costs and improving overall efficiency.

**(3)3D surface analysis** Applying 3D surface analysis allows for the precise and detailed measurement of RCA particle shapes and sizes, even in complex and dynamic environments. This overcomes the limitations of traditional 2D imaging techniques, leading to better quality control and more reliable data for optimizing PSD.

**(4)PSD optimization** The algorithm enables the achievement of optimal PSD with the minimal addition of various RCA particle sizes, facilitating the development of high-performance concrete.

**(5)Real-time capability** The real-time capability of the system enables prompt feedback and adjustment of recycling processes, leading to improved productivity and optimal resource utilization.

While this study shows some clear benefits, it also acknowledges certain limitations that necessitate additional investigation. Future research could beneficially explore the scalability of the proposed method, particularly its applicability across diverse aggregate types. Moreover, addressing the existing constraints in the algorithm's performance remains a crucial area for further refinement. Subsequent studies might productively focus on enhancing the algorithm's efficiency, extending the method's applicability to a broader range of conveyor systems, and strategically integrating this technology within other quality control frameworks to optimize overall process efficiency.

# BIBLIOGRAPHY


Akashi, M., Otani, T., Shimosaka, A., Shirakawa, Y., & Hidaka, J. (2010). Estimation of particle size distribution from cross-sectional particle diameter on the cutting plane [Special Issue of 4th Asian Particle Technology Symposium (APT 2009) - I]. *Advanced Powder Technology*, *21*(6), 676–680.

Al-Bayati, H. K. A., Das, P. K., Tighe, S. L., & Baaj, H. (2016). Evaluation of various treatment methods for enhancing the physical and morphological properties of coarse recycled concrete aggregate. *Construction and Building Materials*, *112*, 284–298.

Al-Thyabat, S., & Miles, N. (2006). An improved estimation of size distribution from particle profile measurements. *Powder Technology*, *166*(3), 152–160.

Bai, F., Fan, M., Yang, H., & Dong, L. (2021). Image segmentation method for coal particle size distribution analysis. *Particuology*, *56*, 163–170.

Bamford, T., Esmaeili, K., & Schoellig, A. P. (2021). A deep learning approach for rock fragmentation analysis. *International Journal of Rock Mechanics and Mining Sciences*, *145*, 104839.

Bi, Z., & Wang, L. (2010). Advances in 3d data acquisition and processing for industrial applications. *Robotics and Computer-Integrated Manufacturing*, *26*(5), 403–413.

Brand, A. S., Roesler, J. R., & Salas, A. (2015). Initial moisture and mixing effects on higher quality recycled coarse aggregate concrete. *Construction and Building Materials*, *79*, 83–89.

Braun, J., & Willett, S. D. (2013). A very efficient o(n), implicit and parallel method to solve the stream power equation governing fluvial incision and landscape evolution. *Geomorphology*, *180-181*, 170–179.

Chang, C., Di Maio, F., Rem, P., Gebremariam, A. T., Mehari, F., & Xia, H. (2022). Cluster-based identification algorithm for in-line recycled concrete aggregates characterization using laser-induced breakdown spectroscopy (libs). *Resources, Conservation and Recycling*, *185*, 106507.

Chatterjee, S., Bhattacherjee, A., Samanta, B., & Pal, S. K. (2010). Image-based quality monitoring system of limestone ore grades. *Computers in Industry*, *61*(5), 391–408.

Engin, I. C., & Maerz, N. H. (2019). Size distribution analysis of aggregates using lidar scan data and an alternate algorithm. *Measurement*, *143*, 136–143.

Etxeberria, M. (2020). 13 - the suitability of concrete using recycled aggregates (ras) for high-performance concrete. In F. Pacheco-Torgal, Y. Ding, F. Colangelo, R. Tuladhar, & A. Koutamanis (Eds.), *Advances in construction and demolition waste recycling* (pp. 253–284). Woodhead Publishing.

Evangelista, L., Guedes, M., de Brito, J., Ferro, A., & Pereira, M. (2015). Physical, chemical and mineralogical properties of fine recycled aggregates made from concrete waste. *Construction and Building Materials*, *86*, 178–188.

Florea, M., & Brouwers, H. (2013). Properties of various size fractions of crushed concrete related to process conditions and re-use. *Cement and Concrete Research*, *52*, 11–21.

Galdames, F. J., Perez, C. A., Estévez, P. A., & Adams, M. (2017). Classification of rock lithology by laser range 3d and color images. *International Journal of Mineral Processing*, *160*, 47–57.

Gao, L., Wang, D., & Miao, Y. (2024). A review of two-dimensional image-based technologies for size and shape characterization of coarse-grained granular soils. *Powder Technology*, *445*, 120115.

Gebremariam, A. T., Di Maio, F., Vahidi, A., & Rem, P. (2020). Innovative technologies for recycling end-of-life concrete waste in the built environment. *Resources, Conservation and Recycling*, *163*, 104911.

Hamzeloo, E., Massinaei, M., & Mehrshad, N. (2014). Estimation of particle size distribution on an industrial conveyor belt using image analysis and neural networks. *Powder Technology*, *261*, 185–190.

Han, J., & Thakur, J. K. (2015). Sustainable roadway construction using recycled aggregates with geosynthetics. *Sustainable Cities and Society*, *14*, 342–350.

Ibrahim, M. I. M. (2016). Estimating the sustainability returns of recycling construction waste from building projects. *Sustainable Cities and Society*, *23*, 78–93.

Jayasuriya, A., Adams, M. P., & Bandelt, M. J. (2018). Understanding variability in recycled aggregate concrete mechanical properties through numerical simulation and statistical evaluation. *Construction and Building Materials*, *178*, 301–312.

Kelley, H. J. (1962). Method of gradients. In *Mathematics in science and engineering* (pp. 205–254, Vol. 5). Elsevier.

Khoury, E., Ambrós, W., Cazacliu, B., Sampaio, C. H., & Remond, S. (2018). Heterogeneity of recycled concrete aggregates, an intrinsic variability. *Construction and Building Materials*, *175*, 705–713.

Kistner, M., Jemwa, G. T., & Aldrich, C. (2013). Monitoring of mineral processing systems by using textural image analysis [Process Mineralogy]. *Minerals Engineering*, *52*, 169–177.

Kou, S.-c., & Poon, C.-s. (2015). Effect of the quality of parent concrete on the properties of high performance recycled aggregate concrete. *Construction and Building Materials*, *77*, 501–508.

Lotfy, A., & Al-Fayez, M. (2015). Performance evaluation of structural concrete using controlled quality coarse and fine recycled concrete aggregate. *Cement and Concrete Composites*, *61*, 36–43.

Mazhoud, B., Sedran, T., Cazacliu, B., Cothenet, A., & Torrenti, J.-M. (2022). Influence of residual mortar volume on the properties of recycled concrete aggregates. *Journal of Building Engineering*, *57*, 104945.

Meddah, M. S., Zitouni, S., & Belâabes, S. (2010). Effect of content and particle size distribution of coarse aggregate on the compressive strength of concrete. *Construction and Building Materials*, *24*(4), 505–512.

Mohammadinia, A., Arulrajah, A., Haghighi, H., & Horpibulsuk, S. (2017). Effect of lime stabilization on the mechanical and micro-scale properties of recycled demolition materials. *Sustainable Cities and Society*, *30*, 58–65.

Mollaei, A., Bachmann, C., & Haas, C. (2023). Estimating the recoverable value of in-situ building materials. *Sustainable Cities and Society*, *91*, 104455.

Moon, D., Chung, S., Kwon, S., Seo, J., & Shin, J. (2019). Comparison and utilization of point cloud generated from photogrammetry and laser scanning: 3d world model for smart heavy equipment planning. *Automation in Construction*, *98*, 322–331.

Nedeljković, M., Visser, J., Šavija, B., Valcke, S., & Schlangen, E. (2021). Use of fine recycled concrete aggregates in concrete: A critical review. *Journal of Building Engineering*, *38*, 102196.

O'Callaghan, J. F., & Mark, D. M. (1984). The extraction of drainage networks from digital elevation data. *Computer Vision, Graphics, and Image Processing*, *28*(3), 323–344.

Olivier, L. E., Maritz, M. G., & Craig, I. K. (2020). Estimating ore particle size distribution using a deep convolutional neural network [21st IFAC World Congress]. *IFAC-PapersOnLine*, *53*(2), 12038–12043.

Pacheco, J., de Brito, J., Chastre, C., & Evangelista, L. (2019). Experimental investigation on the variability of the main mechanical properties of concrete produced with coarse recycled concrete aggregates. *Construction and Building Materials*, *201*, 110–120.

Pedro, D., de Brito, J., & Evangelista, L. (2017). Mechanical characterization of high performance concrete prepared with recycled aggregates and silica fume from precast industry. *Journal of Cleaner Production*, *164*, 939–949.

Sinoh, S. S., Othman, F., & Onn, C. C. (2023). Circular economy potential of sustainable aggregates for the malaysian construction industry. *Sustainable Cities and Society*, *89*, 104332.

Siregar, A., Rafiq, M. I., & Mulheron, M. (2017). Experimental investigation of the effects of aggregate size distribution on the fracture behaviour of high strength concrete. *Construction and Building Materials*, *150*, 252–259.

Standard, B. (2002). Aggregates for concrete. *BS EN*, *12620*.

Steer, P., Guerit, L., Lague, D., Crave, A., & Gourdon, A. (2022). Size, shape and orientation matter: Fast and semi-automatic measurement of grain geometries from 3d point clouds. *Earth Surface Dynamics*, *10*(6), 1211–1232.

Sun, H., Fan, B., Memon, S. A., Cen, Z., Gao, X., Lin, B., Liu, B., Li, D., Xing, F., & Zhang, X. (2017). 3d particle size distribution of inter-ground portland limestone/slag cement from 2d observations: Characterization and distribution evaluation. *Construction and Building Materials*, *147*, 550–557.

Tafesse, S., Fernlund, J., & Bergholm, F. (2012). Digital sieving-matlab based 3-d image analysis. *Engineering Geology*, *137-138*, 74–84.

Tessier, J., Duchesne, C., & Bartolacci, G. (2007). A machine vision approach to on-line estimation of run-of-mine ore composition on conveyor belts. *Minerals Engineering*, *20*(12), 1129–1144.

Thurley, M. J. (2011). Automated online measurement of limestone particle size distributions using 3d range data [Special Issue on Automation in Mining, Minerals and Metal Processing]. *Journal of Process Control*, *21*(2), 254–262.

Wang, B., Yan, L., Fu, Q., & Kasal, B. (2021). A comprehensive review on recycled aggregate and recycled aggregate concrete. *Resources, Conservation and Recycling*, *171*, 105565.

Wang, Y., Yu, B., Zhang, X., & Liang, J. (2022). Automatic extraction and evaluation of pavement three-dimensional surface texture using laser scanning technology. *Automation in Construction*, *141*, 104410.

Wilson, J. P., & Gallant, J. C. (2000). *Terrain analysis: Principles and applications*. John Wiley & Sons.

Wu, C.-R., Hong, Z.-Q., Zhang, J.-L., & Kou, S.-C. (2020). Pore size distribution and itz performance of mortars prepared with different bio-deposition approaches for the treatment of recycled concrete aggregate. *Cement and Concrete Composites*, *111*, 103631.

Wu, J., Feng, M., Mao, X., Xu, J., Zhang, W., Ni, X., & Han, G. (2018). Particle size distribution of aggregate effects on mechanical and structural properties of cemented rockfill: Experiments and modeling. *Construction and Building Materials*, *193*, 295–311.

Wu, X., Liu, X.-Y., Sun, W., Mao, C.-G., & Yu, C. (2019). An image-based method for online measurement of the size distribution of iron green pellets using dual morphological reconstruction and circle-scan. *Powder Technology*, *347*, 186–198.

Yaghoobi, H., Mansouri, H., Ebrahimi Farsangi, M. A., & Nezamabadi-Pour, H. (2019). Determining the fragmented rock size distribution using textural feature extraction of images. *Powder Technology*, *342*, 630–641.

Yoshida, H., Yamamoto, T., Mori, Y., Masuda, H., Okazaki, K., & Sugasawa, H. (2014). Particle size measurement of reference particle candidates and uncertainty region of count and mass based cumulative distribution. *Advanced Powder Technology*, *25*(6), 1748–1753.

Zeng, Z., Wei, Y., Wei, Z., Yao, W., Wang, C., Huang, B., Gong, M., & Yang, J. (2022). Deep learning enabled particle analysis for quality assurance of construction materials. *Automation in Construction*, *140*, 104374.

Zhang, Z., Liu, Y., Hu, Q., Zhang, Z., Wang, L., Liu, X., & Xia, X. (2020). Multi-information online detection of coal quality based on machine vision. *Powder Technology*, *374*, 250–262.

Zhang, Z., Yang, J., Ding, L., & Zhao, Y. (2012). An improved estimation of coal particle mass using image analysis. *Powder Technology*, *229*, 178–184.

Zhou, Y., Zhou, H., Chen, T., Hu, C., Liang, Z., Zhao, C., & Wang, F. (2023). Detection of rockfill gradation based on video image recognition. *Automation in Construction*, *154*, 104965.

# 5

# Optimizing Contaminant Detection Precision in Recycled Coarse Aggregates via Surface-Condition-Adaptive Method

*Recycling coarse aggregates from construction and demolition waste is essential for sustainable construction practices. However, the quality of recycled coarse aggregates (RCA) often fluctuates significantly, in contrast to the more stable quality of natural aggregates. Contaminants in RCA notably compromise its quality and usability. Therefore, automating the quality control of RCA is necessary for the recycling industry. This study introduces an industry-focused, innovative, and rapid quality control system that combines Laser-Induced Breakdown Spectroscopy (LIBS) with 3D scanning technologies to enhance the detection of contaminants in RCA streams. The system involves a synchronized application of LIBS for spectral analysis and 3D scanning for the physical characterization of different materials. Results reveal that the dependability of single-shot LIBS analysis has been enhanced, thus elevating the precision of contaminant detection. This improvement is achieved by accounting for the laser shot's angle of incidence and focal length adjustments. The introduced technology holds potential for application in the real-time examination of substantial volumes of RCA, facilitating a rapid and reliable quality control method. This rapid assessment technique delivers online data about the concentration*

Apart from minor updates, this chapter has been published in C. Chang et al., 2025.

*of contaminants in RCA, including recycled fine aggregates, cement paste, bricks, foam, glass, gypsum, mineral fibers, plastics, and wood. This data is both essential and sufficient for choosing a cost-effective mortar recipe and guaranteeing the performance of the final concrete product in terms of strength and durability in construction projects. The system can monitor the quality of RCA flows at throughputs of 50 tons per hour per conveyor, characterizing approximately 4,000 particles in every ton of RCA, in this way signaling the most critical contaminants at levels of less than 50 parts per million. With these characteristics, the system could also become relevant for other applications, such as characterizing mining waste or solid biofuels for power plants.*

## 5.1. INTRODUCTION

THE global shift towards sustainable construction practices has increasingly emphasized the importance of recycling materials, particularly in the context of construction and demolition waste. Among these materials, recycled coarse aggregates (RCA) are of significant interest due to their potential to reduce environmental impact and contribute to resource conservation (de Andrade Salgado and de Andrade Silva, 2022; Silva et al., 2017). The quality of the aggregate improves with more thorough waste treatment (Martín-Morales et al., 2011). Despite its potential, the effective recycling of RCA is hampered by significant challenges in accurately detecting contaminants, a crucial step to ensure the quality and safety of recycled materials.

The challenge primarily arises from the frequent and significant fluctuations in RCA quality (Lux et al., 2023). Natural aggregates originate from relatively uniform geological sources, maintaining stable quality over long periods. In contrast, RCA quality can exhibit considerable fluctuations over relatively short intervals due to the diverse nature of demolition waste. Such waste includes materials from different sections of various demolition sites and is processed with differences in recycling methods. Therefore, the non-uniform composition and properties of the input demolition waste directly influences the uniformity of the resulting RCA.



Research on RCA has predominantly examined how contaminants affect concrete quality (Abid et al., 2018; Ahmad et al., 2023; Bai et al., 2020). However, precise detection and classification of these contaminants in RCA have received less attention. Vegas et al. analyzed mixed recycled aggregates from various European countries, revealing that near-infrared sorting effectively reduces, if not eliminates, problematic fractions (Vegas et al., 2015). Serranti and Bonifazi developed strategies to detect asbestos-containing materials and other contaminants in concrete aggregates derived from demolition waste (Serranti and Bonifazi, 2020). Xia and Bakker examined different material particle samples, concluding that the success of practical testing depends on the training set's quality and the management of potential false positives (Xia and Bakker, 2014). Despite these advancements, a significant gap remains in methods for in-situ evaluation of contaminants in RCA, particularly their application in industrial scenarios (Bonifazi et al., 2018; Serranti et al., 2023).

A primary challenge in the field of recycling RCA remains the accurate detection of contaminants that might evade initial sorting processes. This is particularly crucial in quality control, where even a small percentage of undetected contaminants can compromise the final product's integrity. False positives in sorting are less critical, as they result in acceptable losses of non-contaminated material. However, the accurate detection and minimization of false positives in quality control are essential to ensure the reliability and high quality of the recycled aggregates. A high rate of false positives can lead to RCA being mistakenly identified as contaminated, which can diminish the quality and value of what was originally high-quality and valuable material. Currently, the field lacks a rapid and precise method for detecting a wide range of contaminants in RCA. This gap is largely due to the inconsistent and unpredictable nature of these contaminants. These inconsistencies hinder the accurate detection of contaminants, complicating the development of a universal, straightforward method for detecting all contaminants. Consequently, this leads to considerable discrepancies in the quality assessments of RCA. Ad-

dressing these challenges requires the adoption of efficient, reliable, non-destructive, and cost-effective sensor technologies. Such technologies would enable automatic contaminant detection, addressing the diverse nature of recycled materials. Implementing this approach will enhance quality control in the use of RCA, ensuring a more consistent and reliable end product.

Laser-induced breakdown spectroscopy (LIBS) is emerging as a highly promising technology for real-time, on-site elemental analysis, particularly within the expansive market of concrete production industries (Mansoori et al., 2011; Yin et al., 2016). LIBS offers numerous advantages for practical operations, including minimal or no sample preparation, real-time analysis, and comprehensive element measurement capabilities (J. Wang et al., 2020). In the concrete sector, LIBS is commonly employed for both identifying and quantifying chemical elements (qualitative and quantitative) (Cabral et al., 2023). However, its application in classifying, recognizing, and recycling various construction materials remains underexplored (C. Chang et al., 2022; Elfaham and Eldemerdash, 2019; Xia and Bakker, 2014). Gottlieb et al. introduced an algorithm for heterogeneous concrete to isolate spectral data of non-relevant aggregates and cement matrix (Gottlieb et al., 2017). Völker et al. investigated cement paste prisms to distinguish cement types and noted that additional moisture changes the laser material interaction and the composition of vaporized material volume, affecting classification (Völker et al., 2020). Živković et al. used LIBS with microscopic-scale spatial resolution to map elemental distribution in archaeological samples from the Smederevo Fortress, Serbia (Živković et al., 2021). Junwei et al. noted that in the cement industry, the matrix of the cement raw meal varies due to different sources, possibly extending beyond the calibration sample concentration range (Junwei et al., 2018). Most studies are confined to laboratory environments, emphasizing the need for environmental considerations during measurements (Dietz et al., 2019; Mansoori et al., 2011). Hence, practical application in concrete industrial production is limited.

A significant challenge for LIBS in quantitative measurements is its relatively high uncertainty or low repeatability (Z. Wang et al., 2021). This uncertainty in collected spectral data significantly impacts classification accuracy. This is due to various factors, but most research work was concentrated superficially on the impact of different system parameters on the emission signals (Kim et al., 2013; J. Wang et al., 2020), temperatures (Palanco et al., 1999) and ambient gas (Yu et al., 2020) on LIBS performance. While many algorithms have been developed to classify materials using LIBS, less attention has been given to surface information analysis to enhance spectral signals. Zhang et al. found that adjusting lens-to-sample distances improves LIBS's analytical performance, enhancing precision and detection limits (Zhang et al., 2012). Wang et al. investigated the effect of surface roughness on solid samples, concluding that preparing smooth surfaces leads to more consistent laser-sample interactions and fewer plasma fluctuations (Z. Wang et al., 2021). However, in practical scenarios, the uneven surfaces of materials like RCA pose challenges for LIBS to obtain high-quality spectral information.

This study presents an innovative and rapid quality control system that enhances contaminant detection precision in RCA streams by employing surface-condition-adaptive LIBS. This advancement results from merging LIBS with 3D scanning technology, providing vital data on surface conditions at each laser shooting point. Con-

sequently, this integration substantially enhances the reliability of analytical results obtained from each single LIBS laser shot. For effective operation, precise synchronization and calibration of the two sensors are essential. The technique involves a detailed analysis of the LIBS laser focal length and angle of incidence at the shooting point. The process continues by filtering the collected spectral data, omitting laser shots that do not meet the required standards. Then, both the angles of incidence and corresponding spectral values are incorporated into the cluster-based classification algorithm. This approach enables the LIBS system to dynamically adjust its analysis based on the real-time surface conditions of each laser shot, significantly reducing the false-positive rates of material misclassification. This adaptive strategy markedly elevates the accuracy of material classification, thereby facilitating rapid quality control processes for RCA streams on the conveyor belt. The research thoroughly assesses this surface-condition-adaptive LIBS method, highlighting its proficiency in precisely identifying a variety of materials commonly encountered in construction waste. Figure 5.1 illustrates the procedural flowchart, offering a visual summary of the methodological sequence employed in this study.



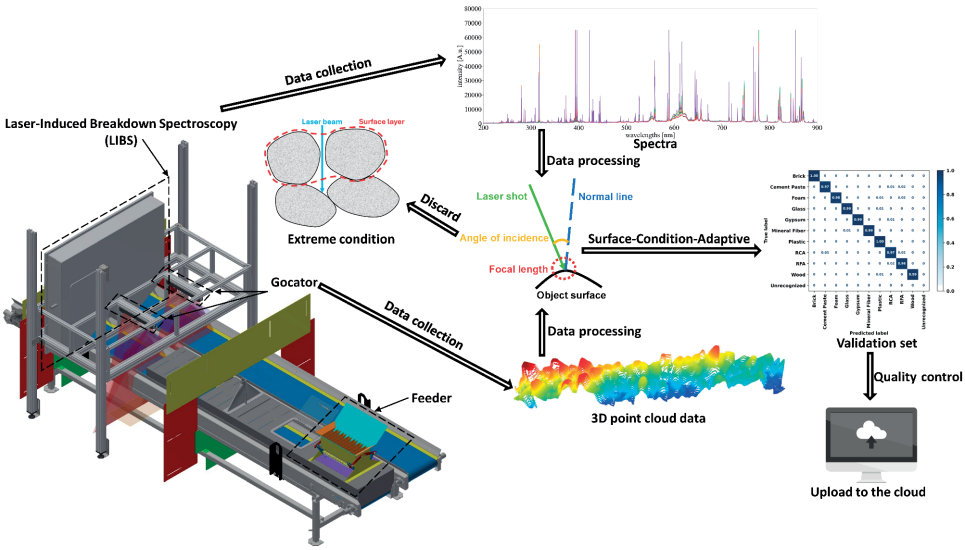


Figure 5.1: Schematic of quality control process

## 5.2. MATERIALS AND METHODS

### 5.2.1. MATERIALS

Demolition waste samples (Figure 5.2) were gathered from sites in the Netherlands for analysis. Distinct materials (bricks, foam, glass, gypsum, mineral fibers, plastics, and wood) were separated either by hand or with the help of inline sorters available at the recycling facility. The End-of-Life (EoL) concrete was obtained relatively clean through selective demolition. This EoL concrete was then processed using the Concrete to Cement

and Aggregate (C2CA) technology (Gebremariam et al., 2020). The output was divided into three categories: RCA ranging from 4.0 to 16.0 mm, recycled fine aggregates (RFA) between 0.25 and 4.0 mm, and cement paste-rich powder sized 0 to 0.25 mm.


Figure 5.2: Demolition waste samples



### 5.2.2. Equipment

#### Sensor-based Quality Control System

The sensor-based quality control system depicted in Figure 5.3 begins with the process of transporting the to-be-inspected objects via a feeder to the conveyor belt, which then conveys them under the sensor system for analysis. This system encompasses two principal sensors: the 3D scanner Gocator and the LIBS. Both sensors are mounted on a fixed frame directly above the conveyor belt. The LIBS is aligned perpendicularly to the direction of the conveyor belt's movement, while the Gocator is oriented parallel to it. The Gocator specializes in detecting the surface conditions of target objects, generating high-resolution (x-direction: 0.378 mm, y-direction: 0.393 mm, z-direction: 0.083 mm), three-dimensional point cloud data that effectively captures the detailed surface topography. On the other hand, LIBS plays a pivotal role in the recognition and classification of various objects.

A distinctive feature of the system's design is the integration of multiple reflective mirrors. The laser beam is divided and directed using a series of beam splitters and mirrors (as shown by the red arrows in Figure 5.3) onto two separate conveyor belts. To further fine-tune the position of the laser beam, a dual-stage system is employed, with each stage directing a laser beam to one of the conveyor belts. The laser's position can be adjusted based on the specific characteristics of the objects being inspected. The laser beams' positioning can be adjusted according to the specific attributes of the objects being inspected. This design enables the simultaneous monitoring of objects on two distinct conveyor belts using just a single Nd : TAG laser.

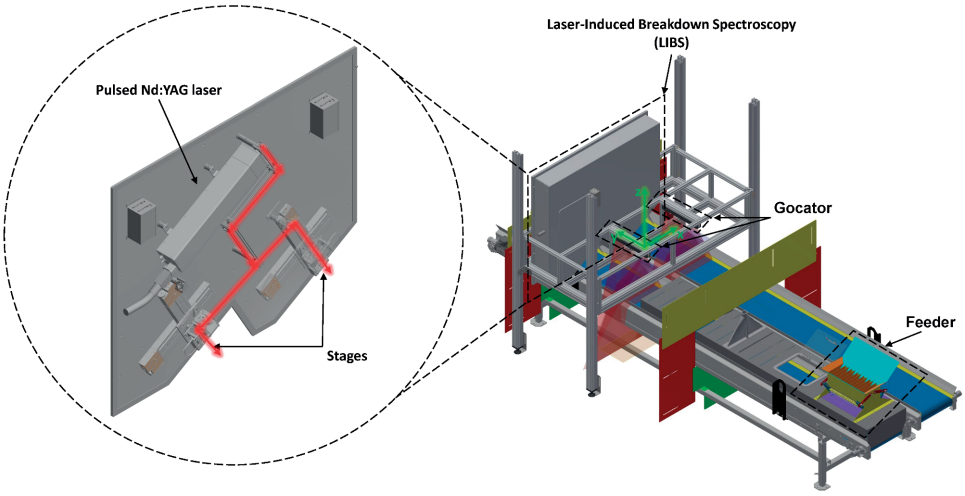


Figure 5.3: Sensor-based quality control system



### SYNCHRONIZATION

To enhance spectral analysis through surface information, it is crucial to synchronize the two sensors. This approach enables enhancement of the analysis of spectra obtained from LIBS by incorporating surface conditions of the target points captured by the Gocator. An integrated encoder is employed for the control and logging of the conveyor belt, Gocator, and LIBS systems. The integrated encoder's resolution is set at 4098 pulses per revolution. Given the conveyor belt's wheel perimeter of 402.116 mm, the belt advances 0.098 mm with each pulse of the integrated encoder. Considering the maximum scanning frequency of the Gocator, its internal encoder resolution is configured at 1024 pulses per revolution. This implies that for every four pulses emitted by the integrated encoder, the Gocator executes one scan. Consequently, the calculated resolution of the Gocator along the conveyor belt's direction of travel is 0.393 mm.

Experimental data indicates a horizontal distance of 6025 integrated encoder pulses, equivalent to 591.203 mm, between the linear scans of the Gocator and the LIBS laser shooting point. Based on this, synchronization of the Gocator and LIBS signals is achieved through the pulse values recorded by the integrated encoder. When the LIBS emits a laser shot, the corresponding pulse value of LIBS recorded by the integrated encoder at that moment is $pv$. Therefore, the surface targeted at that instant corresponds to the $(pv\text{-}6025)/4$ scan in the Gocator's dataset.

### CALIBRATION

Within this setup, two sensors have been securely mounted on the same frame. The LIBS is oriented vertically, while the Gocator sensor maintains a horizontal position and is perpendicular to the plane of the LIBS (as shown in Figure 5.4). The relative positioning of the sensors has been precisely pre-calibrated, ensuring no displacement occurs between them. The conveyor belt, however, is distinct and separate from this frame. In practice, the conveyor belt is inserted beneath the frame to align with the operation

of the sensors. Should the positioning be incorrect, recalibration is required to ensure accuracy.

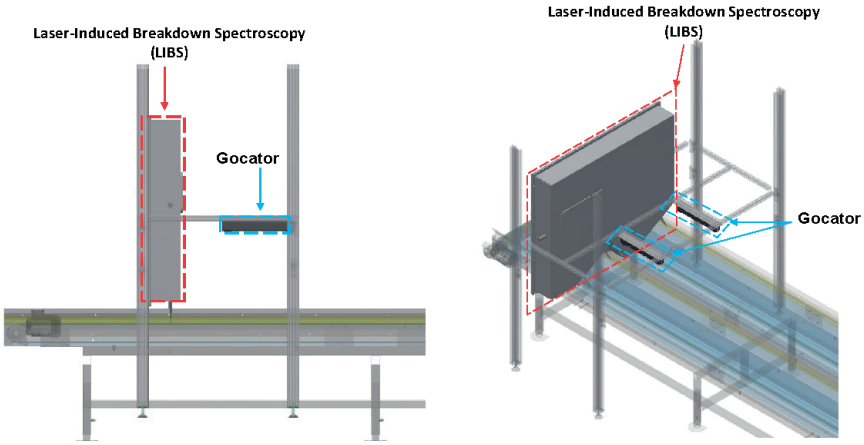


(a) Side view (b) 3D view

Figure 5.4: Pre-calibrated sensors

To enhance clarity, a spatial coordinate system, as illustrated in Figure 5.3, is established. The $x$-axis is defined as the direction perpendicular to the Gocator body, pointing towards the direction of the conveyor belt's movement. The $y$-axis runs parallel to the Gocator body, and the $z$-axis is oriented vertically upwards from the Gocator body.

To address misalignments between the sensor system and the conveyor belt, which can introduce measurement inaccuracies, a calibration methodology is necessary. Specifically, in practical operations, the conveyor belt does not maintain a perfect horizontal position and deviates from the ideal alignment along the $z$-axis, as well as exhibits variations along the $x$ and $y$-axes. The correction approach involves the use of a flat calibration plate placed on the conveyor belt. Two arbitrary points labeled $A$ and $B$, are selected on the plate, ensuring that their $y$-axis coordinates are not identical. The differences along the $x$-axis ($\Delta$x) and the $y$-axis ($\Delta$y) between points $A$ and $B$ are recorded.

As the conveyor belt operates, the calibration plate undergoes scanning by the Gocator. Initially, the Gocator captures the coordinates of point A$\left(x_a, y_a, z_a\right)$. After a span of number t pulses, the Gocator records the coordinates of point B$\left(x_b, y_b, z_b\right)$. The respective differences in the coordinates of points $A$ and $B$ are then calculated as follows:

$$\begin{cases} \Delta x' = x_b - x_a \\ \Delta y' = y_b - y_a \\ \Delta z' = z_b - z_a \end{cases} \tag{5.1}$$

If the conveyor belt is positioned correctly, it should satisfy the following relationships:

$$\begin{cases} \Delta x' = \Delta x \\ \Delta y' = \Delta y \\ \Delta z' = 0 \end{cases} \tag{5.2}$$

If the relationships are not satisfied, this indicates a misalignment in the placement of the conveyor belt, necessitating an adjustment. Referring to Equation Set 5.3, the values for the offset in each pulse along the $x$, $y$, and $z$ axes $(\varepsilon_x, \varepsilon_y, \varepsilon_z)$ can be accurately calculated. These values are then employed to implement the required corrective measures.

$$\begin{cases} x_b = x_a + \Delta x + \varepsilon_x \cdot t \\ y_b = y_a + \Delta y + \varepsilon_y \cdot t \\ z_b = z_a + \varepsilon_z \cdot t \end{cases} \tag{5.3}$$

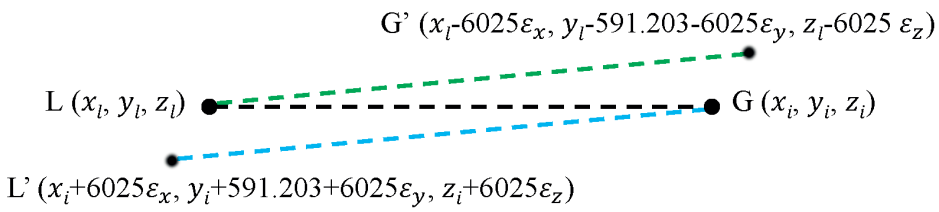


Figure 5.5: Correlation between the LIBS laser shooting point and the Gocator's scanning data

The LIBS and the Gocator are both affixed to the same framework, with their relative positions meticulously pre-calibrated. This ensures that the spatial relationship between the LIBS and the Gocator remains invariant. This alignment allows for a direct and synchronized correlation between the LIBS laser shooting point and the Gocator's scanning data. As illustrated in Figure 5.5, a point $G$ captured by the Gocator travels along the conveyor belt. When the LIBS is set to emit the laser after 6025 pulses, the target point $G$ shifts to a new position, denoted as $L$', due to certain deviations. At this precise moment, the actual shooting point of the LIBS laser is at $L$, corresponding to the point $G$' previously scanned by the Gocator. The spatial correlation of points $L$ and '$G$' are related as follows:

$$\begin{cases} x_l = x_i \\ y_l = y_i + 591.203 \\ z_l = z_i \end{cases} \tag{5.4}$$

After correction, it can be calculated that the actual corresponding point $G$' for the LIBS laser shooting point $L$ is located at the coordinates $(x_i - 6025\varepsilon_x, y_i - 6025\varepsilon_y, z_i - 6025\varepsilon_z)$. This representation effectively maps the corrected laser shooting point to the scanner's coordinate system, ensuring precise spatial alignment and data integration.

### 5.2.3. ANALYSIS METHODS

#### CALCULATION OF 3D POINT CLOUD NORMAL VECTOR

Analyzing the surface condition of objects at laser shooting points requires the determination of the object's surface normal. This step aids in calculating the laser shot's angle of incidence relative to the object's surface. In this study, a hybrid approach is used

to estimate normal vectors within 3D point clouds. This method synergistically combines fixed-radius and K-Nearest neighbors (KNN) algorithms (Corral and Almendros-Jiménez, 2007) to calculate within the smallest possible range around a target point, enabling efficient and precise identification of each point's geometric characteristics in the cloud.

**Neighborhood Definition**

The initial step involves defining each point's neighborhood using a set radius. Given a point $P_u$ with coordinates $(x_u, y_u, z_u)$ in the 3D point cloud, the neighborhood $N(P_u)$ of $P_u$ within a starting radius $r$ is defined as:

$$N(P_u) = \left\{ P_v \middle| \sqrt{(x_u - x_v)^2 + (y_u - y_v)^2 + (z_u - z_v)^2} \leq r, \forall u \neq v \right\} \tag{5.5}$$

where $P_v$ are the points in the point clouds. Considering resolutions along the $x$, $y$, and $z$ axes of 0.378 mm, 0.393 mm, and 0.083 mm, respectively, the starting radius $r$ of 1 mm is set to guarantee a uniform search area, regardless of point density variations. This radius-based search encompasses all points within the specified boundary, providing a comprehensive dataset for further analysis.

**Refinement to K-Nearest Neighbors**

From the initial neighborhood $N(P_u)$, the set is refined to the k-nearest neighbors, constrained to a maximum count based on the Euclidean distance - in this case, $k = 9$. This refined neighborhood is denoted as $N_k(P_u)$.

**Covariance Matrix Computation**

Upon identifying the relevant neighborhood points, for each point $P_u$ and its neighborhood $N_k(P_u)$, calculate the covariance matrix $CM_{P_u}$ as:

$$CM_{P_u} = \frac{1}{k} \sum_{P_v \in N_k(P_u)} \left( P_v - \overline{P_u} \right) \left( P_v - \overline{P_u} \right)^T \tag{5.6}$$

where $\overline{P_u}$ is the centroid of the neighborhood points and is given by:

$$\overline{P_u} = \frac{1}{k} \sum_{P_v \in N_k(P_u)} P_v \tag{5.7}$$

This covariance matrix captures the spatial distribution of the points, forming the basis for the next steps.

**Eigenvalue Decomposition**

The core of the normal vector estimation process involves the eigenvalue decomposition of the covariance matrix $CM_{P_u}$. Through this decomposition, eigenvalues $\phi_1, \phi_2, \phi_3$ and their corresponding eigenvectors $\vec{\tau}_1, \vec{\tau}_2, \vec{\tau}_3$ are obtained. Eigenvectors signify the predominant axes of the point distribution. The eigenvalues are ordered as $\phi_1 \geq \phi_2 \geq \phi_3$.

**Normal Vector Estimation**

The normal vector $\overrightarrow{N_u}$ at point $P_u$ is the eigenvector $\overrightarrow{\tau_3}$ corresponding to the smallest eigenvalue $\varphi_3$, thus:

$$\overrightarrow{N_u} = \overrightarrow{\tau_3} \tag{5.8}$$

This choice is grounded in the principle that the smallest eigenvalue's direction exhibits the least variance, aligning with the surface normal.

**Preprocessing for Noise and Outliers**

It is imperative to recognize that irregularities in point cloud density, along with noise and outliers, can significantly affect the accuracy of normal vector estimation. When the scanning laser of the Gocator encounters gaps between particles, particularly in areas that are deeper and darker than the surrounding particle surface, the scanning laser's reflectivity may decrease. This reduction in reflectivity results in abnormal elevation data, often producing negative values. Such anomalies can introduce substantial errors in normal vector estimation, especially when calculating the boundary points of particles based on adjacent data. To enhance the reliability of the results, preprocessing steps such as noise filtering and smoothing are essential.

It is important to emphasize that these preprocessing steps are specifically designed for the normal vector estimation process. When processing LIBS spectral data later, the original Gocator scanning data, including any negative elevation values, should still be used. The presence of these negative elevation data indicates the areas where gaps between particles exist, and accurately identifying these areas is critical for subsequent corrections in LIBS spectral data analysis.



### SURFACE-CONDITION-ADAPTIVE CLASSIFICATION ALGORITHM

The quality of the detected spectrum is highly influenced by two factors: the distance of the focal point of the laser to the object's surface and the laser shot's angle of incidence relative to the object's surface normal during laser shooting. To ensure optimal analysis, it is essential to exclude spectral data obtained outside the focal length. Moreover, incorporating the angle values into the spectral data analysis improves accuracy. By integrating these angle values as parameters, the performance of the classification algorithm is refined and enhanced.

The surface-condition-adaptive classification algorithm for analyzing single-shot spectral data utilizes chemometric methods that integrate principal component analysis with the chi-square distribution (C. Chang et al., 2022). To effectively perform principal component analysis (PCA), distinct preprocessing methods are required for angle values and spectral values. This ensures comparability in magnitude and optimal representation of each data set's characteristics. For angle values, normalization is applied. Given their range of 0 to 90 degrees, they are normalized to a scale of 0 to 1. This is achieved by employing Min-Max Normalization for each angle value. This transformation maintains the proportional relationships while making the values more manageable. In contrast, spectral values are processed through standardization. The key information in spectral data, the distribution patterns of peaks and troughs, is best captured by z-score standardization. This approach maintains the data's overall distribution but

adjusts the mean and standard deviation to a zero mean and unit standard deviation. By doing so, spectral values are effectively scaled, ensuring a standardized framework for further analysis.

When shooting material $X$, each laser shot yields an angle of incidence value $d$, and a corresponding spectrum $\mathbf{x} = (x_1, x_2, \ldots, x_N)$, where $x_s$ denotes the plasma emission intensity at wavelength $\lambda_s (s = 1, 2, \ldots, N)$, with $N$ representing the total number of recorded spectral wavelengths. By assessing the angle of incidence and the actual focal length, spectra that do not meet the criteria are filtered out. Subsequently, by combining the normalized angle value $d'$ with the spectrum $x$, a composite value $C = (d', x_1, x_2, \ldots, x_N)$ is created. Consequently, each laser shot can be considered as a point in an $N+1$ dimensional space. In this space, laser shots from the same material form a unique group of point clouds. Different materials are represented by distinct groups of point clouds. Each new laser shot creates a new point, which is either assigned to an existing point cloud group or labeled as unrecognizable if it significantly deviates from known groups.

After PCA processing, the database for material $X$ records a selected principal component number $n$. This corresponds to a new, rotated orthonormal coordinate system with axes aligned along $n$ unit vectors $(e_1, e_2, \ldots, e_n)$. The database also includes a set of vectors of principal components $(\xi_1, \xi_2, \ldots, \xi_n)$, and a center point $\left(\overline{\xi_1}, \overline{\xi_2}, \ldots, \overline{\xi_n}\right)$ along with variances $\left(\overline{\Delta\xi_1^2}, \overline{\Delta\xi_2^2}, \ldots, \overline{\Delta\xi_n^2}\right)$ to describe the multi-dimensional normal distribution of the spectra for material $X$.

Following the process of $z$-score normalization, for each principal component value $Z_m$ $(m = 1, 2, \ldots, n)$, calculated from the obtained principal components $(\xi_1, \xi_2, \ldots, \xi_n)$, it's presumed to align with chi-square distributions for categorization purposes. Specifically, each $Z_m$ is calculated by the equation:

$$Z_m = \frac{\xi_m - \overline{\xi_m}}{\sqrt{\overline{\Delta\xi_m^2}}} \tag{5.9}$$

showing that it conforms to a standard normal distribution, characterized by a zero mean and unit variance. Leveraging the chi-square distribution framework, the statistic:

$$\chi^2 = \sum_1^n Z_m^2 = \sum_1^n \frac{\left(\xi_m - \overline{\xi_m}\right)^2}{\overline{\Delta\xi_m^2}} \tag{5.10}$$

is scrutinized to verify its alignment with the expected $\chi_n^2$-distribution by checking if it is adequately small. This $\chi^2$ metric is then converted into a probability $p$-value reflective of the $\chi_n^2$-distribution, with an inverse relationship between $\chi^2$ and the $p$-value indicating an increased confidence level. A $p$-value below a selected significance level suggests significant statistical relevance. This significance level for material $X$ is set based on its associated $p$-value, categorizing spectra with $p$-values exceeding this significance level as attributable to material $X$.

#### QUALITY CONTROL METHOD

Initially, the RCA is thoroughly mixed to ensure a uniform distribution. This homogeneity is achieved through the utilization of the feeder mechanism, which evenly disperses the RCA onto the conveyor belt, preparing it for further analysis. Subsequently, the Gocator continuously scans the surface of the RCA streams, calculating and detecting vital parameters such as the actual focal length (corresponding $z$-values $z$) and the angle of incidence $d$ in real-time. These measurements are crucial for the accurate classification of material types.

Parallel to the scanning process, LIBS targets fixed points on the RCA streams, shooting continuously. It integrates the obtained spectral data $x$ with the previously calculated focal length and angle of incidence to identify the material accurately. This classification process is enhanced by periodically summarizing the frequency of occurrence $FC_{md}$ for each material type $X_{md}$ within fixed time intervals $FI$, thereby estimating the content $CE_{md}$ of various materials in the RCA streams rapidly and efficiently. The specific quality control process is outlined in Algorithm 1.

The quantified material content data is then synchronized to the cloud in real-time, allowing for immediate access and analysis. This capability is instrumental in maintaining quality control, as it facilitates the quick classification of any material content that exceeds predefined limits. Once an anomaly is detected, the system enables swift marking and manual intervention, ensuring that only materials meeting the desired specifications are utilized.



## 5.3. RESULTS AND DISCUSSION

### 5.3.1. EFFECTS OF FOCAL LENGTH

To determine the effective focal length of the LIBS system, it is essential first to calculate the diameter $w_0$ of the focal spot. This is achieved using Formula 5.11:

$$w_0 = \frac{2M^2 \lambda f}{\pi D} \tag{5.11}$$

Formula 5.11 is employed to determine the $1/e^2$ spot diameter for a collimated Gaussian beam (Dickey, 2018). This beam is characterized by a wavelength $\lambda$ and a diameter $D$ at the lens when it is focused using a lens with a focal length $f$. If the beam deviates from an ideal Gaussian, the beam quality parameter $M^2$ is introduced to adjust the calculation. In this LIBS system, the parameters are $\lambda = 1064\,\text{nm}$, $D = 2.5\,\text{mm}$, $f = 300\,\text{mm}$, and $M^2 = 1.2$. With these parameters, the calculated diameter $w_0$ of the focal spot is $195.1\,\mu\text{m}$.

The effective focal length range is defined by the depth of field (DOF) of the focused beam, calculated as twice the Rayleigh range $Z_R$:

$$\text{DOF} = 2Z_R \tag{5.12}$$

The Rayleigh range (Herman and Wiggins, 1998), a pivotal concept in optics and laser physics, describes the characteristics of a Gaussian beam. It is the distance from the beam's narrowest point (the beam waist) to the point where the beam's diameter increases by a factor of $\sqrt{2}$. Within this distance, the beam is considered to be approxi-

**Algorithm 1** Quality control module

**Input:** Laser shooting point $P_u(x_u, y_u, z_u)$ and spectrum $x$
**Output:** Estimated content $CE$ of each material type $X_{md}$

**If** a **then**ny point in the neighborhood has $z_u < 0$
  **Delete** spectrum $x$
**Else**
  $z \leftarrow$ Calculate the corresponding $z$-value at the point $P_u$
  $d \leftarrow$ Calculate the angle of incidence at the point $P_u$
  **If** $z >$ focal length limit or $d >$ angle of incidence limit **then**
    **Delete** spectrum $x$
  **Else**
    $d' \leftarrow$ Apply Min-Max normalization to $d$
    $x' \leftarrow$ Apply z-score standardization to $x$
    $C \leftarrow$ Combine $d'$ and $x'$
    **For** each material database $X_{md}$ $(md = 1, 2, ..., 10)$ **do**
      $(\xi_1, \xi_2, ..., \xi_n) \leftarrow$ Apply PCA to $C$
      $Z_m = \frac{\xi_m - \overline{\xi_m}}{\sqrt{\overline{\Delta\xi_m^2}}}$ $(m = 1, 2, ..., n)$
      $p$-value $\leftarrow \chi^2 = \sum_1^n Z_m^2 = \sum_1^n \frac{\left(\xi_m - \overline{\xi_m}\right)^2}{\overline{\Delta\xi_m^2}}$
      **If** $p <$ significance level **then**
        Spectrum $x$ is classified as the material type $X_{md}$
      **Else**
        Spectrum $x$ is classified as not the material type $X_{md}$
      **End If**
    **End For**
  **End If**
**End If**
**Initiate** Frequency summary process
**Set** fixed time intervals $FI$ for summarization
**For** each interval $fi \in FI$ **do**
  **Initialize** frequency count $FC_{md}$ for each material type $X_{md}$
  **For** each classification result within the interval $fi$ **do**
    **Increment** the frequency count $FC_{md}$ for the corresponding material type $X_{md}$
  **End For**
  **Calculate** the content estimate $CE_{md}$ for each material type $X_{md}$
  **Store** the content estimate $CE_{md}$
**End For**
**Aggregate** all interval content estimates $CE_{md}$ to obtain the total estimated content $CE$
**Return** Estimated content $CE$ for each material type
**End** frequency summary process

mately collimated, meaning that the spread of the beam is very minimal. The mathematical expression for the Rayleigh range is typically:

$$Z_R = \frac{\pi w_0^2}{M^2 \lambda} \tag{5.13}$$

where the parameter $M^2$ is included to accommodate for the increased divergence in non-ideal beams. In this study, $Z_R$ is calculated to be 23.4 mm.

At the Rayleigh range $Z_R$, although the beam's expansion results in a doubling of the cross-sectional area and corresponding changes in energy density, the impact on the generated spectra remains relatively stable, as demonstrated in Figure 5.6 (a) and (b) for the RCA example. This stability can be attributed to several key factors:



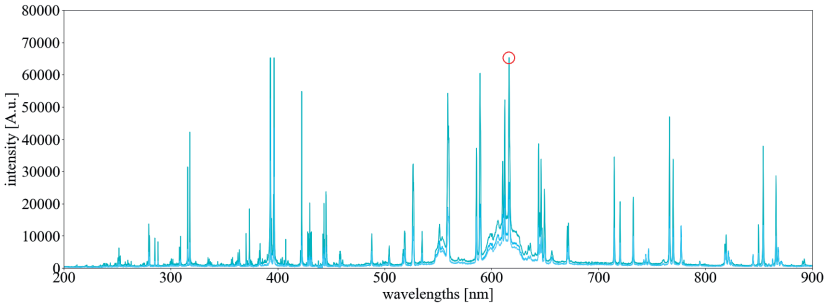


(a) Angle of incidence at 0° and positioned at the focal point

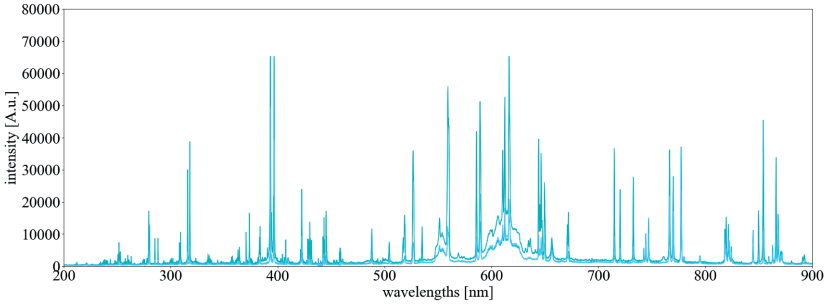


(b) Angle of incidence at 0° and positioned 23.4 mm from the focal point

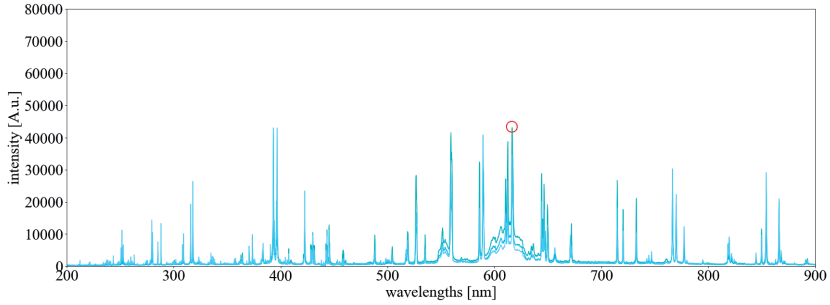


(c) Angle of incidence at 60° and positioned at the focal point

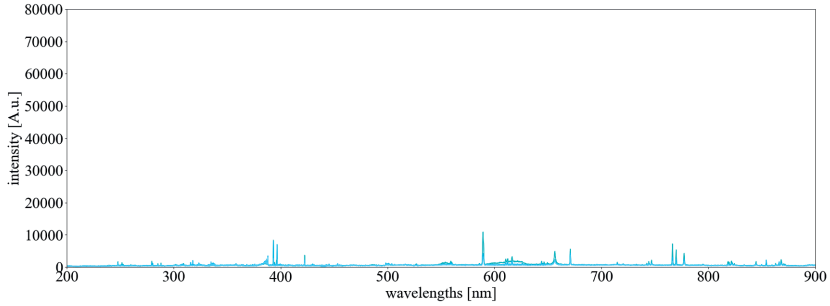


(d) Angle of incidence at 70° and positioned at the focal point

Figure 5.6: Effect of parameters on spectra (RCA)

**(1) Beam collimation within the Rayleigh range** The Rayleigh range defines the distance over which a laser beam remains relatively collimated during propagation (Herman and Wiggins, 1998). Within this range, although the cross-sectional area of the beam increases, the beam remains well-collimated, meaning the energy is still concentrated in a relatively small region (Musazzi and Perini, 2014). As a result, the changes in energy density do not significantly affect the laser-sample interaction. This interaction is sufficiently strong to generate a consistent plasma, leading to relatively stable spectral intensity.

**(2) Nonlinear effects in plasma formation** LIBS relies on the formation of plasma at the sample surface by the laser beam. The formation of plasma and the intensity of the emitted spectra often involve nonlinear processes. Even with variations in energy density, these nonlinear responses—such as saturation effects or plasma shielding—can partially compensate for the changes, resulting in less significant variations in spectral intensity compared to the energy density changes (Z. Wang et al., 2021).

**(3) Tolerance to focal changes** Within the Rayleigh range, the focal spot of the laser, though expanding, still falls within a relatively narrow depth of focus. Within this depth of focus, the conditions of interaction between the laser beam and the sample surface remain relatively consistent, ensuring that the conditions for plasma formation remain within an effective range. These conditions preserve the uniformity of the spectral signals (Gravel et al., 2011). As long as the energy density does not drop below the threshold required for plasma formation, the spectral signal can still maintain a high intensity. In other words, even if the energy density is halved, it remains within the effective range necessary to sustain plasma generation. Therefore, even though the beam's cross-sectional area doubles, the energy density remains sufficiently uniform within this depth of focus, limiting the extent of spectral intensity variations (Dickey, 2018).

These factors collectively ensure that, within the Rayleigh range, the spectral intensity remains within a controllable range despite variations in the energy density due to beam expansion.

Experimental results from various materials reveal that optimal spectra can be successfully obtained within a 30.0 mm distance from the focal point. Thus, a focal length range of 23.4 mm is identified as the optimal limit for effective spectral acquisition. This conclusion draws upon both empirical evidence and theoretical analysis, which shows that this specific focal distance consistently produces the most accurate and reliable spectral data across different material types, enhancing the precision of the spectroscopic analysis.



Considering the size of the measured particles, which are all smaller than 23.4 mm, it is reasonable to assume that laser shooting points are typically within the effective focal length. However, there is a possibility that the laser shoots may pass through the gap between two surface particles, penetrating below the surface layer, which is the outermost layer of the particle pile, as illustrated in Figure 5.7. Laser shots in such scenarios, potentially beyond the Rayleigh range, are challenging to evaluate. This is also reflected in the Gocator scanning data, where the corresponding z-values are negative. Consequently, this laser shot's incidence angle on the material's surface cannot be precisely determined. Based on this unique characteristic, these laser shot data can be excluded.

### 5.3.2. EFFECTS OF THE ANGLE OF INCIDENCE

Experiments conducted on various materials revealed that spectral data, which are capable of characterizing material properties, is obtained when the laser shot's angle of incidence is between 0 and 60 degrees relative to the object's surface normal. For example, in the case of RCA, as illustrated in Figure 5.6 (a) and (c), the peak values of the spectral maxima indicated by the red circles are 65,269.526 A.U. and 43,072.738 A.U. at incidence angles of 0 degrees and 60 degrees, respectively. This represents a decrease of approximately 34%. Despite differences in specific numerical values, the overall trend of the spectra is highly consistent. Particularly, both spectra exhibit similar peak and trough distributions across different wavelength ranges, indicating that the characteristic peak positions remain relatively stable at both 0 degrees and 60 degrees incidence angles, with only variations in intensity.

When the angle of incidence exceeds 60 degrees, spectral values tend to be signifi-

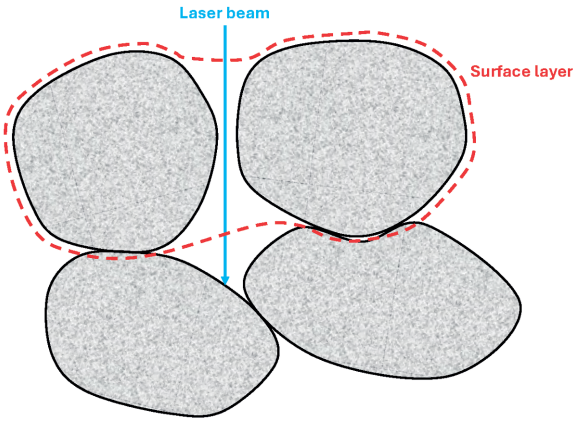


Figure 5.7: Laser shoots the gap between two particles



cantly lower. For instance, in the case of RCA, at a 70-degree angle (Figure 5.6 (d)), the spectral intensity not only drops substantially compared to the spectra at 0 degrees (Figure 5.6 (a)) and 60 degrees (Figure 5.6 (c)) but also loses many characteristic peaks, making them challenging to correct algorithmically. This reduction is primarily attributed to the increased surface area impacted by the laser shots at steeper angles, leading to diminished reflected energy and consequently lower spectral values detected. Other studies indicate that LIBS signal intensity decreases markedly when the angle of incidence exceeds 60 degrees (Brennetot et al., 2003; López-Moreno et al., 2007; Palanco et al., 2002).

Both angle of incidence and focal distance variations lead to changes in the laser spot size on the sample surface, thereby affecting the energy density and, consequently, the spectral intensity in LIBS. However, angle variation generally exerts a more significant impact on spectral intensity than focal distance changes. The reasons are as follows:

**(1) Energy density distribution** As the angle of incidence increases, the laser beam projects onto the sample surface as an elongated ellipse (Képeš et al., 2021), leading to a less uniform energy density distribution. This non-uniformity is particularly pronounced along the major axis of the ellipse, where the energy density is lower, reducing the efficiency of plasma formation and, consequently, the spectral intensity. Additionally, the matrix effect of the sample's surface morphology on LIBS should not be overlooked (Xiang et al., 2024). In contrast, when changes in the focal distance affect the energy density by altering the spot size, this effect is typically less pronounced within the Rayleigh range, where the beam remains relatively well-collimated and energy is still concentrated (Fortes et al., 2013).

**(2) Variation in reflection and absorption** As the angle of incidence increases, the proportion of laser energy reflected from the sample surface also increases, while the energy absorbed by the sample decreases. This reduction in absorbed energy further dimin-

ishes the formation of plasma and reduces the intensity of the resulting spectral signal (Palanco et al., 2002). In contrast, focal distance changes primarily affect the focusing of the laser on the sample surface. Although this also impacts spectral intensity, the effect is relatively minor compared to the substantial differences in reflection and absorption efficiency caused by angle variation.

**(3) Effects in plasma formation** The angle of laser incidence significantly affects plasma formation and consequently influences the intensity of the spectral signal. Plasma formation is highly dependent on the energy density delivered to the sample surface, exhibiting a distinct nonlinear behavior with a clear energy density threshold. As the incidence angle increases, the laser irradiance decreases, making plasma formation more challenging. Larger incidence angles alter the ablation geometry and reduce the efficiency of laser ablation, leading to a decrease in the ablated mass and a significant weakening of plasma emission intensity (Breves et al., 2017; Képeš et al., 2021; Lei et al., 2019). Plasmas generated at larger ablation angles are typically smaller and potentially less dense (Breves et al., 2017).

Under orthogonal incidence, plasma expansion primarily occurs perpendicular to the target surface. In contrast, with non-orthogonal incidence, the majority of the sample material's emission is observed along the sample surface normal, despite plasma expansion following the incident laser pulse (J. J. Chang and Warner, 1996; Ilyin et al., 2015). Variations in the incidence angle result in decreased energy density due to a larger interaction area and the enhanced plume shielding effect of the expanding plasma (Zhang et al., 2012). This reduction in energy density can fall below the threshold needed for effective plasma formation, resulting in reduced excitation of plasma particles and a significant decrease in spectral intensity (Brennetot et al., 2003; Fortes et al., 2013).

The spatial distribution of plasma on the sample surface is not uniform but rather diffuses outward in a hemispherical shape, with the highest radiation intensity occurring in the direction normal to the sample surface and decreasing around it. As the incidence angle increases, the non-uniform distribution of plasma and the directionality of radiation intensity contribute to weaker LIBS signals (Z. Wang et al., 2021). Additionally, changes in the incidence angle can induce plasma asymmetry (Képeš et al., 2021). In non-orthogonal ablation, the initial plasma is divided into two components: one that follows the ablation pulse and primarily emits continuous radiation, and another composed of sample material expanding along the sample normal (Képeš et al., 2021). The interaction between these two plasma components and the position of the collection system significantly impacts the quality of the LIBS signal (Képeš et al., 2021; Z. Wang et al., 2021).

Non-orthogonal incidence makes the interaction between the laser pulse and the plasma more complex. The plasma structure generated under non-orthogonal incidence is more intricate, with less homogeneous ionic emissivity profiles compared to the orthogonal case. This discrepancy is likely due to the varying height dependency of the interaction between the laser radiation and the shockwave (Képeš et al., 2021). Even small deviations from orthogonal incidence significantly reduce the vertical homogeneity of the ionic emissivity profiles, likely because ionization predominantly occurs at the shockwave boundaries (Képeš et al., 2020). Furthermore, the shockwave produced by

non-orthogonal ablation is more complex than that generated by orthogonal ablation (Liu et al., 2013). This non-homogeneity in the distribution of emitting species in the plasma may result in self-absorption, which decreases emission line intensity as the observation angle varies (Képeš et al., 2021).

In summary, increasing the incidence angle reduces the fluence of the laser ablation pulse, which affects plasma uniformity and spectral signal strength. Therefore, it is essential to account for the impact of angle variation on plasma formation and spectral collection when conducting quantitative LIBS analysis.

While focal length variations can also affect energy density, the uniformity of the laser energy distribution means that the plasma formation is less likely to be severely compromised, resulting in a less dramatic impact on the spectral signal.

Although both angle and focal length variations within the Rayleigh range can lead to changes in the interaction area, angle variation has a more significant impact on spectral intensity. Angle variations disrupt the uniformity of energy delivery to the sample and result in a less efficient plasma formation process, leading to a more substantial reduction in LIBS signal strength compared to focal length variations. These combined factors make angle variation a more critical parameter in determining the strength of the spectral signal in LIBS.



RCA are generally more angular and irregular in shape compared to natural aggregates, leading to significant variations in surface conditions. These irregularities can cause inconsistent laser-sample interactions, particularly when the laser's angle of incidence varies across the surface. Such variations in angle directly affect the energy density of the laser on the sample, leading to fluctuations in the intensity and accuracy of the spectral data obtained.

To mitigate these effects, we have normalized the angle of incidence and integrated it into our cluster-based classification algorithm. By doing so, the algorithm accounts for the changes in spectral data resulting from different incidence angles, ensuring that the analysis remains accurate regardless of these variations. This adjustment is especially critical in situations where maintaining a consistent angle of incidence is difficult, such as when dealing with the rough and uneven surfaces typical of RCA. As a result, this approach enhances the reliability and precision of spectral analysis, ensuring more consistent material classification and quality control.

### 5.3.3. Quality Control Test Results

In this study, we meticulously collected data for a variety of materials, each characterized by specific angle and spectral values. To rigorously evaluate our classification methodology, we partitioned this dataset into two subsets: a training set and a validation set. The partitioning adhered to a 9:1 ratio, ensuring a balanced distribution for effective model training and validation. Specifically, for the purpose of validation, we randomly selected 100 entries for each material, resulting in a comprehensive validation set encompassing a total of 1000 entries. Conversely, the training set comprised the remaining 900 entries per material. This extensive dataset facilitated the development of a robust standard library, pivotal for the accurate classification of materials based on their spectral signatures and surface conditions.

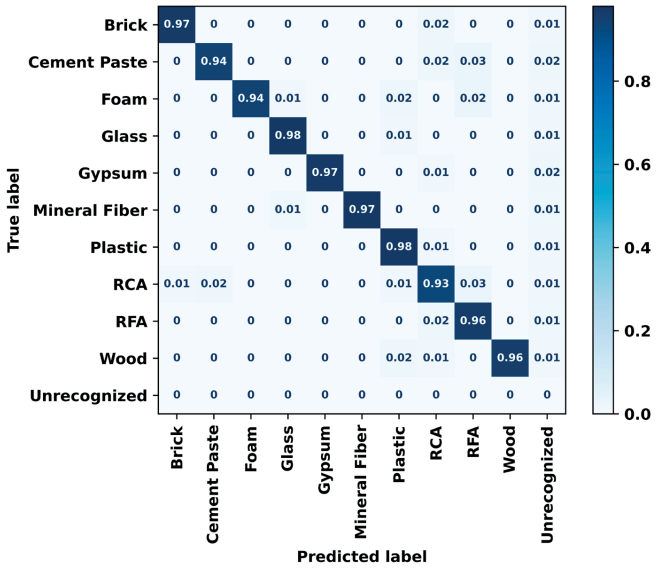


(a) Without consideration of surface information

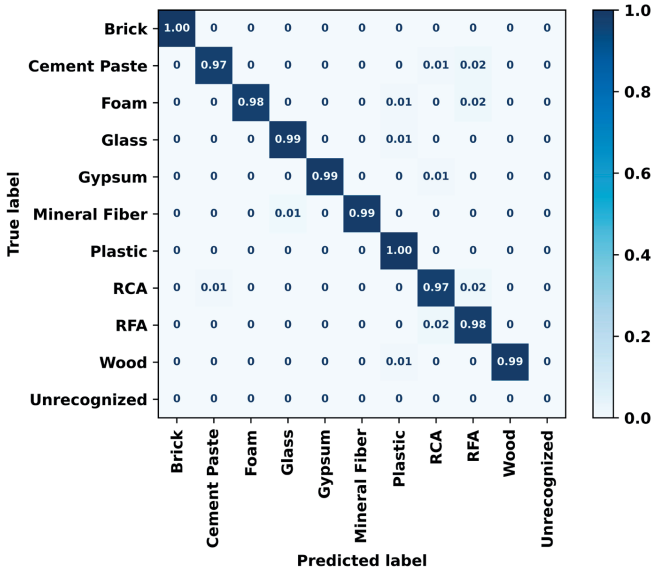


(b) With consideration of surface information

Figure 5.8: Confusion matrix of the validation set

Figure 5.8 delineates the classification outcomes, offering a comparative analysis of the results obtained without considering surface conditions against those that are factored in these conditions. Further, the validation set's classification efficacy is docu-

mented in Table 5.1 and Table 5.2. These tables provide an insightful examination of the classification performance, highlighting the precision, recall, and F1 score among other metrics, thereby offering a transparent overview of our methodological accuracy and efficacy.

Table 5.1: Classification report of the validation set without consideration of surface information

| | Precision | Recall | F1-score | Support |
|---|---|---|---|---|
| Brick | 0.98 | 0.97 | 0.98 | 100 |
| Cement Paste | 0.98 | 0.94 | 0.96 | 100 |
| Foam | 1.00 | 0.94 | 0.97 | 100 |
| Glass | 0.98 | 0.98 | 0.98 | 100 |
| Gypsum | 1.00 | 0.97 | 0.99 | 100 |
| Mineral Fiber | 1.00 | 0.97 | 0.99 | 100 |
| Plastic | 0.94 | 0.98 | 0.96 | 100 |
| RCA | 0.91 | 0.93 | 0.92 | 100 |
| RFA | 0.94 | 0.96 | 0.95 | 100 |
| Wood | 1.00 | 0.96 | 0.98 | 100 |
| Unrecognized | 0.00 | 0.00 | 0.00 | 0 |
| weighted avg | 0.97 | 0.96 | 0.96 | 1000 |

Subsequently, the constructed standard library was employed in a real-world scenario to continuously monitor the quality of RCA streams transported on the conveyor belt, following its processing through the C2CA treatment. The monitoring experiments were specifically designed to assess the content of various contaminants within the RCA streams. The experimental findings reveal that the concentration of contaminants in the RCA streams was within the permissible limits set forth by the EN 12620 standard (Standard, 2002), which delineates the requirements for aggregates to be used in concrete.

### 5.3.4. Accuracy and Efficiency in Quality Control

Significant enhancements in the algorithm are noted when incorporating surface conditions. The algorithm with consideration of surface conditions demonstrates improvements in precision (weighted average), recall (weighted average), and F1-score (weighted average), all reaching 0.99. This is a significant advancement over the algorithm that did not account for surface conditions, which achieves a precision (weighted average) of 0.97, recall (weighted average) of 0.96, and F1-score (weighted average) of 0.96. It is important to acknowledge that the test set was approximately 40 times too small to ensure that materials, such as wood and plastics with stringent maximum concentration specifications, can be detected at the highest quality limit levels (0.1 $cm^3$ per

Table 5.2: Classification report of the validation set with consideration of surface information

| | Precision | Recall | F1-score | Support |
|---|---|---|---|---|
| Brick | 1.00 | 1.00 | 1.00 | 100 |
| Cement Paste | 0.99 | 0.97 | 0.98 | 98 |
| Foam | 1.00 | 0.98 | 0.99 | 98 |
| Glass | 0.99 | 0.99 | 0.99 | 99 |
| Gypsum | 1.00 | 0.99 | 1.00 | 99 |
| Mineral Fiber | 1.00 | 0.99 | 0.99 | 99 |
| Plastic | 0.97 | 1.00 | 0.99 | 99 |
| RCA | 0.96 | 0.97 | 0.96 | 97 |
| RFA | 0.96 | 0.98 | 0.97 | 99 |
| Wood | 1.00 | 0.99 | 1.00 | 98 |
| Unrecognized | 0.00 | 0.00 | 0.00 | 0 |
| weighted avg | 0.99 | 0.99 | 0.99 | 987 |



kg, or about 1 in 4,000 particles).

Nevertheless, the system has demonstrated high efficiency, accuracy, and significant market potential. It can monitor the quality of RCA flows at a throughput of 50 tons per hour per conveyor, analyzing approximately 4,000 particles per ton of RCA. This allows the system to detect critical contaminants at concentrations below 50 parts per million. For materials with stringent content regulations, such as wood, the system can meet the required limit of 0.2 $cm^3$/kg, equivalent to about 0.08 g/kg or a mass concentration of 80 ppm, further demonstrating its reliability.

Notably, the most significant improvements include the complete elimination of the unrecognized category and a reduction in confusion primarily to materials with similar chemical compositions. These improvements are highlighted by the disappearance of previously unrecognized classifications and the significant reduction in misclassifications involving materials with similar chemistry, particularly where RCA was previously misclassified as other materials.

Specifically, the improvements include both the removal of previously unrecognized laser shots and a reduction in misclassifications. The elimination of these previously unrecognized laser shots arises from two factors. Firstly, it is evident that some ineffective data have been removed from various materials (except for brick). This is attributed to the probability of laser shooting the gaps between particles during consecutive laser shots. These laser shots are highly beyond the focal point, resulting in the exclusion of previously unrecognized laser shots. Secondly, the incorporation of the angle parameter aids in identifying and correcting these unrecognized laser shots. A notable instance of

this improvement is observed in the case of brick. Analysis of prior literature (C. Chang et al., 2022) reveals that misclassified laser shots typically display smaller scales than normal and are obscured by typical values. The diminished spectral values of these laser shots, possibly caused by the angle of incidence issues, make classification challenging. By incorporating the angle of incidence of laser shots into the algorithm, these small-scale shots can be accurately identified and classified, leading to a decrease in misclassification.

However, RCA, RFA, and cement paste remain susceptible to classification errors. Challenges arise from multiple factors. One major issue is the difficulty of ensuring the complete removal of residues during the material processing stage. In particular, the adhesion of cement paste to RCA surfaces complicates differentiation. Additionally, the size overlap between RCA and RFA, both sharing a boundary at 4.0 mm, further complicates their distinction, especially in this marginal size range where they exhibit greater similarity. The inherent heterogeneity of the materials adds another layer of complexity to the classification task. Moreover, the chemical compositional similarities among RCA, RFA, and cement paste amplify the presence of misclassifications. RCA, obtained by crushing concrete from demolished structures, generally consists of larger fragments of original aggregates, such as gravel or crushed stone, along with adhered mortar. Its chemical composition is primarily characterized by calcium oxide (CaO), silicon dioxide ($SiO_2$), aluminum oxide ($Al_2O_3$), iron oxide ($Fe_2O_3$), and magnesium oxide (MgO). The presence of residual mortar in RCA introduces additional variability in its chemical profile, distinguishing it from natural aggregates. In contrast, RFA, which comes from the finer fractions of the same source as RCA, consists of sand-sized material and finer residues from the original concrete. Although the chemical composition of RFA is similar to that of RCA, it contains higher proportions of calcium hydroxide [$Ca(OH)_2$] and other hydrated compounds due to its finer particle size and greater surface area. Cement paste, which acts as the binding phase in concrete, mainly consists of calcium silicate hydrate (C-S-H), calcium hydroxide, and unhydrated cement particles, with a notable presence of calcium carbonate ($CaCO_3$) due to carbonation. The similar yet heterogeneous chemical compositions of RCA and RFA lead to minimal differences in their spectral signatures (as shown in 5.9) when analyzed using LIBS. These inconsistencies in data acquisition complicate the development of a reliable database, as the collected spectra may not accurately represent the material's true characteristics. Consequently, this leads to reduced recognition accuracy when these databases are used for material classification. To overcome these challenges, more precise analysis and algorithms are necessary to improve accuracy.

Several strategies can enhance classification effectiveness. Exploring alternative methods, such as the integration of additional sensors (e.g., moisture sensors) and considering scale differences in classification, could lead to improved outcomes. Alternatively, increasing the ratio of training and validation and using a greater number of spectral data for database construction can align data distribution more closely with a normal distribution. This alignment is beneficial for PCA, resulting in more accurate predictions. Therefore, extensive future experimentation is recommended to develop a robust database and improve overall accuracy.

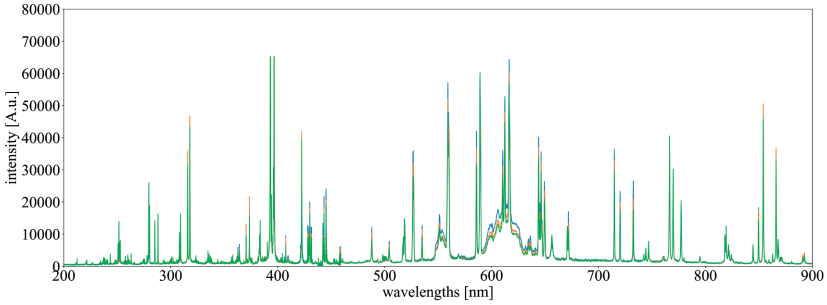


(a) RCA

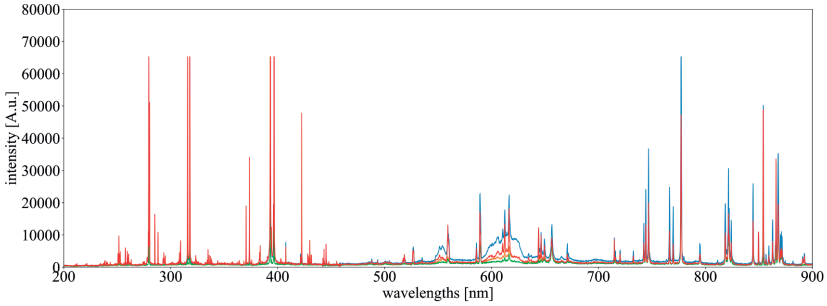


(b) RFA

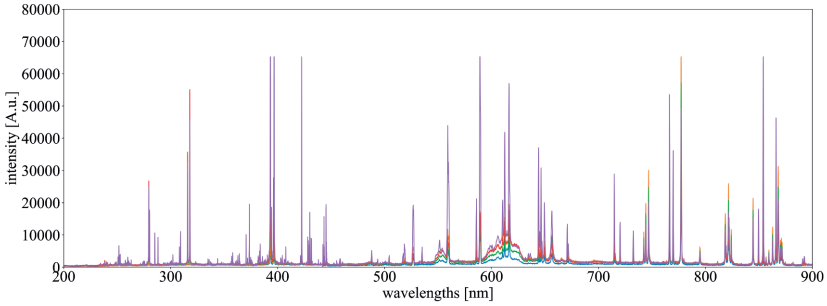


(c) Cement Paste
Figure 5.9: LIBS data

### 5.3.5. ECONOMIC FEASIBILITY

This quality control system is designed for a plant that processes approximately 150 tons per hour of EoL concrete. Similar plants in Europe typically operate around 4,000 hours per year, with downtime ranging from 10% to 20%. To justify the investment, the system needs to process 500,000 tons annually. The facility cost is approximately €300,000,

which equates to an additional 0.60 euro/ton of input material or around 1.00 euro/ton for RCA and RFA if the facility is to break even within one year. Given that typical aggregate prices in the EU range from 10.00 to 15.00 euro/ton, investing in a quality control system that not only ensures product quality but also supports a digital concrete recycling process and reduces labor costs is economically feasible.

## 5.4. Conclusion

This study introduces a novel rapid quality control system for contaminant detection in RCA streams via surface-condition-adaptive LIBS. A key advancement is the integration of a synchronized system that merges spatial data from a 3D scanner with the spectral data from LIBS. This novel approach effectively tackles the issue of variable surface conditions on objects, which affect the laser shot's focal length and angle of incidence. These factors have previously impeded the precision of traditional LIBS applications. By adapting the spectra based on the surface position and orientation, as determined by 3D scanning, this method significantly reduces unrecognizable classifications and misclassification rates, enhancing the reliability of material classification. The surface-condition-adaptive LIBS method demonstrates improvements in precision (weighted average), recall (weighted average), and F1-score (weighted average), all reaching 0.99. This level of accuracy is pivotal for the rapid quality control of RCA streams on the conveyor belt, underpinning its utility in ensuring the quality of RCA utilized in construction projects.



The advancements of this study enhance the reliability of single-shot analyses of LIBS, thereby reducing the occurrence of false positives during the material classification process. In situations where the concentration of contaminants is extremely low, false positives can significantly influence the results of theoretical simulations. For example, with a 1% wood content that is uniformly distributed, the likelihood of detecting wood is only once in every 100 samples. However, false positives in other materials could falsely inflate the estimated wood content, greatly impacting the quality assessment of RCA. By precisely adjusting the angle of incidence and eliminating spectra outside the focal range, the quality of the spectra has been improved, and the incidence of false positives has been substantially lowered. This enhancement is essential for preserving the integrity and reliability of recycling processes.

This study highlights the potential of surface characterization in the recognition of different materials. The diversity in surface properties of different materials presents a unique opportunity for precision in material classification. Detailed analysis of these surface characteristics, combined with existing technologies, enables more accurate recognition of various materials. The integration of 3D scanning with LIBS allows for a detailed understanding of surface conditions, which plays a pivotal role in enhancing the accuracy of material classification. This research underscores the significance of surface properties in the classification process and paves the way for further advancements in material recognition technology. Moreover, future research should investigate automated analysis techniques for discerning particle size distributions in different materials. The use of advanced sensors allows for the swift collection of particle size data of a specific material in mixed material streams, augmenting the efficiency and precision of recycling processes.

Beyond waste management and recycling, this research has broader implications

across various industries where material classification and detection of particle flows are pivotal. However, the study also acknowledges the complexities in distinguishing materials with similar spectral signatures. The challenge remains in fine-tuning the LIBS methodology to distinguish between such materials with greater specificity. Future research could focus on enhancing the algorithmic aspect of LIBS data interpretation, potentially incorporating machine learning techniques to refine the classification process. Moreover, exploring the synergy of LIBS with other analytical techniques could offer a more comprehensive understanding of material classification and detection.

Importantly, this study has broader implications for environmental sustainability. It exemplifies the potential of combining advanced scanning and spectroscopy technologies with real-time data analysis and cloud synchronization to enhance construction material recycling processes. Through the rapid quality control of RCA streams, it promotes more efficient recycling of construction waste, thereby reducing the environmental impact of building materials and prompting their use in the building sector. This approach aligns with global efforts towards circular economies, where maximizing the reuse and recycling of materials is paramount.

# BIBLIOGRAPHY


Abid, S. R., Nahhab, A. H., Al-aayedi, H. K., & Nuhair, A. M. (2018). Expansion and strength properties of concrete containing contaminated recycled concrete aggregate. *Case Studies in Construction Materials*, *9*, e00201.

Ahmad, S., Upadhyay, S., Umar, A., & Al-Osta, M. A. (2023). Effect of recycled crushed glass and recycled coarse aggregate on the properties of self-compacting concrete. *Case Studies in Construction Materials*, *19*, e02532.

Bai, G., Zhu, C., Liu, C., & Liu, B. (2020). An evaluation of the recycled aggregate characteristics and the recycled aggregate concrete mechanical properties. *Construction and building materials*, *240*, 117978.

Bonifazi, G., Palmieri, R., & Serranti, S. (2018). Evaluation of attached mortar on recycled concrete aggregates by hyperspectral imaging. *Construction and Building Materials*, *169*, 835–842.

Brennetot, R., Lacour, J. L., Vors, E., Rivoallan, A., Vailhen, D., & Maurice, S. (2003). Mars analysis by laser-induced breakdown spectroscopy (malis): Influence of mars atmosphere on plasma emission and study of factors influencing plasma emission with the use of doehlert designs. *Appl. Spectrosc.*, *57*(7), 744–752.

Breves, E., Lepore, K., Dyar, M., Bender, S., Tokar, R., & Boucher, T. (2017). Laser-induced breakdown spectra of rock powders at variable ablation and collection angles under mars-analog conditions. *Spectrochimica Acta Part B: Atomic Spectroscopy*, *137*, 46–58.

Cabral, J. S., Menegatti, C. R., & Nicolodelli, G. (2023). Laser-induced breakdown spectroscopy in cementitious materials: A chronological review of cement and concrete from the last 20 years. *TrAC Trends in Analytical Chemistry*, *160*, 116948.

Chang, C., Di Maio, F., Bheemireddy, R., Posthoorn, P., Gebremariam, A. T., & Rem, P. (2025). Rapid quality control for recycled coarse aggregates (rca) streams: Multisensor integration for advanced contaminant detection. *Computers in Industry*, *164*, 104196.

Chang, C., Di Maio, F., Rem, P., Gebremariam, A. T., Mehari, F., & Xia, H. (2022). Cluster-based identification algorithm for in-line recycled concrete aggregates characterization using laser-induced breakdown spectroscopy (libs). *Resources, Conservation and Recycling*, *185*, 106507.

Chang, J. J., & Warner, B. E. (1996). Laser-plasma interaction during visible-laser ablation of methods. *Applied Physics Letters*, *69*(4), 473–475.

Corral, A., & Almendros-Jiménez, J. M. (2007). A performance comparison of distance-based query algorithms using r-trees in spatial databases. *Information Sciences*, *177*(11), 2207–2237.

de Andrade Salgado, F., & de Andrade Silva, F. (2022). Recycled aggregates from construction and demolition waste towards an application on structural concrete: A review. *Journal of Building Engineering*, *52*, 104452.

Dickey, F. M. (2018). *Laser beam shaping: Theory and techniques*. CRC press.

Dietz, T., Gottlieb, C., Kohns, P., & Ankerhold, G. (2019). Comparison of atomic and molecular emission in laser-induced breakdown spectroscopy for the quantification of harmful species in cement-based materials. *Spectrochimica Acta Part B: Atomic Spectroscopy*, *161*, 105707.

Elfaham, M. M., & Eldemerdash, U. (2019). Advanced analyses of solid waste raw materials from cement plant using dual spectroscopy techniques towards co-processing. *Optics & Laser Technology*, *111*, 338–346.

Fortes, F. J., Moros, J., Lucena, P., Cabalín, L. M., & Laserna, J. J. (2013). Laser-induced breakdown spectroscopy. *Analytical Chemistry*, *85*(2), 640–669.

Gebremariam, A. T., Di Maio, F., Vahidi, A., & Rem, P. (2020). Innovative technologies for recycling end-of-life concrete waste in the built environment. *Resources, Conservation and Recycling*, *163*, 104911.

Gottlieb, C., Millar, S., Grothe, S., & Wilsch, G. (2017). 2d evaluation of spectral libs data derived from heterogeneous materials using cluster algorithm. *Spectrochimica Acta Part B: Atomic Spectroscopy*, *134*, 58–68.

Gravel, J.-F. Y., Doucet, F. R., Bouchard, P., & Sabsabi, M. (2011). Evaluation of a compact high power pulsed fiber laser source for laser-induced breakdown spectroscopy. *Journal of Analytical Atomic Spectrometry*, *26*(7), 1354–1361.

Herman, R., & Wiggins, T. (1998). Rayleigh range and the m 2 factor for bessel–gauss beams. *Applied optics*, *37*(16), 3398–3400.

Ilyin, A., Nagorny, I., & Biryukova, Y. (2015). Optical breakdown on the inclined target: The features of the erosive plume formation. *Applied Mechanics and Materials*, *723*, 825–828.

Junwei, J., Hongbo, F., Zongyu, H., Huadong, W., Zhibo, N., & Fengzhong, D. (2018). Calibration curve and support vector regression methods applied for quantification of cement raw meal using laser-induced breakdown spectroscopy. *Plasma Science and Technology*, *21*(3), 034003.

Képeš, E., Gornushkin, I., Pořízka, P., & Kaiser, J. (2020). Tomography of double-pulse laser-induced plasmas in the orthogonal geometry. *Analytica Chimica Acta*, *1135*, 1–11.

Képeš, E., Gornushkin, I., Pořízka, P., & Kaiser, J. (2021). Spatiotemporal spectroscopic characterization of plasmas induced by non-orthogonal laser ablation. *Analyst*, *146*, 920–929.

Kim, C. K., In, J. H., Lee, S. H., & Jeong, S. (2013). Influence of laser wavelength on the laser induced breakdown spectroscopy measurement of thin cuin 1- xgaxse2 solar cell films. *Spectrochimica Acta Part B: Atomic Spectroscopy*, *88*, 20–25.

Lei, B., Wang, J., Li, J., Tang, J., Wang, Y., Zhao, W., & Duan, Y. (2019). Signal enhancement of laser-induced breakdown spectroscopy on non-flat samples by single beam splitting. *Opt. Express*, *27*(15), 20541–20557.

Liu, T., Gao, X., Hao, Z., Liu, Z., & Lin, J. (2013). Characteristics of plasma plume expansion from al target induced by oblique incidence of 1064 and 355 nm nanosecond nd: Yag laser. *Journal of Physics D: Applied Physics*, *46*(48), 485207.

López-Moreno, C., Palanco, S., & Laserna, J. J. (2007). Stand-off analysis of moving targets using laser-induced breakdown spectroscopy. *Journal of Analytical Atomic Spectrometry*, *22*(1), 84–87.

Lux, J., Hoong, J. D. L. H., Mahieux, P.-Y., & Turcry, P. (2023). Classification and estimation of the mass composition of recycled aggregates by deep neural networks. *Computers in Industry*, *148*, 103889.

Mansoori, A., Roshanzadeh, B., Khalaji, M., & Tavassoli, S. (2011). Quantitative analysis of cement powder by laser induced breakdown spectroscopy. *Optics and Lasers in Engineering*, *49*(3), 318–323.

Martín-Morales, M., Zamorano, M., Ruiz-Moyano, A., & Valverde-Espinosa, I. (2011). Characterization of recycled aggregates construction and demolition waste for concrete production following the spanish structural concrete code ehe-08. *Construction and building materials*, *25*(2), 742–748.

Musazzi, S., & Perini, U. (2014). Libs instrumental techniques. In S. Musazzi & U. Perini (Eds.), *Laser-induced breakdown spectroscopy: Theory and applications* (pp. 59–89). Springer Berlin Heidelberg.

Palanco, S., Baena, J., & Laserna, J. (2002). Open-path laser-induced plasma spectrometry for remote analytical measurements on solid surfaces. *Spectrochimica Acta Part B: Atomic Spectroscopy*, *57*(3), 591–599.

Palanco, S., Cabalin, L., Romero, D., & Laserna, J. (1999). Infrared laser ablation and atomic emission spectrometry of stainless steel at high temperatures. *Journal of Analytical Atomic Spectrometry*, *14*(12), 1883–1887.

Serranti, S., & Bonifazi, G. (2020). Detection and classification of asbestos and other contaminants in c&dw by advanced technologies. In *Advances in construction and demolition waste recycling* (pp. 407–437). Elsevier.

Serranti, S., Palmieri, R., Bonifazi, G., Gasbarrone, R., Hermant, G., & Bréquel, H. (2023). An automated classification of recycled aggregates for the evaluation of product standard compliance. *Sustainability*, *15*(20), 15009.

Silva, R., De Brito, J., & Dhir, R. K. (2017). Availability and processing of recycled aggregates within the construction and demolition supply chain: A review. *Journal of Cleaner Production*, *143*, 598–614.

Standard, B. (2002). Aggregates for concrete. *BS EN*, *12620*.

Vegas, I., Broos, K., Nielsen, P., Lambertz, O., & Lisbona, A. (2015). Upgrading the quality of mixed recycled aggregates from construction and demolition waste by using near-infrared sorting technology. *Construction and Building Materials*, *75*, 121–128.

Völker, T., Millar, S., Strangfeld, C., & Wilsch, G. (2020). Identification of type of cement through laser-induced breakdown spectroscopy. *Construction and Building Materials*, *258*, 120345.

Wang, J., Li, X., Li, H., Li, X., & Li, Z. (2020). Lens-to-sample distance effect on the quantitative analysis of steel by laser-induced breakdown spectroscopy. *Journal of Physics D: Applied Physics*, *53*(25), 255203.

Wang, Z., Afgan, M. S., Gu, W., Song, Y., Wang, Y., Hou, Z., Song, W., & Li, Z. (2021). Recent advances in laser-induced breakdown spectroscopy quantification: From fun-

damental understanding to data processing. *TrAC Trends in Analytical Chemistry*, *143*, 116385.

Xia, H., & Bakker, M. (2014). Reliable classification of moving waste materials with libs in concrete recycling. *Talanta*, *120*, 239–247.

Xiang, Y., Yang, L., Li, X., Sun, W., Pan, C., Dong, J., Xu, M., Chen, J., & Lu, R. (2024). Spectral correction study to reduce the influence of sample surface morphology on laser-induced breakdown spectroscopy. *Journal of Analytical Atomic Spectrometry*, *39*(6), 1470–1481.

Yin, H., Hou, Z., Zhang, L., Zhang, X., Wang, Z., & Li, Z. (2016). Cement raw material quality analysis using laser-induced breakdown spectroscopy. *Journal of Analytical Atomic Spectrometry*, *31*(12), 2384–2390.

Yu, J., Hou, Z., Ma, Y., Li, T., Fu, Y., Wang, Y., Li, Z., & Wang, Z. (2020). Improvement of laser induced breakdown spectroscopy signal using gas mixture. *Spectrochimica Acta Part B: Atomic Spectroscopy*, *174*, 105992.

Zhang, Y., Jia, Y.-H., Chen, J.-W., Shen, X.-J., Zhao, L., Yang, C., Chen, Y.-Y., Zhang, Y.-H., & Han, P.-C. (2012). Study on parameters influencing analytical performance of laser-induced breakdown spectroscopy. *Frontiers of Physics*, *7*, 714–720.

Živković, S., Botto, A., Campanella, B., Lezzerini, M., Momčilović, M., Pagnotta, S., Palleschi, V., Poggialini, F., & Legnaioli, S. (2021). Laser-induced breakdown spectroscopy elemental mapping of the construction material from the smederevo fortress (republic of serbia). *Spectrochimica Acta Part B: Atomic Spectroscopy*, *181*, 106219.

# 6

# Conclusion

## 6.1. SUMMARY OF RESEARCH CONTRIBUTIONS

### 6.1.1. KEY FINDINGS AND DISCUSSIONS

THE overarching goal of this dissertation was to enhance the efficiency and reliability of RCA quality inspection, thereby supporting sustainable construction practices and advancing the circular economy. The research specifically focused on developing a novel sensor-based system capable of assessing RCA quality in real-time during processing at recycling sites. Through this research, it is anticipated that more efficient, economically viable, and environmentally friendly methods will be developed, significantly impacting the construction industry's approach to material recycling and reuse.

#### INNOVATIONS IN RCA QUALITY INSPECTION

The core of this dissertation was the development and empirical validation of a novel mobile sensor-based system designed to enhance the efficiency and accuracy of RCA quality assessment. This system integrates advanced sensor technologies, including 3D scanning and LIBS, to provide real-time, on-site quality checks of RCA at demolition sites. The implementation of these technologies marks a significant improvement over traditional manual and labor-intensive quality assessment methods.



The 3D scanner, specifically the Gocator, was employed to measure the PSD of RCA. The Gocator's ability to generate high-resolution three-dimensional point cloud data enabled it to capture geometrical properties of the RCA particles with high precision. This method proved crucial in overcoming the limitations of previous image-based techniques, which often struggled with accuracy due to lighting conditions and the physical characteristics of the materials.

Furthermore, the integration of the LIBS sensor facilitated the detection of various contaminants within the RCA. The sensor's capability to perform rapid spectroscopic analysis allowed for the identification of materials such as gypsum, glass, and plastics, which can adversely affect the quality and durability of recycled concrete. The combination of these technologies within a single mobile platform provided a comprehensive tool for RCA quality assessment that is both scalable and adaptable to various operational environments.

#### EFFECTIVENESS OF THE IMPLEMENTED TECHNOLOGIES

The effectiveness of the introduced technologies was validated through extensive testing and comparison with traditional methods. The findings revealed that the sensor-based system could process and analyze over 100 tons of RCA per hour, demonstrating a substantial increase in efficiency compared to older methods. Moreover, the system achieved a RMSE of less than 5% in its PSD analysis, indicating a high level of accuracy.

This research highlighted significant improvements in the operational efficiency and reliability of RCA quality assessments. By enabling real-time feedback, the system allows for immediate adjustments in the recycling process, enhancing the overall quality of the RCA. Such capabilities are crucial for meeting industry standards and ensuring the structural integrity of constructions utilizing RCA.

### 6.1.2. IMPLICATIONS FOR SUSTAINABLE CONSTRUCTION

The findings from this research underscore the significant potential for RCA to contribute to more sustainable construction practices. By improving the methods for inspecting, grading, and certifying RCA, the construction industry can reduce its environmental impact and reliance on virgin materials. The methodologies developed in this thesis offer practical solutions that can be adopted by industry stakeholders to meet increasing demands for sustainability.

#### ENVIRONMENTAL IMPACT REDUCTION

One of the primary implications of integrating RCA into construction practices is the significant reduction in environmental impact. Traditional construction methods heavily rely on the extraction of virgin materials, which not only depletes natural resources but also causes considerable environmental degradation including habitat destruction, water pollution, and increased carbon emissions due to the transportation and processing of these materials. In contrast, the use of RCA conserves natural resources by diverting waste materials from landfills and reducing the need for virgin aggregate extraction. This shift not only alleviates the pressure on natural aggregates but also minimizes the ecological disturbances associated with mining operations.

The methodologies developed in this thesis, particularly the novel systems for inspecting and grading RCA, ensure that the quality of recycled materials meets the stringent requirements of modern construction standards. By improving the reliability of RCA through enhanced quality control measures, this research supports the broader adoption of recycled materials, contributing to circular economy principles in the construction sector. This circular approach not only reduces waste but also lowers greenhouse gas emissions by decreasing the energy consumption associated with the production and transportation of new construction materials.



#### ECONOMIC BENEFITS AND MATERIAL EFFICIENCY

The adoption of RCA is not only environmentally advantageous but also economically beneficial. By utilizing waste materials, construction companies can significantly reduce material costs. The cost of extracting and processing virgin materials is steadily increasing due to stricter environmental regulations and decreasing availability. RCA offers a cost-effective alternative that can provide substantial savings on material expenses. Furthermore, the methodologies for efficient sorting and grading of RCA, as developed in this thesis, enhance the usability of recycled materials, thereby increasing their market value and attractiveness to industry stakeholders.

Material efficiency is another critical aspect underpinned by the use of RCA. Efficient material use involves not only the recycling of waste but also optimizing the lifecycle performance of the materials. The advanced inspection and grading systems introduced in this thesis enable the precise classification of RCA, ensuring that the right quality of material is used for appropriate construction applications. This tailored approach maximizes the functional performance of recycled materials and extends the lifespan of construction projects, further contributing to sustainability goals.

#### MEETING SUSTAINABILITY DEMANDS

The methodologies outlined in this thesis align with the increasing demands for sustainable construction practices. Stakeholders across the construction industry—including policymakers, builders, and consumers—are increasingly prioritizing sustainability due to its environmental, economic, and social benefits. The practical solutions provided by this research equip industry players with the tools needed to implement sustainable practices effectively. These tools not only facilitate compliance with environmental regulations but also enhance the overall sustainability profile of construction projects, making them more appealing to eco-conscious consumers and investors.

Moreover, the integration of RCA as a key component of sustainable construction practices serves as a model for other industries looking to adopt circular economy principles. The success of RCA can inspire similar innovations in the use of recycled materials across different sectors, broadening the impact of sustainable practices on a global scale.

## 6.2. CHALLENGES AND LIMITATIONS

### 6.2.1. TECHNOLOGICAL CHALLENGES

**Complexity of RCA Quality Assessment**

RCA are inherently variable due to their origin from diverse demolition sites. This variability poses a significant challenge for quality assurance and control. The sensor-based technologies implemented, including 3D scanning and LIBS, although innovative, still struggle with accurately characterizing materials with highly heterogeneous properties. Differentiating between various contaminants and RCA in a mixed stream, especially at high throughput rates, occasionally led to errors in material classification.



**Sensor Sensitivity and Calibration**

The sensors used, particularly the LIBS, require frequent recalibration to maintain accuracy, which can be cumbersome in a high-throughput industrial environment. Environmental factors such as dust, moisture, and varying ambient temperatures also affect sensor performance, complicating the consistent application of this technology on different demolition sites.

**Data Processing and Analysis**

The large volume of data generated by real-time, high-resolution 3D scanning presents significant challenges in data processing and analysis. The computational load to process and analyze this data in real-time requires substantial processing power, which can be a limiting factor in deploying these systems in mobile settings or where resources are constrained.

### 6.2.2. METHODOLOGICAL LIMITATIONS

**Sampling Representativeness**

While the methodologies developed aimed to provide a comprehensive analysis of RCA, the representativeness of sampling continues to be a challenge. The method of selecting specific strips or sections of the RCA stream for analysis may not consistently capture the

complete variability of the aggregate properties. This sampling issue could lead to an underestimation or overestimation of qualities such as strength, durability, and purity across the entire batch of RCA.

**Scale of Implementation**
The transition from laboratory-scale or pilot-scale studies to full-scale industrial applications highlighted several scalability challenges. Issues such as the integration of sensor systems into existing recycling operations, adapting to different types of recycling equipment, and the economic implications of technology retrofitting were significant. These factors often restrict the immediate adoption of advanced technologies in existing RCA processing facilities.

### 6.2.3. ECONOMIC AND PRACTICAL LIMITATIONS

**Cost Implications**
The high cost of advanced sensor technologies and the necessary computational and data storage infrastructure can be prohibitive. The initial setup cost, ongoing maintenance, and operation costs pose significant barriers to widespread adoption, especially in regions or markets where cost-efficiency is a critical deciding factor.

**Training and Expertise**
The operation of advanced sensor-based systems requires specialized knowledge and training. The lack of skilled personnel capable of managing these sophisticated systems can limit the practical deployment of such technologies. Moreover, the ongoing need for technical support and expertise to troubleshoot and maintain these systems adds to the operational complexity.



**Regulatory and Standardization Issues**
There is a lack of standardized protocols for the use of sensor-based technologies in RCA quality assessment. Regulatory uncertainties and the absence of universally accepted guidelines for the use of such technologies in construction material recycling further complicate their adoption. Ensuring compliance with local and international standards for construction materials remains a challenge when new technologies are introduced.

### 6.2.4. ENVIRONMENTAL AND SUSTAINABILITY LIMITATIONS

**Energy Consumption**
The energy requirements for operating high-power sensors and data processing systems are significant. This aspect is often at odds with the sustainability goals of recycling operations, particularly in scenarios where the energy source is not renewable. Balancing technological advancement with environmental sustainability is a critical consideration that needs further exploration.

**Technology Lifecycle**
The environmental impact of manufacturing, maintaining, and eventually disposing of advanced technological equipment used in RCA processing has not been fully explored.

The lifecycle assessment of such technologies is necessary to ensure that their environmental footprint does not negate the sustainability benefits offered by recycling RCA.

These challenges and limitations highlight the complexities involved in integrating advanced sensor-based technologies into RCA processing operations. While the potential benefits of these technologies are significant, addressing these hurdles is essential for their successful implementation and for maximizing their impact on sustainable construction practices. Future research should focus on overcoming these challenges through innovative solutions, improved system designs, and strategies that enhance the practical and economic feasibility of technology deployment in the recycling of construction and demolition waste.

## 6.3. FUTURE RESEARCH DIRECTIONS

This dissertation has laid a robust foundation for the utilization of RCA in construction, emphasizing sustainability and technological advancement. However, as the domain of sustainable construction evolves, so too must the technologies and methodologies that support it. This section outlines a comprehensive roadmap for future research, focusing on technological enhancements, economic evaluations, scalability assessments, and long-term performance studies of RCA-utilized structures.



### 6.3.1. TECHNOLOGICAL REFINEMENTS

The use of LIBS and 3D scanning has proven transformative in analyzing and ensuring the quality of RCA. Future studies should aim at increasing the resolution and accuracy of LIBS to detect finer compositional nuances that may affect the performance of RCA in concrete. This could involve integrating advanced spectroscopic techniques that allow for deeper material characterization at the molecular or atomic level.

Further, enhancing the speed of 3D scanning technologies can expedite the quality control processes, allowing for real-time data acquisition and analysis. The development of more sophisticated algorithms for faster processing and interpretation of 3D imaging data will significantly reduce the turnaround time from RCA collection to usage. Integration of machine learning models that can predict RCA quality based on historical data and real-time scans could streamline the decision-making process in RCA utilization.

### 6.3.2. ECONOMIC IMPACT AND SCALABILITY

The economic implications of adopting RCA on a large scale are multifaceted. Future research should involve detailed cost-benefit analyses comparing the lifecycle costs of structures built with traditional materials versus those constructed with RCA-enhanced concrete. This analysis should include not only initial construction costs but also long-term maintenance, repair, and eventual decommissioning costs. Environmental cost accounting should also be incorporated to assess the savings in carbon emissions and natural resource depletion.

Scalability studies are essential to understand the barriers and facilitators to the widespread adoption of RCA in different regional markets. These studies should consider local availability of RCA, regulatory environments, and existing supply chains for

construction materials. By identifying specific regional challenges and opportunities, tailored strategies can be developed to promote the adoption of RCA.

### 6.3.3. COMMERCIAL VIABILITY

Investigating the commercial viability of the developed technologies involves assessing market readiness and industry acceptance. Surveys and pilot studies within the construction industry can provide insights into the perceived benefits and drawbacks of RCA usage from a commercial perspective. Furthermore, developing business models that can economically justify the initial higher costs of implementing advanced technologies for RCA processing and utilization may accelerate their adoption.

Partnerships with construction firms and public infrastructure projects could serve as test beds for demonstrating the practical benefits and economic feasibility of RCA. These partnerships could also facilitate adjustments to the technology based on real-world feedback and performance metrics, ensuring that the solutions developed are not only scientifically sound but also commercially viable.

### 6.3.4. LONG-TERM PERFORMANCE AND SUSTAINABILITY

To validate the durability and practicality of RCA-enhanced concrete, longitudinal studies on structures built with this material are crucial. Such studies would track performance over time under various environmental conditions and usage scenarios. This research should also explore the repairability and recyclability of RCA concrete, examining if structures built with RCA can be efficiently maintained or further recycled.

Incorporating sustainability assessments that examine the lifecycle environmental impact of RCA utilization—from extraction and processing of original materials to the end-of-life of the structure—will provide a holistic view of the benefits and potential drawbacks of RCA. This could help in refining RCA processing techniques to further minimize environmental impact.



## 6.4. CONCLUSION

The path forward for RCA and associated technologies involves a blend of technical innovation, economic analysis, and practical testing. By continuing to explore these avenues, the research community can enhance the viability and desirability of RCA in construction, thereby contributing to a more sustainable and economically feasible construction industry.

# ACKNOWLEDGEMENTS

This doctoral journey has been a winding road filled with challenges and transformations. Along the way, I changed universities once and supervisors twice, navigating uncertainty and growth. Yet, I was incredibly fortunate to eventually meet Peter and Francesco at Delft University of Technology. They embodied everything I could have hoped for in supervisors, offering unwavering support, encouragement, and guidance.

Although my PhD project ventured into an entirely new field—one I had no prior experience in—Peter and Francesco always believed in me. Their consistent recognition of even my smallest progress was a source of motivation, far beyond what I could have imagined, instilling in me a deep sense of confidence.

Peter consistently brings remarkable insights to the most challenging problems, inspiring awe with his brilliance. No matter how daunting the issues ahead, he always maintains a smile, addressing each challenge with a calm demeanor and decisive wisdom. Despite his incredibly busy schedule, he always responds swiftly and thoughtfully to my every query, offering an unshakeable sense of reassurance. His office door was always open to me, and whenever I knocked, he would set aside his work to patiently guide me through my questions and doubts. I will never forget one heartfelt conversation we had after a particularly challenging discussion. I confided in him that I felt lost in my research, inadequate in my abilities, and overly reliant on his step-by-step guidance. I worried this made me seem incapable and doubted whether I could ever become an independent researcher. Peter patiently reassured me, explaining that feeling this way is part of the journey for any researcher. He reminded me that publishing my first paper was a clear testament to my abilities and emphasized that expertise comes with time and experience. His words instilled in me a belief in my potential to excel.

Francesco's unwavering diligence and meticulous work ethic have been exemplary, offering me a model of professionalism to emulate. His dedication is profound; even when ill, Francesco managed everything with remarkable orderliness. It seemed he never rested, as no matter when I sent an email, he was always the first to respond. What truly astonishes me is his consistent success in securing funding for projects, maintaining an impressively high success rate. I am deeply grateful to Francesco, who was a constant source of support during this difficult time. He guided me through challenges, helped me communicate effectively, and ensured I had access to critical resources. His reassuring words, "We just need to do the best we can." stayed with me and continued to inspire me throughout this journey. His attention to detail in

reviewing my work was invaluable—he corrected every small error with patience and care, never criticizing but gently guiding me toward improvement. When I arrived in the Netherlands from Switzerland at the height of the COVID-19 pandemic, everything felt overwhelming. I often found myself overthinking and consumed by anxiety. Francesco would frequently make a point to visit my office, urging me to rest more. No matter what new challenge I wanted to tackle, Francesco was there, offering his unconditional encouragement. It was Francesco's steady encouragement and support that helped me regain my footing and find my path.

Lastly, I wish to express my heartfelt gratitude to all the people who have loved, encouraged, and supported me along this path. Thank you for walking beside me through every challenge and triumph. Your belief in me has made all the difference.

玉宇澄清万里埃

*Cheng Chang*
*Delft*
*August,8 2024*

# CURRICULUM VITÆ

## Cheng CHANG

| | |
|---|---|
| 1992 | Born in Taixing, China. |

## EDUCATION

| | |
|---|---|
| 2011–2015 | Bachelor<br>Southeast University |
| 2016–2018 | Master<br>Southeast University |
| 2019–2020 | PhD candidate in Architecture<br>École Polytechnique Fédérale de Lausanne |
| 2021–2024 | PhD in Engineering<br>Technische Universiteit Delft<br>*Thesis:* Quality Assessment & Monitoring of Recycled Coarse Aggregates<br>*Promotor:* Prof. dr. ir. P. C. Rem<br>*Copromotor:* Dr. F. Di Maio |

# LIST OF PUBLICATIONS

8. B. Chen, P. Perumal, C. Liu, Y. Chen, **C. Chang,** M. Pavlin, D. Kvočka, V. Ducman, M. Illikainen, and G. Ye. *Effects of municipal solid waste incineration (MSWI) bottom ash incorporation on the microstructure and performance of blended cementitious materials: a critical review*, submitted.

7. S. Zong, **C. Chang,** P. Rem A.T. Gebremariam, F. Di Maio, and Y. Lu. *Research on the influence of particle size distribution of high-quality recycled coarse aggregates on the elementary mechanical properties of recycled concrete*, submitted.

6. **C. Chang,** F. Di Maio, R. Bheemireddy, P. Posthoorn, A.T. Gebremariam, and P. Rem. *3D surface analysis to optimize particle size distribution in unscreened recycled coarse aggregates for quality assurance*, submitted.

5. **C. Chang,** F. Di Maio, R. Bheemireddy, P. Posthoorn, A.T. Gebremariam, and P. Rem. *Enhancing quality inspection efficiency and reliability of unscreened recycled coarse aggregates (RCA) streams using innovative mobile sensor-based technology*, submitted.

4. **C. Chang,** F. Di Maio, and P. Rem. *Real-time sensor-based characterization of recycled coarse aggregates (RCA)*, The Sixth International Conference on Civil and Building Engineering Informatics (ICCBEI 2025), Hongkong, China, accepted.

3. **C. Chang,** F. Di Maio, R. Bheemireddy, P. Posthoorn, A.T. Gebremariam, and P. Rem. *Rapid quality control for recycled coarse aggregates (RCA) streams: multi-sensor integration for advanced contaminant detection*, Computers in Industry **164**,104196.

2. F. Di Maio, **C. Chang,** A. Vahidi, A.T. Gebremariam, and P. Rem. *Quality control of recycled concrete aggregates using laser-induced breakdown spectroscopy*, Concrete Plant International **01/2023**, 36.

1. **C. Chang,** F. Di Maio, P. Rem, A.T. Gebremariam, F. Mehari, and H. Xia. *Cluster-based identification algorithm for in-line recycled concrete aggregates characterization using laser-induced breakdown spectroscopy (LIBS)*, Resources, Conservation and Recycling **185**, 106507.